



Institute for Advanced Study
Math. - Nat. Sci. Library
Princeton, N. J. 08540

Contract No. DA-36-034-ORD-1330
Project No. TB3-0538

FINAL REPORT

on

CONTRACT NO. DA-36-034-ORD-1330

by

The Staff
Electronic Computer Project

IAS ECP list of reports,
1946-57. no. 17.

THE INSTITUTE FOR ADVANCED STUDY
December 1954

TABLE OF CONTENTS

PREFACE

ACKNOWLEDGMENTS

PART I - ENGINEERING

A. INTRODUCTION	I-1.
B. SUMMARY	I-2.
C. ENGINEERING WORK	I-3.
1. Machine move	I-3.
a. Memory improvements during move	I-3.
i. Deflection bus re-insulation	I-3.
ii. Control plugboard	I-4.
iii. Collected amplifier outputs	I-4.
iv. Other changes	I-7.
b. AC-DC turn-on system	I-7.
The starting control	I-9.
c. The new location	I-13.
i. Layout	I-13.
ii. Power	I-15.
iii. Cooling	I-18.
2. Engineering improvements	I-21.
a. RI digit insertion	I-21.
i. General	I-21.
ii. Detailed description	I-24.
b. New secondary regulators	I-27.
c. Present drum techniques	I-31.
d. Graphing circuit	I-32.
i. Deflection for graphing operation	I-33.
ii. Deflection for slave operation	I-37.
iii. Beam turnon	I-37.
iv. Control	I-41.
e. Division spill check	I-48.
f. Zero shift order	I-50.
g. Memory high voltage change	I-50.
3. Machine operation	I-54.
Table I - Weekly time for the year	I-56.
Table II - Time records for the previous year	I-57.
Table III - Summary of results for two years	I-58.

TABLE OF CONTENTS (continued)

FIGURES IN PART I

Figure 1 - Bleeder chain for CRT	I-5.
Figure 2 - Plugboard photo	I-6.
Figure 3 - Collected amp outputs	I-8.
Figure 4 - Turnon control	I-10.
Figure 5 - AC power wiring	I-11.
Figure 6 - Machine room layout	I-14.
Figure 7 - Power switching center, front view	I-16.
Figure 8 - Power switching center, photo	I-17.
Figure 9 - Air conditioning - Air flow diagram	I-19.
Figure 10 - Primary feed and air conditioning controls .	I-20.
Figure 11 - Neon toggle control	I-23.
Figure 12 - Neon toggle control	I-23.
Figure 13 - NE-2 characteristics	I-26.
Figure 14 - Neon contrd for R_1	I-26.
Figure 15 - Reference and screen supplies for regulators	I-29.
Figure 16 - Typical regulator	I-30.
Figure 17 - Block diagram - Graphing unit	I-34.
Figure 18 - Comparison circuit	I-34.
Figure 19 - Memory beam turnon pulses	I-34.
Figure 20 - Proportional pulse stretcher	I-39.
Figure 21 - Operation of stretcher circuit	I-39.
Figure 22 - Graph priming circuit	I-42.
Figure 23 - Graph priming diagram	I-42.
Figure 24 - False B_3 signal	I-42.
Figure 25 - Graphing control	I-44.
Figure 26 - Division spill	I-49.
Figure 27 - Regulated high voltage supply for Williams memory	I-52.
Figure 28 - Table of regulated power supplies	I-53.

PART II - MATHEMATICS

A. BLAST WAVE CALCULATION	II-1.
0. <u>Introduction</u>	II-1.
1. <u>The differential equations</u>	II-1.
2. <u>The difference equations</u>	II-3.
3. <u>The computational algorithm</u>	II-6.
4. <u>The initial values</u>	II-16.
5. <u>Preliminary remarks on the calculation</u> . . .	II-17.
6. <u>The results</u>	II-26.

TABLE OF CONTENTS (continued)

(PART II - continued)

Figure I - Shock overpressure vs. shock radius	II-28.
Figure II - Time of shock arrival at radius R	II-29.
Table I -	II-30.
Table II -	II-31.
Figure III - Overpressure vs. Eulerian radius	II-32.
Figure IV - Overpressure vs. Eulerian Radius	II-33.
Figure V - Overpressure vs. Eulerian radius $t = 2.9322$. .	II-34.
Figure VI - Overpressure vs. Eulerian radius $t = 14.0989$.	II-35.
Figure VII - Overpressure vs. Eulerian radius $t = 32.3653$	II-36.
Figure VIII - Overpressure vs. Time Eulerian Radius $= 0.625$	II-37.
Figure IX - Overpressure vs. Time Eulerian Radius $= 1.00$.	II-38.
Figure X - Overpressure vs. Time Eulerian Radius $= 1.5$. .	II-39.
Figure XI - Overpressure vs. Time Eulerian Radius $= 2.00$.	II-40.
Figure XII - Overpressure vs. Time Eulerian Radius $= 2.75$	II-41.
Figure XIII - Overpressure vs. Time Eulerian Radius $= 3.75$	II-42.
Figure XIV - Overpressure vs. Time Eulerian Radius $= 5.50$.	II-43.
Figure XV - Overpressure vs. Time Eulerian Radius $= 19.5$.	II-44.
Figure XVI - Overpressure vs. Time Eulerian Radius $= 41.0$	II-45.
Figure XVII - Length of positive phase vs. shock radius .	II-46.
Figure XVIII - Length of positive phase vs. shock radius .	II-47.
B. CONTINUED FRACTION EXPANSIONS OF ALGEBRAIC NUMBERS . .	II-48.
0. <u>Summary</u>	II-48.
1. <u>The continued fraction algorithm for real algebraic irrationalities</u>	II-50.
2. <u>Outline of the basic code</u>	II-50.
3. <u>Checking facilities</u>	II-53.
C. MAGNETOHYDRODYNAMIC THEORY OF SOLAR SPICULES	II-56.
D. CALCULATION OF THE ENERGY BAND STRUCTURE OF IRON WITH APPLICATION TO THE THEORY OF FERROMAGNETISM	II-61.

PART III - METEOROLOGY

A. <u>Computations with a three-level model</u>	III-1.
B. <u>Experiments with a two-level forecasting model</u>	III-5.
C. <u>Experiments with multi-layer non-linear forecasting models</u>	III-7.
D. <u>Barotropic forecasts for low latitudes</u>	III-11.
E. <u>Computations of vertical velocities</u>	III-12.
F. <u>Time series code</u>	III-14.

TABLE OF CONTENTS (continued)

(PART III - continued)

G. <u>Objective analysis</u>	III-17.
H. <u>Wind-driven water waves</u>	III-34.
I. <u>Use of the primitive equations in forecasting</u>	III-40.

PREFACE

The following report has been prepared in accordance with the terms of Contract No. DA-36-034-ORD-1330 and constitutes the Final Report called for under the terms of that contract. It is divided into three parts covering the salient engineering work as well as the mathematical and meteorological investigations for the period July 1, 1953 through June 30, 1954. The actual carrying out of the calculations indicated in Parts II and III was done under the terms of the contract. The mathematical preparations, i.e. the numerical analysis, programming and coding were carried out under the terms of Contract No. N-7-ONR-388, T. O. I and Contract No. N-6-ORI-139, T. O. I between the Institute for Advanced Study and the Office of Naval Research. Since the objectives of the three contracts are substantially overlapping it was felt desirable to include all this material in one report. In this fashion it is hoped to give the maximum possible information to all interested agencies.

John von Neumann
Project Director

Institute for Advanced Study

ACKNOWLEDGMENTS

The present report represents the combined efforts of the staff of the Electronic Computer Project of the Institute for Advanced Study and in particular of the following individuals: J. Callaway, J. Cooley, B. Gilchrist, H. Goldstine, L. Harmon, W. Keefe, Jr., D. Lautmann, J. Pomerene, B. Tuckerman, G. Veronis, J. von Neumann, and S. Wong

In addition, the editors drew freely on material from unpublished works by: J. Charney and G. Cressman.

PART I - ENGINEERING

A. INTRODUCTION

This report describes the operation of and engineering improvements on the electronic computer at the Institute for Advanced Study during the period from 1 July 1953 to 30 June 1954. The engineering discussion is restricted to those features of the present machine which were added during this period. A full technical description of the machine prior to this period is given in the final reports on Contract No. W-36-034-ORD-7481, Contract No. DA-36-034-ORD-19 (Project No. TB3-0007F) and Contract No. DA-36-034-ORD-1023 (Project No. TB3-0007).

B. SUMMARY

During the first month of the period covered by this report the computer was in full scale use at its original construction location. It was then moved to its permanent location in the mathematical wing of the building. Advantage was then taken of the partial disassembly required by the move to carry out several mechanical and electrical improvements on the memory unit. In addition, the control system, power supplies, and cooling system were organized to make operation and maintenance much easier.

Full scale operation was resumed in December 1953 at the new location. In subsequent months the magnetic drum was brought into a state of control, the major work was finished on a graphical output device and several other engineering improvements were made.

C. ENGINEERING WORK

1. Machine move.

The computer was constructed in the experimental area adjacent to the engineering laboratory and the shop, and after its completion was operated in this area through all of 1952 and the first half of 1953. Considerably operating experience was gained during this period and the machine itself was brought into an excellent state of engineering control.

However, the restricted space available made operation cumbersome at best and placed the machine and the operator in the same environment, this latter resulting in a compromise between machine cooling and human comfort. A large space had been provided in the mathematical wing of the building and it was accordingly decided to move the machine into this space and to arrange operating facilities as conveniently as possible. An earnest attempt was made to simplify operating procedures, including turn on and off, so as to make the machine available to non-technical users.

a. Memory improvements during move.

The overall height of the machine was too great to permit passage through doorways so it was necessary to separate the memory and the arithmetic units. This occasion was used to make several improvements in the memory unit which experience had shown desirable:

i. Deflection bus re-insulation.

Because of the already high average voltage level of the deflection bus system (+1300 v) and the possibility of a further increase to improve read-around, the old fish paper insulation was removed and nylon base phenolic installed. In addition, teflon

insulated wire was used for the individual bus-to-socket connections.

ii. Control plugboard.

The focus, astigmatism, and beam current controls for each tube were formerly located with the stage and below it with the result that memory adjustments were executed from a cramped position and further involved stage by stage relocation of the test oscilloscope if all stages were tuned. It was also clear that the potentiometers themselves were causing day to day variations in the memory adjustment, partly because of their necessarily high resistance values. Therefore all cathode ray tube controls were moved to a panel at the 2^{-39} end of the machine and only the individual electrode decoupling filters left at the cathode ray tube sockets. Further, the focus and astigmatism potentiometer ensembles were abandoned altogether and replaced by a single multi-tapped low resistance bleeder with a plugboard arrangement. The focus plugboard supplies 20 voltage steps three volts apart, each step feeding a row of 41 paralleled banana jacks. Each cathode ray tube focus supply wire terminates in a banana plug which can be put into any one of the 20 steps. The astigmatism plugboard is similar except that it provides 12 steps in increments of six volts. Potentiometers were retained for the intensity control but reduced in resistance from 150 K to 20 K ohms. See figure (1) and (2).

iii. Collected amplifier outputs.

Since at least preliminary memory stage adjustments are made according to observed dot and dash waveforms, a resistance divider was installed in each discriminator to feed an attenuated but low impedance signal via a cable to a 40 position switch at the plugboard location. Thus a complete preliminary alignment can

Figure 1 - I-5.

ELECTRONIC COMPUTER PROJECT
INSTITUTE FOR ADVANCED STUDY
PRINCETON, N. J.

BLEEDER CHAIN FOR C.R.T.

DRAWN F.Fell

DATE: 5-7-54

Dwg. No. A = 2006

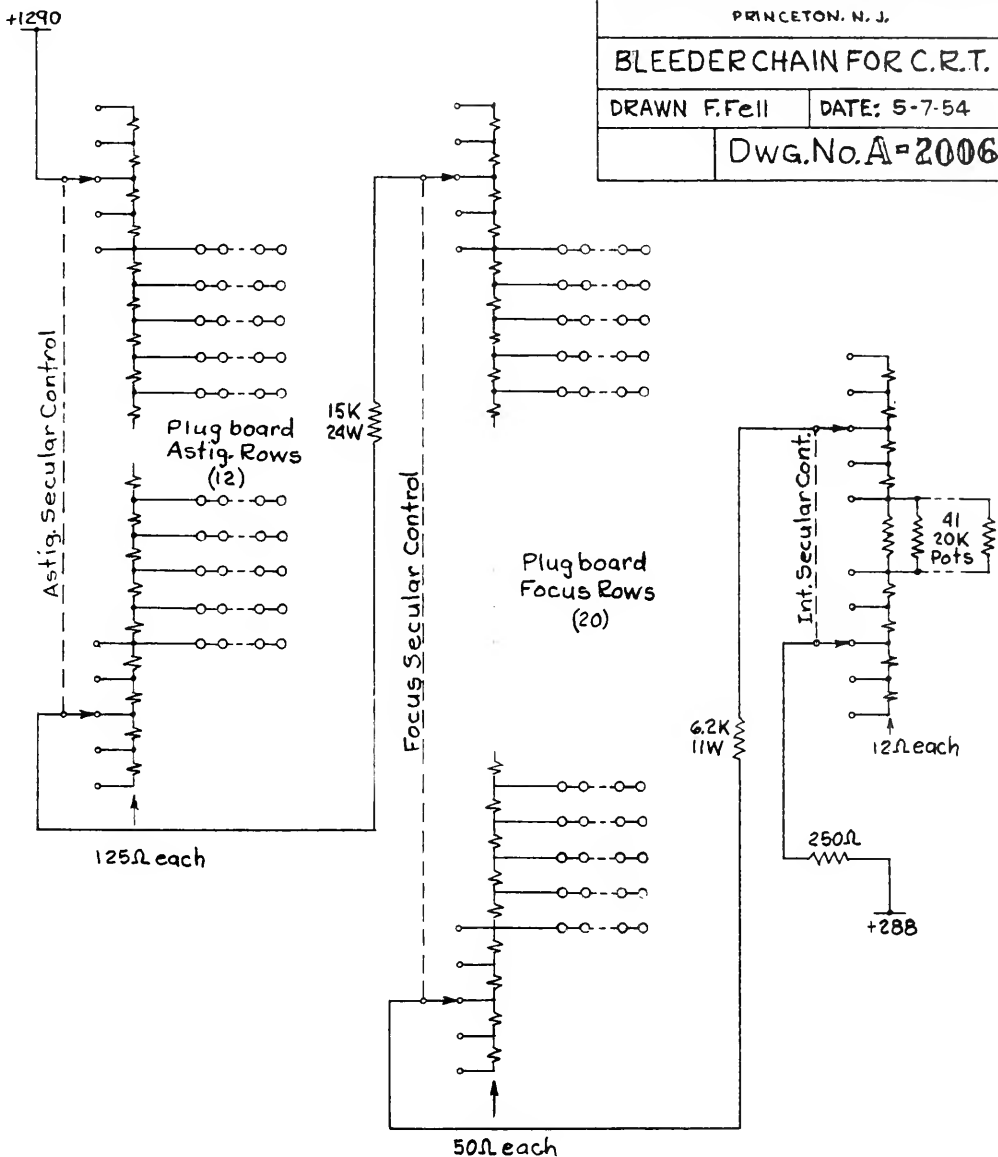
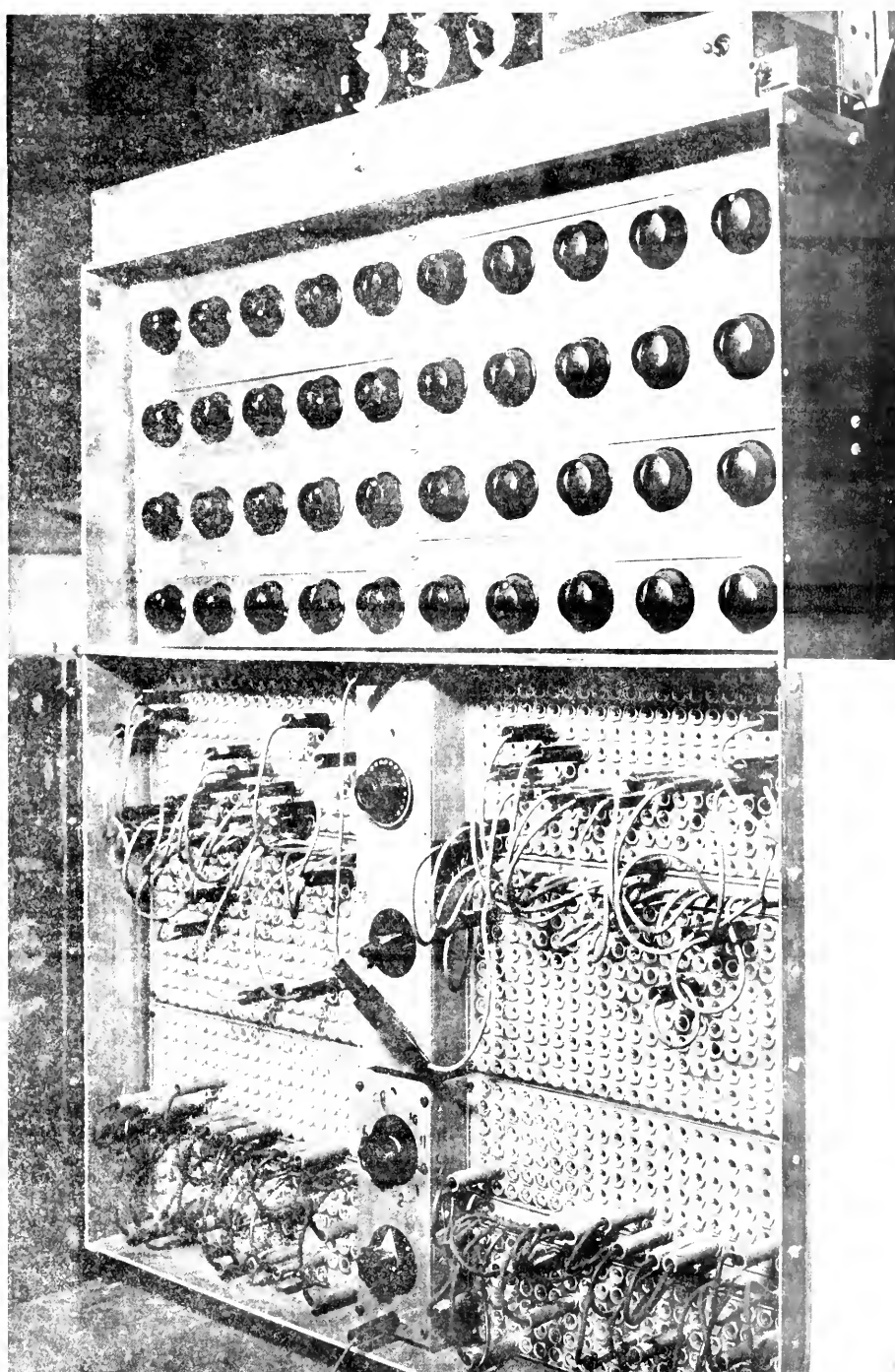
AstigmatismFocusIntensity

Figure 2 - I-6.



be made quickly and conveniently. Final adjustments, made according to read-around test results, are equally convenient in that a standard focus or astigmatism increment is obtained just by shifting the plug one row for the stage in question. The circuit is shown in figure (3).

iv. Other changes.

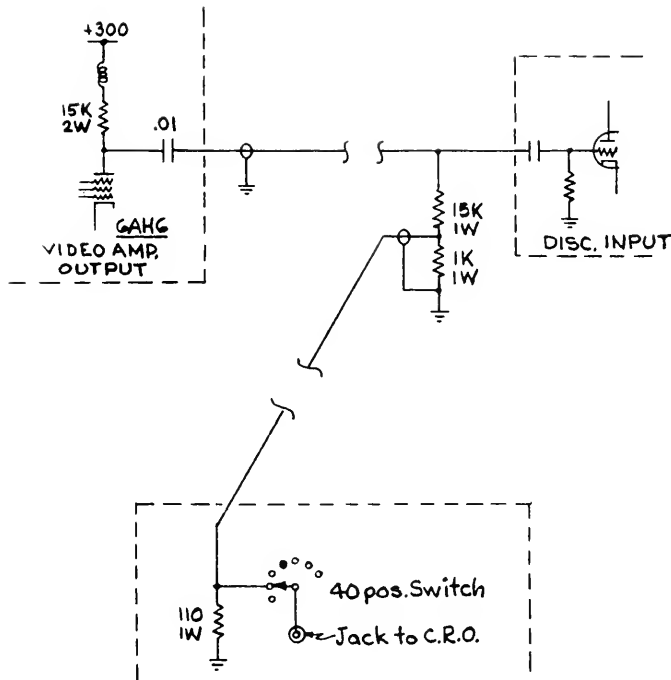
Additional changes were the punching of holes in the cathode ray tube support web to facilitate cooling air flow, provision for a forty-first memory stage (to be completed if needed), consolidation of memory heater transformer banks and automatic screen charging at turn-on.

b. AC-DC turn-on system.

A major consideration in furnishing the new location for the machine was to simplify turning on and turning off procedures so that the computer could be used by the mathematicians and coders without engineering assistance. This would make available the 48 to 88 hours per week not regularly scheduled and staffed by engineering operators. Accordingly, a one button system was visualized in which the single command "turn on" would initiate an automatic sequence of events resulting in a "ready to compute" signal. Similarly one action would be required to "turn off".

This very simple system was elaborated slightly in the realization. The authorization to use the machine was embodied in the requirement of a key to enable the "turn on" switch and the following automatic sequence was terminated at the completion of all AC functions. One additional button was provided to apply DC voltages to the machine. A "DC off" button was also furnished for servicing and standby, but normal "turn off" was left a one-switch function.

Figure 3 - I-8.



COLLECTED AMPLIFIER OUTPUTS

Since the vacuum tube heaters contribute about one-half of the heat output of the machine, it is quite essential that the first turn-on step be to turn on the cooling system and also that continuation of the turn-on sequence be dependent on the blowers coming on. Following this all memory and arithmetic unit heaters are turned up slowly by a motor driven Powerstat bank. In the same period all power supplies are turned on, the large (PEC) units having their own sequencing arrangements. Completion of these steps lights an "AC on" light. Turning the DC on is made a separate operation to insure that someone is present to observe the machine at this critical time. After DC turn-on a time delay arrangement maintains all memory beam currents at a higher than normal value for about two minutes in order to bring the charge on the phosphor to equilibrium. When this delay is over, the machine is ready for use.

A step by step description of the turn-on process follows.
Reference is made to figures (4) and (5).

The starting control.

The whole machine can be turned on only when a key switch is operated. This switch has two functions. After the "AC" switch is turned on:

Turn key clockwise - energizes the air conditioners and blowers.

Return key to normal position - enables the rest of the starting process if either compressor and both blowers are properly energized. This prevents unnecessary starting cycles in case the air conditioner is out of function as the machine cannot be operated without air conditioning for sustained periods of time.

After the key has been returned to its normal position: A limit

Figure 4 - I-10.

TURN ON CONTROL

ELECTRONIC COMPUTER PROJECT
INSTITUTE FOR ADVANCED STUDY

INCERON. N. J.

DR. JON CUNNINGHAM
DATE: 4-20-54

卷之三

卷之二

卷之三

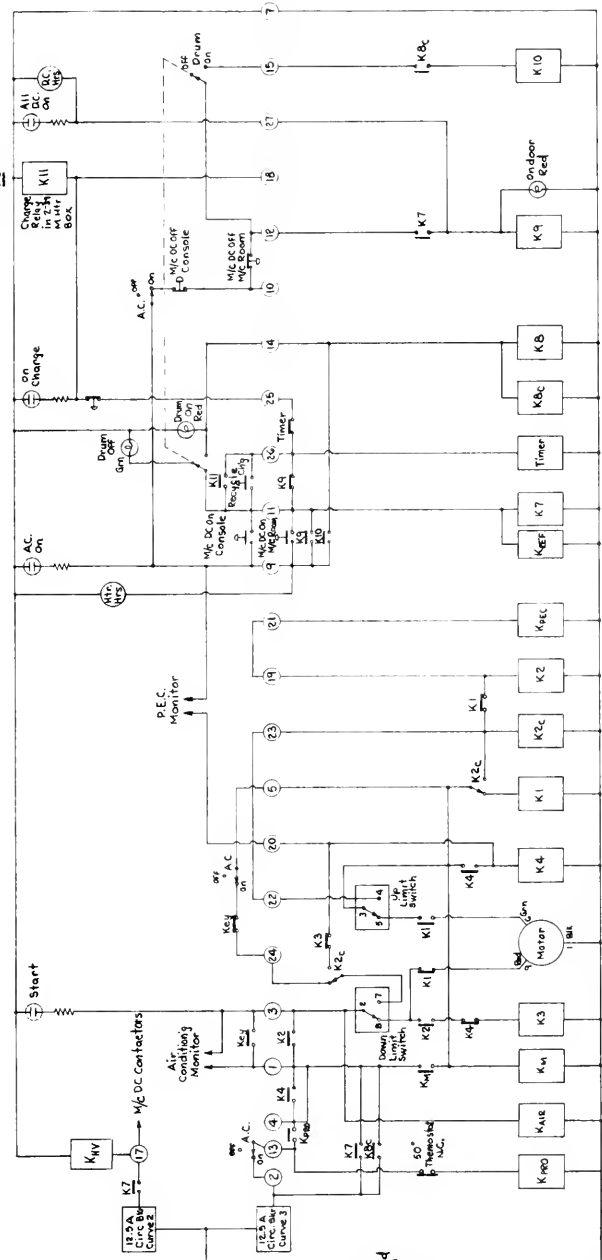
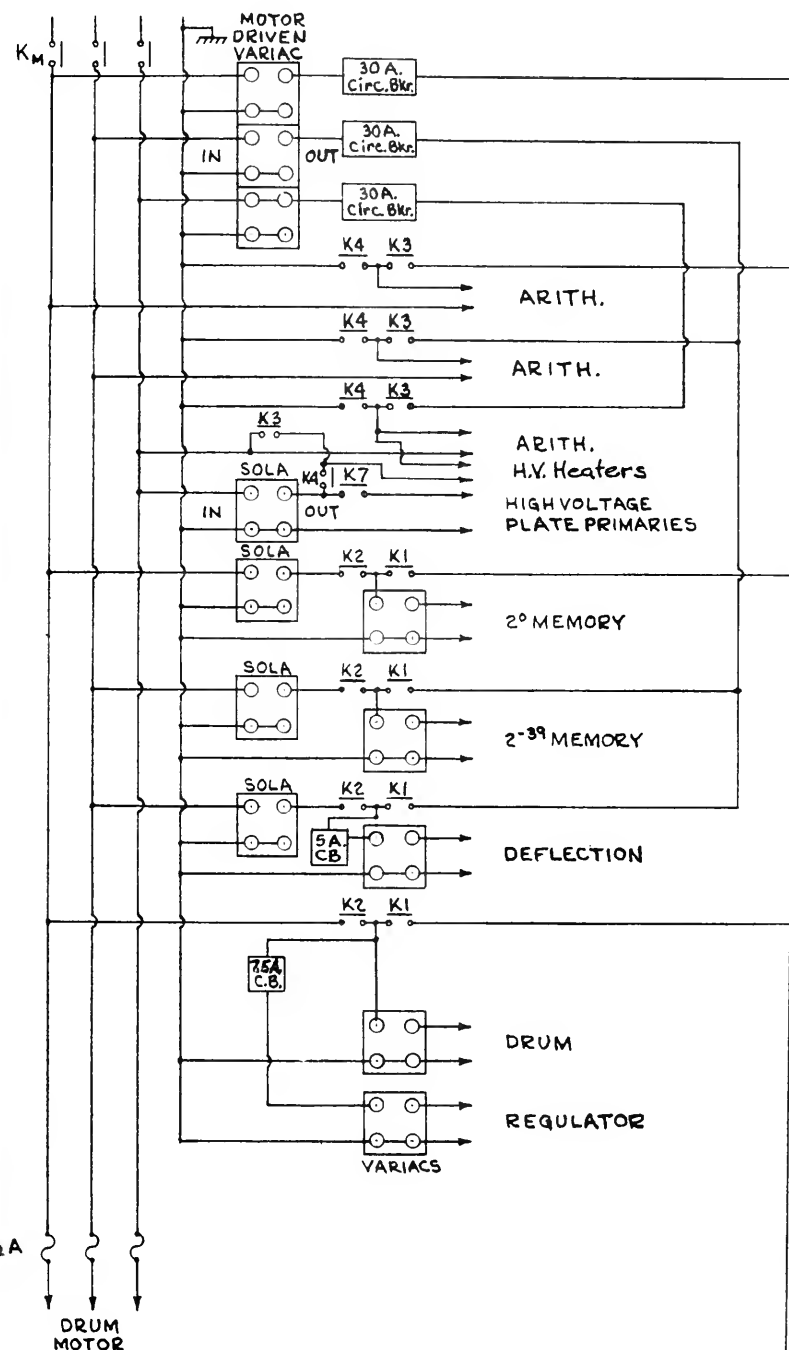


Figure 5 - I-11.



ELECTRONIC COMPUTER PROJECT
INSTITUTE FOR ADVANCED STUDY
PRINCETON, N.J.

A.C. POWER WIRING

DRAWN: F.FELL DATE: 4-29-54

Dwg. No. A-2003

switch on the Powerstat driving motor senses the position of the Powerstat rotor. If the position of the rotor is other than the down limit, the motor is energized so that the down limit is eventually reached. At that instant, due to the operation of the limit switch, the motor is stopped and K_1 and K_M contactors are energized. K_M is the main contactor that energizes the three phase AC supply to all heater circuits. K_1 connects all memory, input-output organ and regulator heater circuits to the output of the Powerstats and starts the motor so that the heater voltages are slowly raised. When the upper limit is reached, the "up" limit switch operates which stops the motor and energizes K_{2c} which in turn drops out K_1 and energizes K_2 . This act switches the memory heaters from the Powerstats to Sola regulating transformers. The main (PEC) power supplies are turned on when K_2 is operated. The PEC supplies contain their slow-raise circuits. At the end of raise, a relay operates to indicate completion. The release of K_1 reverts the control of the Powerstat motor back to the "down" limit switch which starts the motor on the downward trip.

The Powerstat is a voltage divider. The two fixed ends are intrinsically indistinguishable. Regardless of the direction of travel, the voltage between one of the fixed ends of the divider and the rotor is increasing. This fact is used to raise the heater voltages of the arithmetic units by the action of K_3 .

At the end of the downward travel, the "down" limit switch stops the motor and transfers from K_3 to K_4 whereby the arithmetic heaters are now supplied directly from the three phase AC lines.

Notice that after K_2 has been energized, the air conditioning monitoring circuit no longer has control of the machine. This is to

prevent interruption of machine operation by normal cycling of the compressors (under thermostat control).

The DC turn-on is conditional on the PEC supplies. If these supplies are in operating condition, the DC turn-on contactors can be enabled. A manual PEC disable switch is installed to facilitate servicing.

In figure (4) the AC starting circuitry are located on the left of terminal 9, while on its right are DC switching circuitry. The DC switching are arranged such that the input-output organ and drum units can be separately turned off while the machine DC is on, to enable maintenance on those units.

In all cases of on-off procedure, the -300-volt bus is switched on one relay time later than all plus voltages. This is to prevent excessive heater-cathode voltages in the absence of plate voltages on cathode followers and coincidence circuits. On turn-off the reverse is made true. The heaters are also prevented from being turned off while DC is applied to the machine.

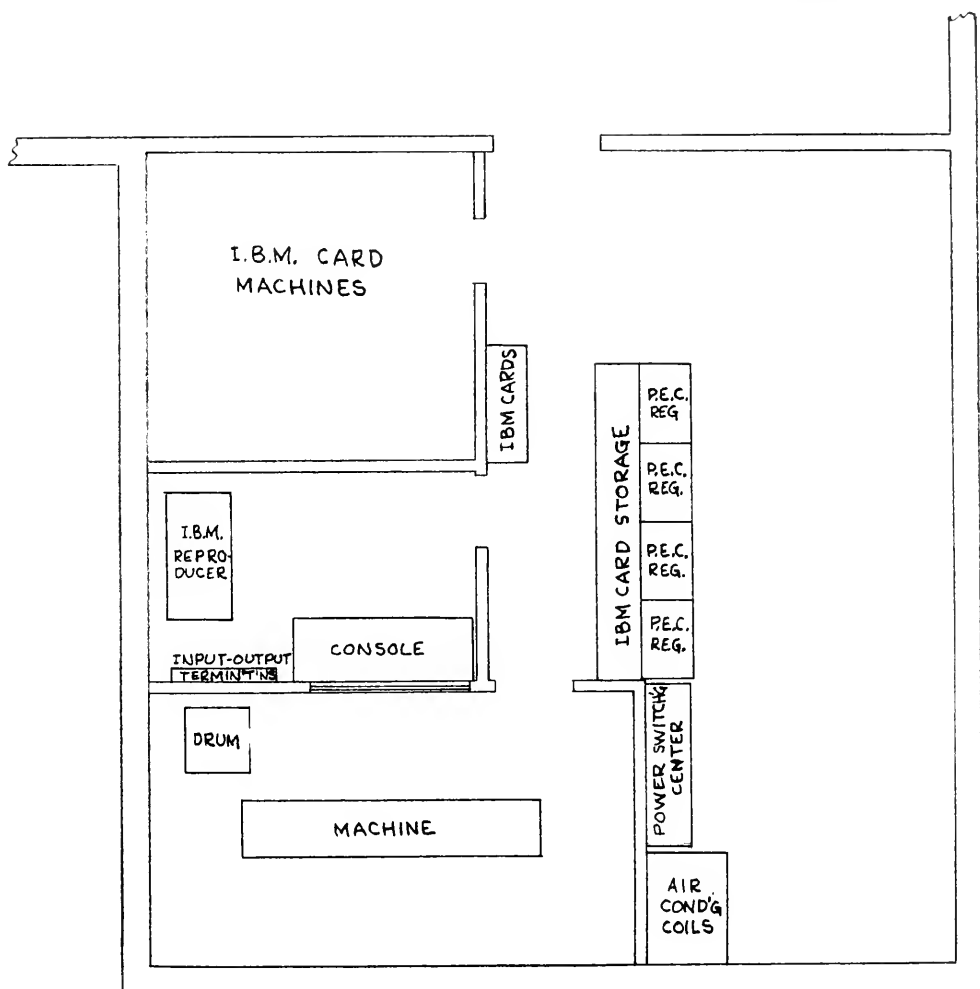
c. The new location.

i. Layout.

Figure (6) shows the physical layout of the new room. The computer is in a separate room from the operator, but can be viewed through a large window in front of the operating table. The computer room itself need not be entered except for maintenance and trouble shooting. It can be kept cooler than human comfort temperature and also more free of dust than if operators were in the same room.

The operating room contains all the needed operating controls, a monitor cathode ray tube for displaying the contents of any memory stage, the graphing device (described elsewhere in this report), and

Figure 6 - I-14.



MACHINE ROOM LAYOUT

an IBM type 514 reproducing punch which is used for input and output.

A third room houses the IBM equipment needed for producing the original machine input decks and for processing outputs. It contains two alphameric key punches, a reproducing punch, an alphameric tabulator and a sorter.

ii. Power.

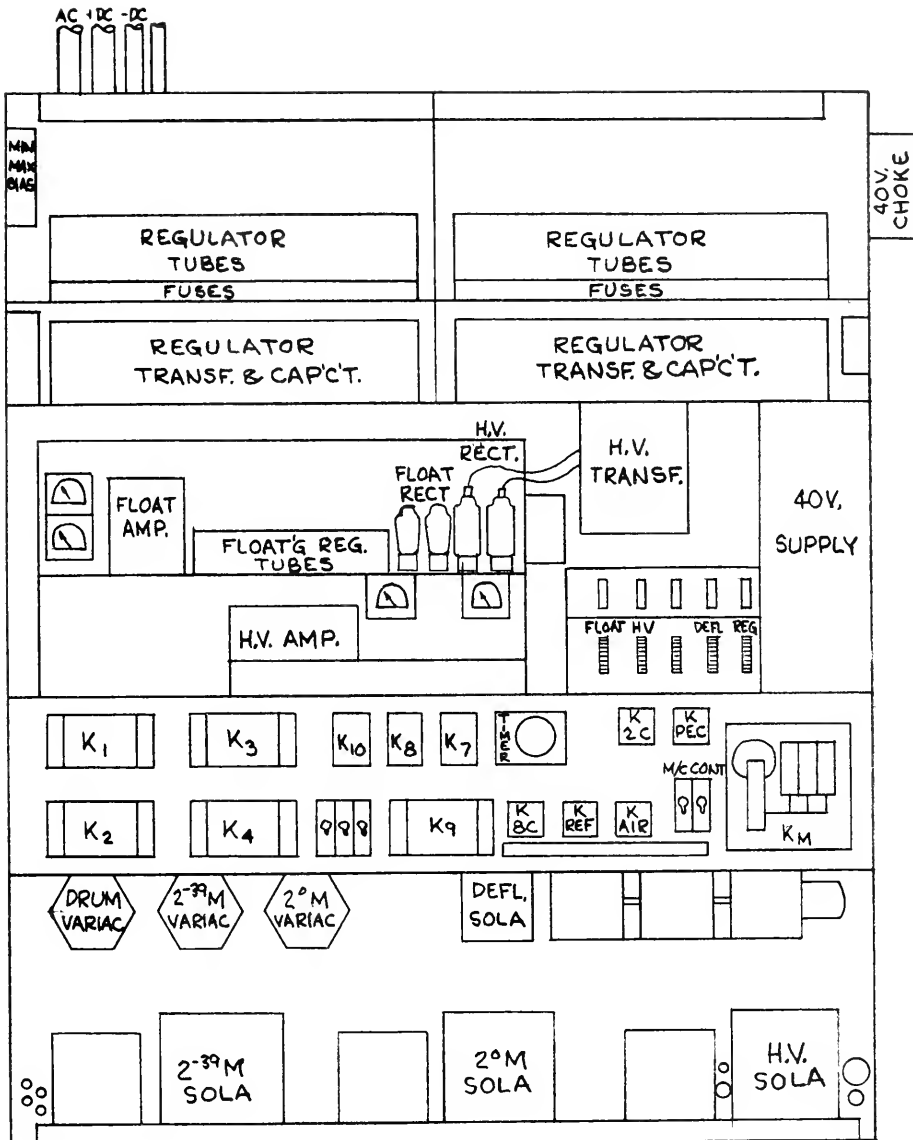
To meet the power requirements of the computer and its associated equipment a 200 ampere feed was installed from the main building load center to the machine location. Here the load was divided into three parts:

- 1) the high current DC supplies - 60 amperes per phase,
- 2) blowers and cooling system - 40 amperes,
- 3) machine vacuum tube heaters and miscellaneous - 50 amperes.

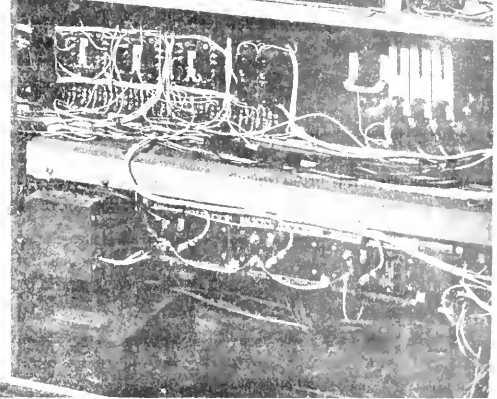
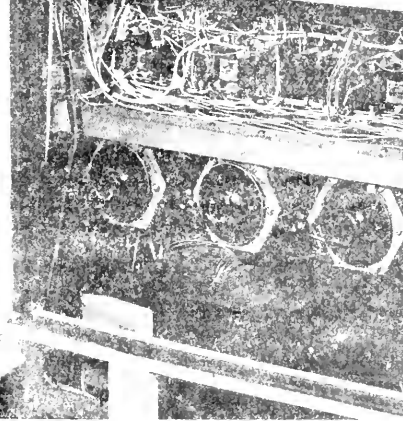
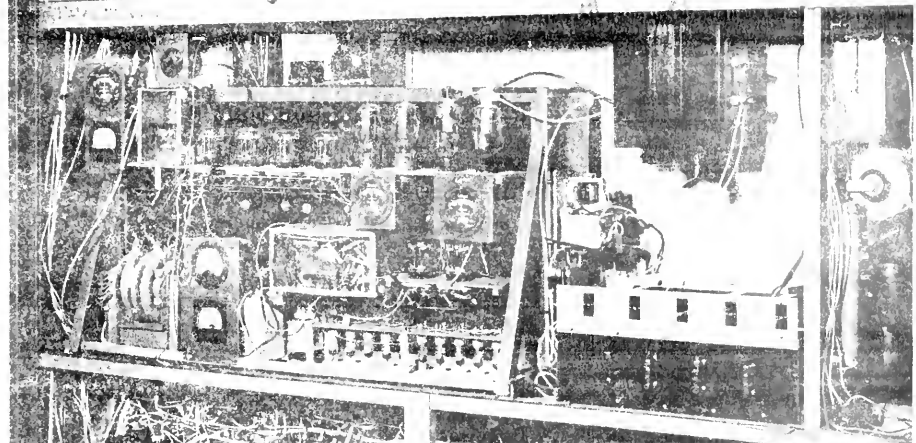
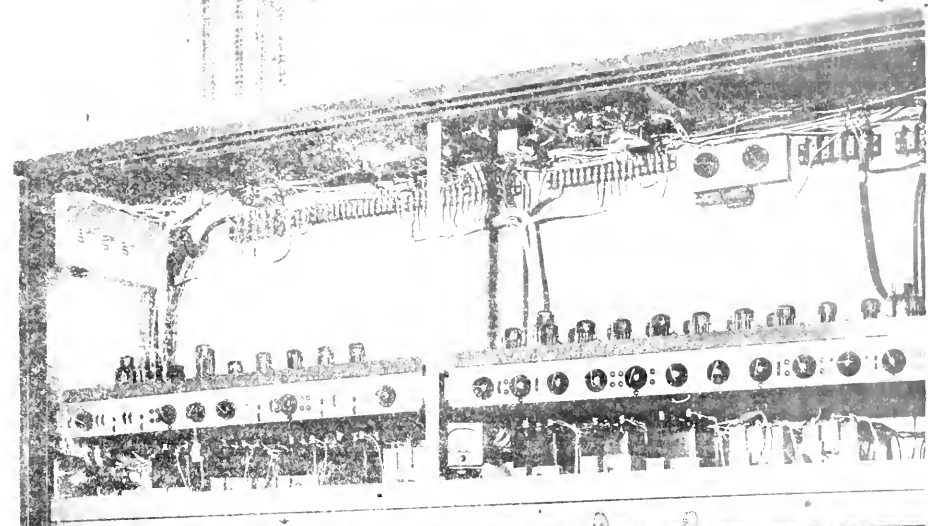
The switching of these loads during normal machine turn-on and off is controlled by the starting control (see C. 1. b.). There are four of the high current DC (PEC) supplies which carry the major DC machine load directly, but some power is also needed at intermediate voltage levels. These are provided by a bank of secondary regulators located in the power switching center. (See C. 2. b.) All power runs to the machine are in conduits under the floor or in the ceiling. As a precaution, wire screen was laid on the floor and ceiling and both interior walls to form an open sided box enclosing the machine. All conduits were bonded to this screen at the point of entry and the machine base bonded to floor screen.

The starting control, regulating transformers, secondary regulators, and the high voltage supplies for the memory are all mounted in a steel frame and constitute the power switching center. This is shown in figures (7) and (8).

Figure 7 - I-16.



POWER SWITCHING CENTER

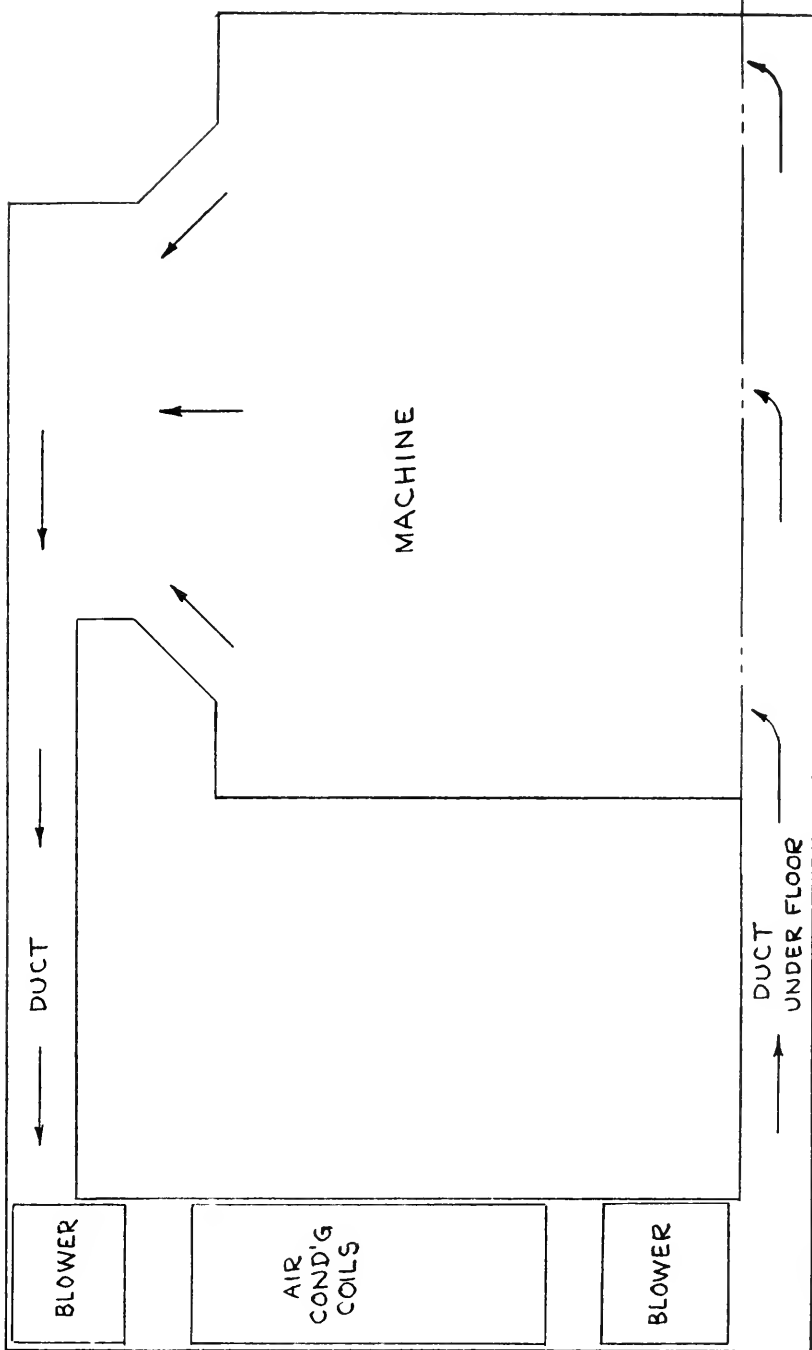


iii. Cooling.

A closed circuit air cooling system was installed in order to provide clean, low humidity cooling air to the machine. Air is blown through a floor duct into the base of the computer, rises through it and exhausts through a ceiling duct, returns through an exhaust blower air filters and cooling coils to the floor duct again. Cooling is provided by two remotely located 7 1/2 ton compressors and heat is dissipated by a Unicon refrigerant to air heat exchanger located on the building roof. The refrigerant system of each compressor is separate so that maintenance can be done on one system while the other temporarily carries the machine. Because this cooling system is intended for year-round operation, pressure regulating bypass valves were installed on the Unicon to maintain constant compressor head pressures regardless of outside air temperature.

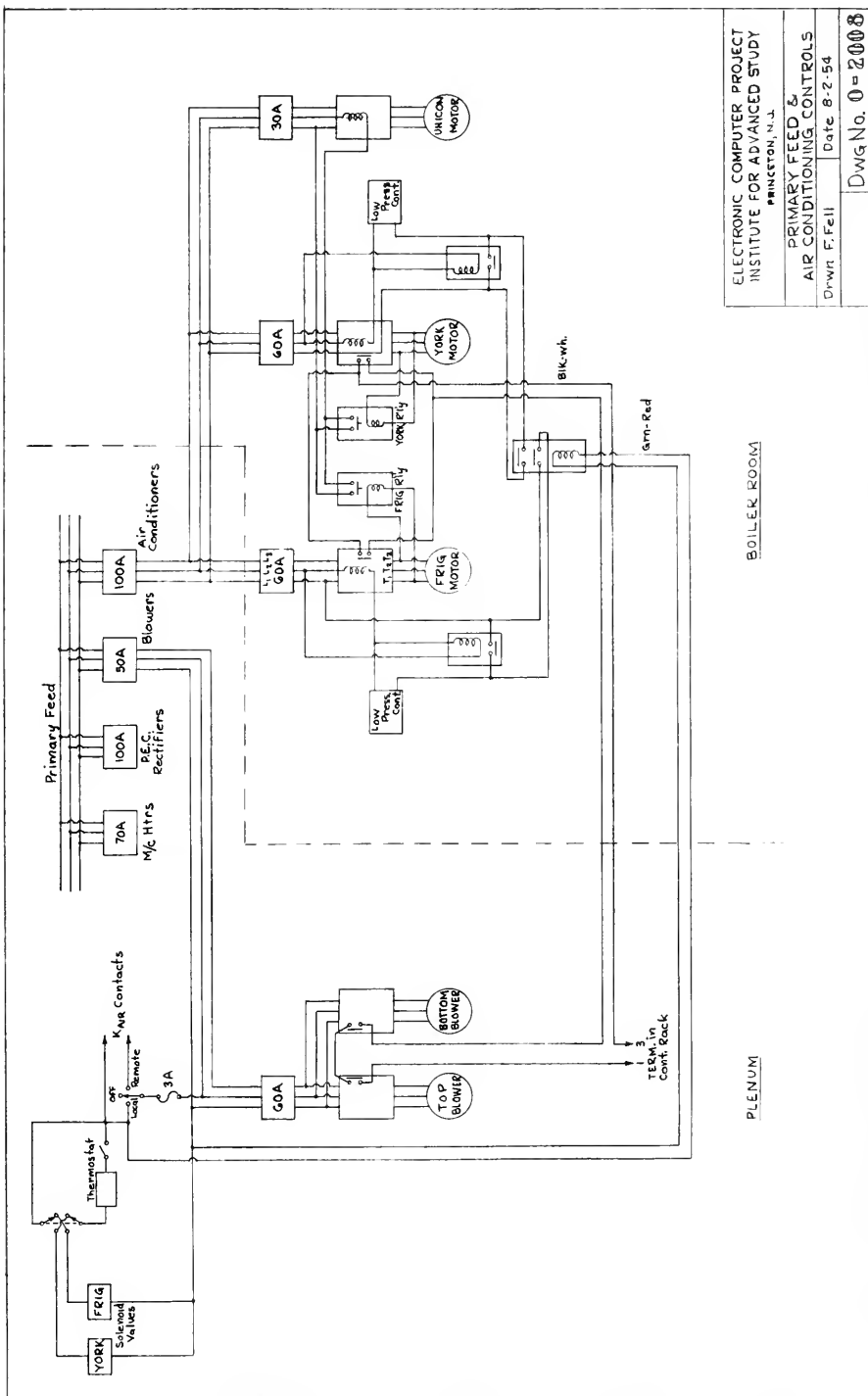
The air circulation path is shown in figure (9) and the power wiring in figure (10).

Figure 9 - I-19.



AIR FLOW DIAGRAM

Figure 10 - I-20.



2. Engineering Improvements.

A number of changes and improvements have been made on the machine to increase ease and versatility of operation and also reliability. These changes are set forth in this section as a series of articles.

a. RI digit insertion.

i. General.

A considerable operating convenience on the machine is a means for manually inserting words in the memory, as, for instance, parameter changes between one run and the next. Since storage into the memory is from RI (the accumulator register), it suffices to provide a means for modifying the contents of RI by a switch bank at the operating position.

Several methods of remote toggle switching have been devised; some of them have been used at this project. One method is to pull on the proper plate of a toggle by means of a voltage impressed on a wire to that plate. A change is enforced in the level of voltage seen at the plate, and the toggle will flip. This process is wasteful of power, requires local decoupling for optimum noise reduction, imposes a large constant capacitative load on the toggle network, and is in general inelegant. Further, it is not simple to get bidirectional control with only one wire in a plate control scheme.

If a grid could be easily swung up and down by a controlling voltage, we should be dealing with information control rather than power control, and one would simply have to apply one of two voltages on a line to obtain either toggle state at will. Obviously it is not desirable to burden a grid control point with an appreciable load. Loss of operating speed and reliability would be an inevitable consequence. It is possible

to use diode or triode elements placed close to the controlled point to act as decoupling agents for the long controlling line. This sort of solution is neither economical nor elegant.

A small neon lamp, such as the NE-2 has interesting properties which lend themselves to this decoupling problem. In the off state, a typical lamp of this type has a capacity between its leads of ≈ 0.7 uuf and a resistance on the order of several thousand megohms. After being turned on, a typical NE-2 has a resistance on the order of 65 K with one ma through it and 35 K when passing 2 ma.

Figure (11) shows a possible use of the NE-2 for toggle control. During the time that no control is being exercised, the point x on the toggle has incurred no more loading than a capacity ≤ 0.7 uuf. This is, for all practical purposes, a trivial perturbation. The bias existing on the control line at this time is chosen to be a value halfway between the ordinary extremes of toggle voltage at point x. This insures that neon firing will not occur accidentally (since x commonly has a stretch of ≈ 40 v.). Most NE-2 samples will not fire at less than 75 applied volts, so we are doubly safe.

Switching either to E_+ or E_- then pulls x, the right toggle grid to a point where stability occurs; on returning the switch to the neutral or bias position, the new toggle state remains.

For the condition of switching to E_+ , grid current will flow in the right side of the toggle due to the grounded cathode. The values of R and E_+ are chosen to limit this current to a safe value. A range of from 1.5 to 1.75 ma has been found to provide certain yet safe operation for these toggle-neon combinations.

A relatively simple extension of circuitry then allows flexible

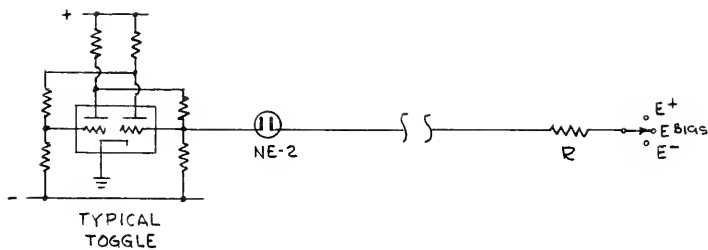


Figure 11.
Neon Toggle Control

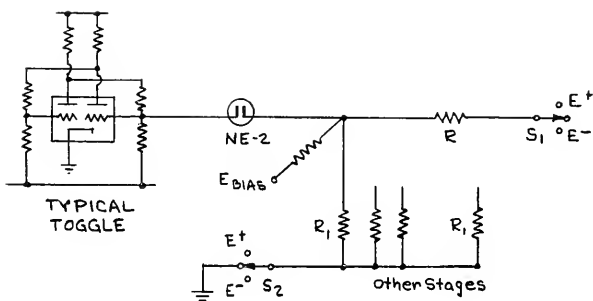


Figure 12.
Neon Toggle Control

control of a number of such stages, single or multiple switching then being possible, as seen in figure (12).

S_1 is seen to be the individual stage control while S_2 will simultaneously switch any number of stages attached to the common bus. It is desirable to apply E bias in such a way as to insure its application at all times, not depending on a set of closed switch contacts. Somewhat more provision against undesirable noise voltages appearing on the control lines is obtained this way.

Modifications of the above system are in use at this project and have been found to operate satisfactorily. A simple arrangement of common components provides remote toggle control with great economy of space, power, and cost.

ii. Detailed description.

A test of ten NE-2 miniature neon lamps selected at random from new stock was conducted to obtain conduction, firing and extinction characteristics. The results are tabulated on the following page.

Of the ten lamps tested the highest voltage required for ignition was 86 v and the lowest voltage which would insure sustained conduction before extinction was 57 v. Thus for an unselected group of NE-2's, we must insure ≥ 86 volts for firing, ≤ 57 volts for extinction, and for nominal currents through the lamp during conduction the voltage must be between ≈ 68 and 74 volts.

A graphic summary of these characteristics is seen in figure (13).

In October 1953 a switching facility incorporating these lamps was built and installed as a control for the R_1 register of the machine. A bank of 81 switches and associated resistors was provided in a control

NE-2 #	M.A. THROUGH LAMP				
	1.0	1.25	1.5	1.75	2.0
1	72.0	74.0	75.0	75.5	76.0
2	70.0	73.0	74.0	75.0	76.0
3	67.0	69.0	69.0	69.5	70.0
4	72.0	75.0	75.5	76.5	78.0
5	60.0	62.0	63.0	63.5	64.0
6	70.0	72.0	73.0	74.0	75.0
7	74.0	76.0	77.0	78.0	78.5
8	72.0	73.0	75.0	76.0	77.0
9	59.0	60.0	62.0	62.5	63.0
10	71.0	74.0	75.0	76.0	77.0
Average	68.7	70.8	71.8	72.65	73.4
Maximum	74.0	76.0	77.0	78.0	78.5
Minimum	59.0	60.0	62.0	62.5	63.0

NE-2 VOLTAGE DROPS FOR CONSTANT CURRENTS

box located at the machine operating position. There are 40 switches for putting ones and 40 for putting zeros into the register. Another switch allows the entire register to be cleared either to one or to zero. The circuit for this control unit is shown in figure (14).

A standby bias potential of 22.5 v is applied to the side of the neons remote from the controlled toggle. Thus at no time will a voltage differential of > 25 v appear across the NE-2 and accidental firing is inhibited.

The 33 K resistors in the switching lines provide sufficient current limiting to protect both toggles and neons. In the event of the

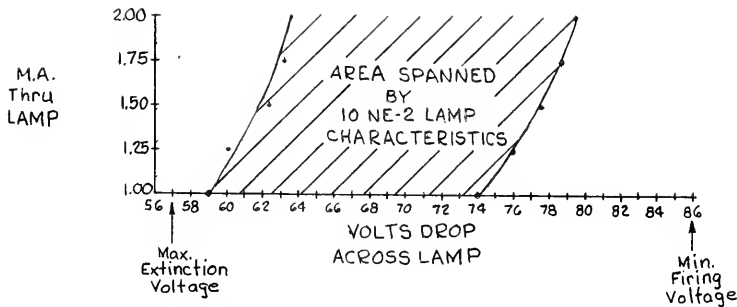


Figure 13.
NE-2 Characteristics

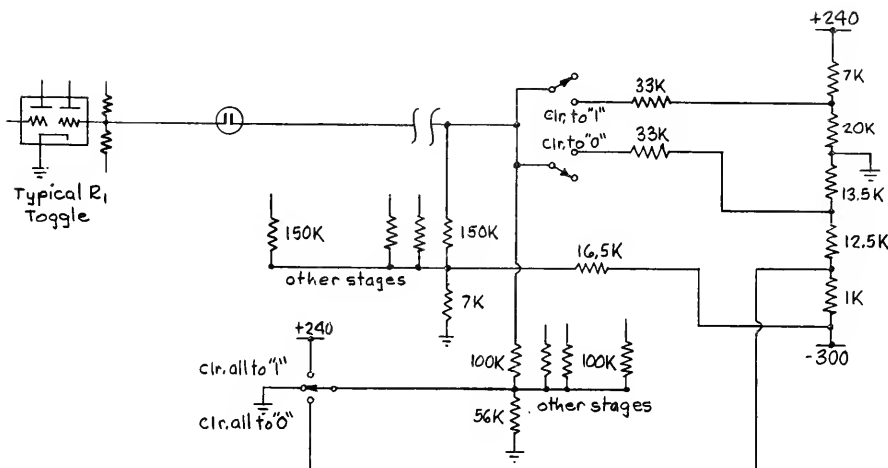


Figure 14.
Neon Control for R₁

worst combination of 10% toggle resistor drifts, less than 3 ma of grid current will flow when the toggle is cleared to the one state. The supply voltages of + 135 volts are sufficient to provide safe operation for any combination of 10% resistor drifts.

This system has been in use for over six months and has given satisfactory, reliable operation. The neon lamp used as a decoupling control device seems to be a feasible solution to a large class of computer operation problems, and will undoubtedly see more service in the present machine.

b. New secondary regulators.

The principal DC load of the machine flows from the high current + 110 volt and + 240 volt supplies and returns through either ground or the -300 volt supply. However, smaller amounts of power are needed at other voltage levels, some of them higher than + 240 so a fourth high current supply is at + 380 volts to provide a memory voltage directly and also to feed a number of secondary regulators which in turn produce the needed intermediate levels, particularly to the adder and digit resolver.

A set of such secondary regulators had been constructed along with the arithmetic unit and were continued in use through the machine move. These were essentially independent units, each with its own heater supply, switching, metering, and voltage reference, mounted in relay racks with the tubes horizontal. They were unsatisfactory for several reasons: the two stage error amplifier used was only conditionally stable; the independent construction led to excess bulk and failure hazard; and the horizontal mounting of the regulator tubes gave considerable grid-cathode short trouble. Therefore a new regulator

system was designed and constructed to meet the now definite power needs of the machine.

The new system consists of two 15" x 33" hinged horizontal chassis side by side with all tubes mounted vertically. Each chassis accommodates only tubes and resistors, with all filament transformers and filter condensers mounted on a shelf below. Fewer tubes are required in the new system because of shunts across the 6080's. These shunts supply the steady component of current. A single reference chassis is provided for all regulators (see figure (15)). The new regulators were installed in May 1954 and to date have proven to be quite trouble-free in that there has been only one failure -- a microphonic 6080. The installation was accompanied by a reduction in the number of voltage levels required for machine operation and a program for further reduction is under study.

A typical regulator is shown in figure (16). The elements include a 6AU6 pentode-amplifier and one or more 6080's as the series tube(s) dependent on load requirements. The 6080's are operated at a maximum of half of rated plate dissipation and half rated zero bias emission, delivering a maximum of about 110 ma. at 55 volts. In series with each section of every 6080 are two 10-ohm resistors, the one nearest the plate serving as a suppressor and the other providing a means of observing the current flow in that section (suitable wiring and tip-jacks allowing these voltage-drop readings to be taken remotely). By periodic observation of the proportionality between the readings for all paralleled sections we can evaluate the relative performance of the series tubes and make any replacements as required. As yet it has not been necessary to make any replacements except for the 6080 mentioned above.

The output voltage of each regulator can be varied about 10 volts

Figure 15 - I-29.

REFERENCE & SCREEN SUPPLIES for REGULATORS

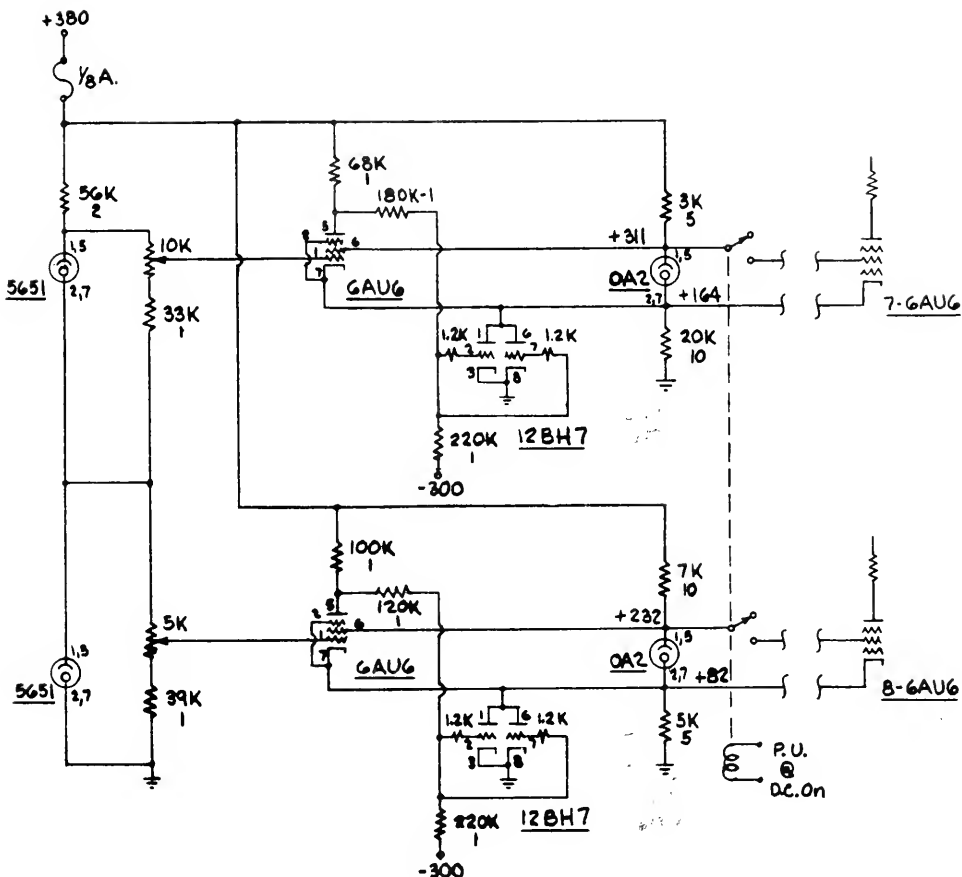
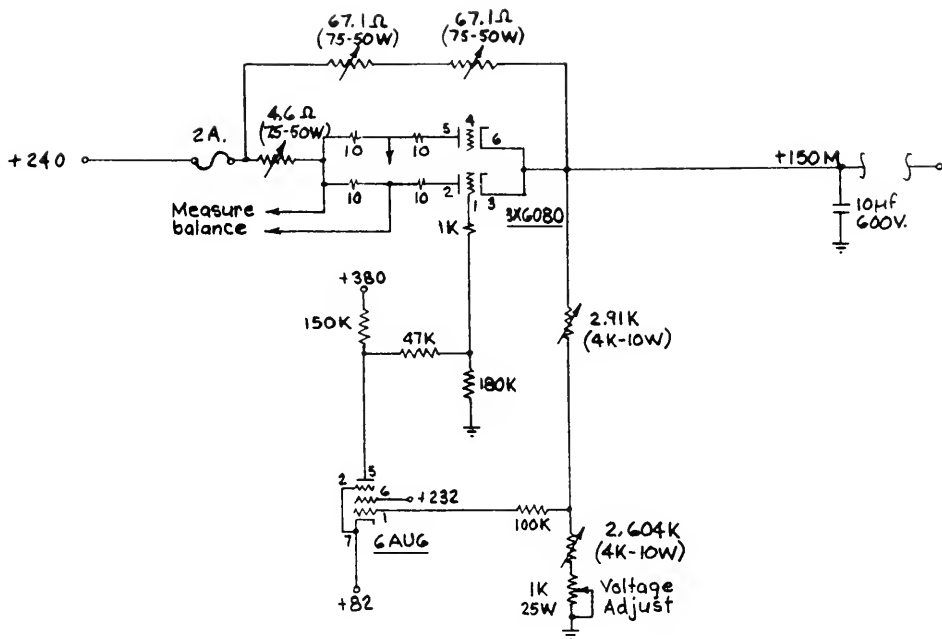


Figure 16 - I-30.



TYPICAL REGULATOR

above or below its nominal value and will regulate to within no more than one volt for all normal loads over this range. DC voltage inputs for all of the regulators and for the reference chassis are derived from commercial high-current regulated power supplys which also feed the computer directly.

The various voltage levels and protective devices associated with the machine are not automatically monitored at present but such a system is in the initial stage of development. This system will detect and record momentary or fixed variations in all DC levels and also indicate the state of the input fuses to the various regulators and power supplies. Any blown fuse will cause all DC to be removed from the machine, but for any DC-level variation which exceeds the normal there will merely be an alarm. The indications of all failures so observed will remain available in the absence of all machine voltages.

c. Present drum techniques.

The drum which has been described in previous reports is now used extensively by practically all coders. Certain engineering changes have been incorporated into its circuitry with the intention of obtaining more trouble-free operation. Among these are a reduction in the number of relays and tubes in the control and also relocation of some elements so as to facilitate preventive maintenance. The surface coating is now erased to magnetic neutral rather than to a polarized state as was previously described. A square-wave generator is used at present, the amplitude being reduced slowly by manual adjustment, but shortly there will be facility for erasing automatically simply by pushing an "ERASE" button. Most of this circuitry now exists and when operative will function as follows: A unique marker (Sync 1-2)

will trigger a one-shot multivibrator and for one complete revolution the drum will be erased "negatively" until the arrival of Sync 1-2 again at which time the multivibrator will provide for "positive" erasing. This alternation persists for about 90 seconds during which time the erasing current is continually reduced by means of an R-C time constant imposed on a 6080 tube in series with all 40 pulsers. Erasing is now done periodically (at least once a week) and it appears that this procedure reduces the occurrence of errors.

d. Graphing circuit.

The design of the graphing function for the machine was initiated early in April 1954. This function is intended to provide an auxiliary facility for maintaining a check on the progress of a computation. It is expected that considerable time and effort can be saved by having available a means for visually observing some of the variables of a solution while the computation is actually being performed. One may see continuity or discontinuity in a function, for instance, or observe the number of oscillations between two given points. It is useful also to know whether two processes being initiated from divergent points tend to approach each other and meet in a smooth fashion. A feeling for scaling quantities as well may be obtained from such a display. These various factors are obtainable without such a visual aid only by means of tedious manual collation and computation. Of further use would be the photographing of graphed displays for future analysis.

The display is designed to be observed on a 7" cathode ray tube. This tube, a 7JP1, has a medium persistence green trace and is similar to the memory and slave tubes used at present in the main machine. Facility for switching either the graphing or the slave function to this

tube is provided, so that when graphing is not desired an auxiliary, enlarged memory slave monitor is available. During such slave monitoring (when it is used in conjunction with the existing memory slave unit) it becomes possible to observe two separate memory stages at once, or to monitor two pairs of "compared" stages. The resolution of the graphing display is 9 binary digits or 512 points in both horizontal and vertical coordinates. Reasons for this choice will be given when the details of the deflection system are described. Resolution during memory slave operation is, of course, the standard raster of 32 x 32 spots.

Information input to the display is obtained from two sources. During graphing we have access to the output of the forty digits of the magnetic drum (Group "0" or "1" heads). We wish to use two groups of nine digits each, one for horizontal and one for vertical deflection. By suitable selection from this 40 digit input it is possible to obtain digits of properly selected weight and position. For slave operation, the digit input comes directly from the ten digit address of the machine's dispatch counter (center rank).

i. Deflection for graphing operation.

Forty digits are available from the output of the magnetic drum from either of the two groups of heads. Either group (zero or one) is selected at the will of the operator and the forty digits are then fed from the drum over a cable to 40 corresponding triodes in the graphing unit. These digit lines have originated from the drum head amplifiers which, with the IBM output circuitry are wired to cathodes of triodes at the main machine's input for these signals. It is necessary that each of these digit lines be isolated from the machine during ordinary computation and that they be connected for an external order. The

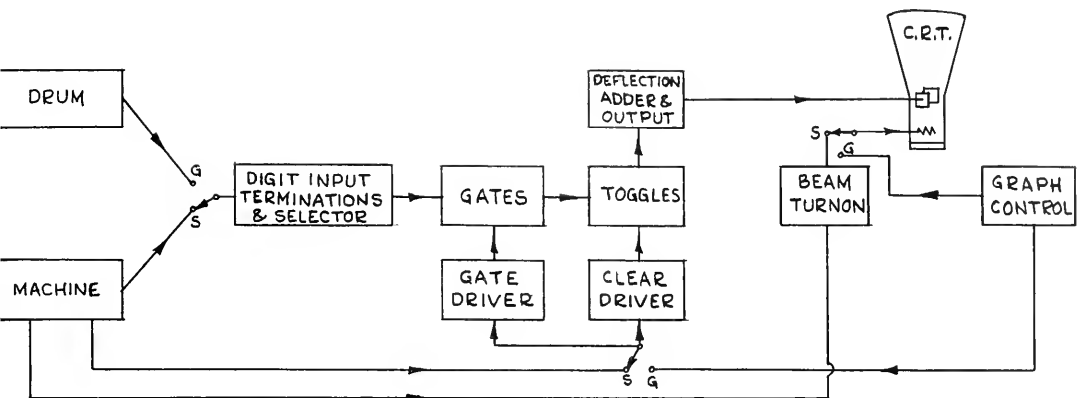


Figure 17.
Block Diagram - Graphing Unit.

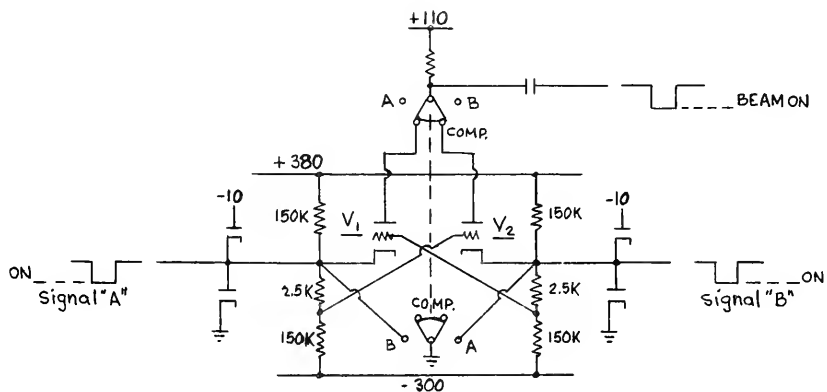


Figure 18.
Comparison Circuit.

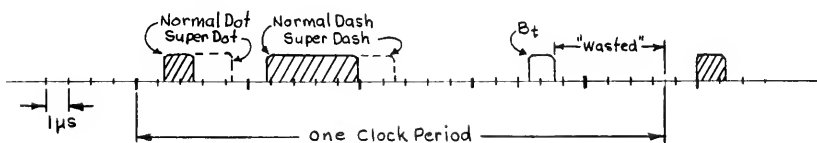


Figure 19.
Memory Beam Turnon Pulses.

requirement then is that for computing these lines be at $\geq + 5$ v. and during an external order they fall to $\geq - 25$ v. A condition which is unique at these times is the presence or absence of ING_2 , and this signal may be used to change the state of these lines. The grids of each of the 40 digit input line triodes on the graphing chassis therefore are returned to a common bus which is supplied by a driver system under the control of ING_2 . During an external order then these grids, hence their cathodes are down and the digit lines are in communication with the computer. At all other times the grids being up, pull their respective cathodes to $\approx + 5$ v. which insures the isolation of the lines from the machine yet retains the function of transfer of information from the drum amplifier outputs to graphing input.

The outputs of the digit line triodes are wired to a circular array of connector jacks. Two "combs" of plugs may then be inserted into these jacks so that two sets of nine consecutive digits each may be picked off. Thus it is possible to select the 18 digits to be used from among the 40 available in order to obtain the desired position and "weighting" of digits. An alternative patch plug arrangement is provided so that one may choose other than consecutive sequences of digits.

The selected signals (nine for horizontal deflection and nine for vertical) are then applied through relay contacts (the upper level of these signals being diode dumped at ground) into gates. At the proper moment in time this information is gated into a set of toggles which feed the deflection circuitry.

Each toggle (one for each of the 18 digits) controls the current in one or the other side of a dual triode deflection adder tube which supplies two deflection summing buses. This is essentially the scheme

used in the computer Williams memory system and is described in detail in a previous report.

There are now two pairs of summed, balanced deflection currents, one pair for horizontal and one for vertical, which are passed through the deflection driver tubes. Voltages developed across the plate resistors of these tubes are then directly applied to the deflection plates of the cathode ray tube.

The choice of a 512 x 512 array was arrived at from the following considerations. The usable projection area of a 7" cathode ray tube is roughly that defined by a 6 inch diagonal or a square with 4 1/4 inch sides. One thousand and twenty-four spots along a 4 1/4 inch line would have a spacing of \approx 4 mils while 512 spots would be spaced \approx 8 mils apart. Considering the currents necessary in the adder tubes, let us assume that 25 m.a. is a reasonable maximum current for the largest deflection digit. Then for 1024 spots obtained from 10 binary digits, the smallest deflection current would be $\frac{25 \text{ m.a.}}{2^{n-1}}$ (where n = 10) or approximately 50 u.a. For 512 spots, the minimum digits current is 100 u.a. The amount of noise and uncertainty which would be found in any practical circuit is not inconsiderable compared to 50 u.a., and requiring a miniature tube to pass as much as 50 m.a. is not a simple task. Since the eye cannot easily resolve 500 lines or dots in a 4 or 5 inch length when viewed a foot or two distant, it is considered reasonable to design for a nine digit or 512 spot resolution. For all practical purposes a function plotted with this resolution will appear as a continuous line, and with care a circuit can be made to function reliably with adder currents ranging between 25 m.a. and 100 u.a.

ii. Deflection for slave operation.

The five digits each for horizontal and vertical deflection are brought over to the graphing unit from the machine's dispatch counter. After passing through amplifier tubes the digits are applied through relay contacts to the most significant digit lines entering the set of deflection toggles. Thus with the relays R_1 and R_2 in the slave position, the normal machine raster deflection is produced by the adder in the same manner that the graphing raster, just described, is produced. A 32×32 spot pattern is then seen on the cathode ray tube.

iii. Beam turnon.

Beam turnon control for the graphing operation is derived from the graphing control circuit and will be described below in the section dealing with the control.

For slave operation the beam turnon signals are generated by a circuit comprising a selector, comparator, and a stretching circuit. The 40 signals are brought over cables from the machine's beam turnon circuits to two 40 position selector switches on the graphing chassis. The signals thus selected (A and B) are amplified and bumped between ground and - 10. Ground level represents beam turnon. Each signal is then introduced into the channel comparator-selector circuit shown in figure (18).

If the selector switch is in the "A" position, the plate of V_1 is connected to the output line. V_2 is cut off at this time by the transpose network. The grid of V_1 is pegged at ≈ -5 v. Its cathode being bumped at ground by the diode on the signal line, cannot rise above 0 v. V_1 is then essentially cut off until a beam turnon signal of - 10 comes along. At this time V_1 will conduct and the pulse will be seen as a down-

going signal on the output line. Similarly channel "B" will conduct turnon signals with the selector switch in the "B" position.

For comparison the outputs of V_1 and V_2 are connected together and their plates observed. Each grid will be at ≈ -5 v. when each cathode normally rests at ground, thus both tubes are cut off. If similar signals are applied to each input, both grids and cathodes will dip similarly and no output signal will be developed. However, if dissimilar signals are present, an output signal, showing that a difference exists, is developed. Suppose signal "A" is present and "B" is absent. The grid of V_1 is at -5 v. while the cathode of V_1 goes to -10 . V_1 conducts and a signal appears on its plate. The cathode of V_2 remains pegged at ground but its grid drops to -15 v. and thus V_2 is cut off.

The beam turnon signals appearing on the output line are then ready for transmission to the cathode ray tube. For slave operation the relatively short times during which the beam turnon signals exist (1.2 us . for normal dot and 4.1 us. for normal dash) are insufficient to guarantee maximum slave brightness. If these turnon pulses could be lengthened, the slave intensity would correspondingly improve.

A "boot-strap" circuit is used to stretch the beam turnon pulse. The present, normal signals are shown in figure (19).

The turnon pulses can be lengthened by a factor of ≈ 3 to 1 for slave without exceeding the clock period limitations.

The circuit used to lengthen the signals is shown in figure (20).

During beam off time E_{in} is at $+10$ and E_c is bumped at $+110$, its lower level by grid current in V_2 . The output at the plate of V_2 at this time is "down" or the beam turnon signal is in the off condition.

When E_{in} goes negative the left half of V_1 is cut off and E_c

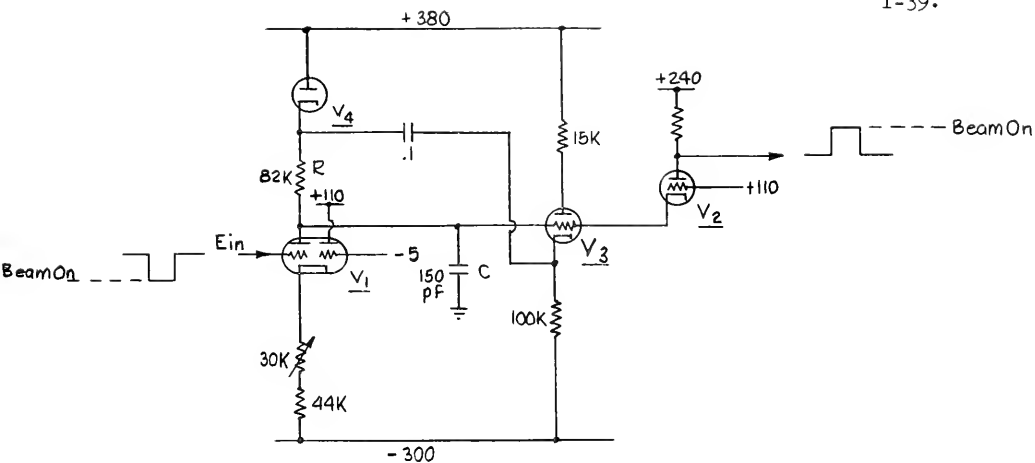


Figure 20.
Proportional Pulse Stretcher

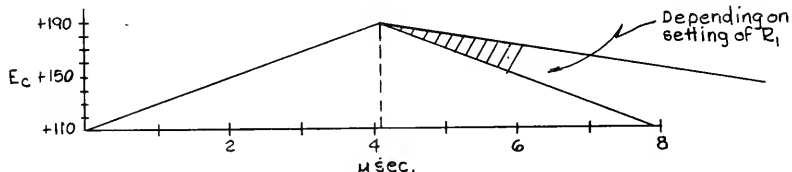
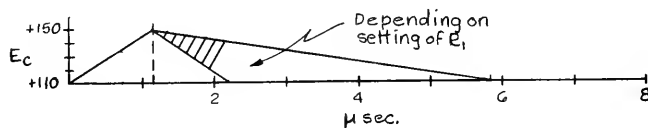
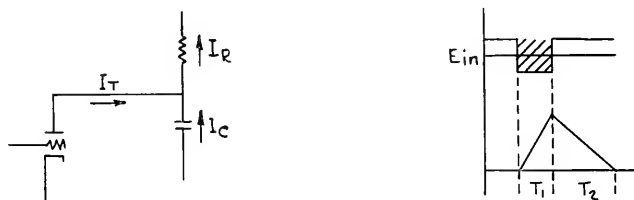


Figure 21.
Operation of Stretcher Circuit

rises from its lower level of +110 at a rate determined by the current through R which is charging C. This current $I_R = (380 - 110)/82 \text{ K} = 3.3 \text{ ma.}$ which will charge a 150 p f. capacitor at the rate of 22 v./usec.

When E in. goes positive, the "constant" cathode current of the switching tube V_1 is impressed on capacitor C to bring Ec back down to its standby condition of + 110v. Depending on the setting of potentiometer R_1 this cathode current will be:

$$\begin{aligned} & 7 \text{ ma if } R_1 = 0 \\ & 4.2 \text{ ma if } R_1 = 30 \text{ K.} \end{aligned}$$

When Ec moves more than a few volts above + 110, V_2 cuts off and its plate signals the CRO grid to turn the beam on. The beam will remain on until Ec returns close enough to + 110 to cause V_2 to conduct again. For our purposes here we may assume that V_2 cuts off as soon as Ec begins its rise.

The actual stretching may be considered as follows (see figure (21)):

$$\text{During time } T_1 : I_c = I_{c1} = I_R \quad (I_T = 0)$$

$$\text{During time } T_2 : I_c = I_{c2} = I_T - I_R \quad (\text{note that})$$

$$\frac{I_T}{I_R} > \frac{I_T}{I_R} \quad)$$

$$\text{Stretching ratio} = \frac{T_1 + T_2}{T_1} = \frac{T_1/T_2 + 1}{T_1/T_2}$$

$$\text{but } T_1/T_2 = I_{c2}/I_{c1} = \frac{I_T - I_R}{I_R}$$

$$\text{or} \quad = \frac{I_T}{I_T - I_R}$$

$$\text{the range of} \quad = \frac{4.2}{4.2 - 3.3} = 4.7 \text{ to } \frac{7}{7 - 3.3} = 1.9$$

iv. Control.

The graphing operation is very similar to the normal magnetic drum operation in that blocks of 32 words each are selected for use by a ten digit "priming order". The first five digits of this order specify the number of the starting block while the second five digits (the right half of the order) specify the number of blocks to be read out. During normal drum operation this priming order is derived from the computer while for graphing the ten priming digits are set up by a bank of switches on the graphing control panel. As long as a graphing cycle is in progress (the machine not executing an external order), the graphing priming order takes precedence over the normal priming number in the drum register.

For graphing the priming order which has been set up on the control panel is waiting to be transferred to and recognized by the drum's coincidence circuit input selector. The ten digits of the order are applied to the coincidence circuit input through NE-2 neon lamps acting as isolating switches. The use of these neons as linkage devices has been described in another section of this report. Sufficient compliance is inserted between the toggles of the priming register and the coincidence gates to insure that the remote insertion of priming digits does not affect the state of the priming toggles. This provision allows the last regularly stored priming number to remain intact for use or reference at any time.

A typical stage is shown in figure (22). If the digit being inserted into the right half of the gate, as shown is one of the first five digits of the priming number, then the left half of the gate will be assigned to a digit in the second half of the priming number. If the second half digit is being switched to the negative switching potential, the left half of the gate will not be affected during the period of no

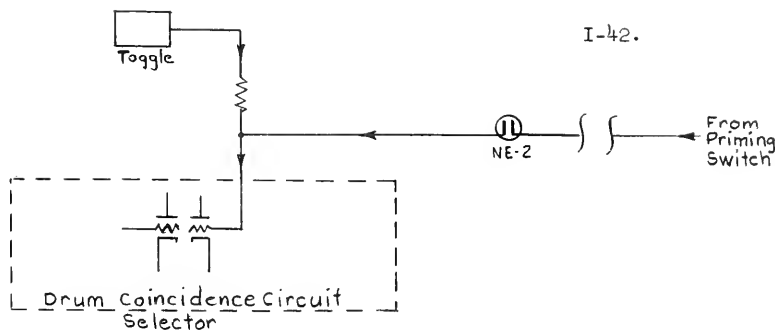


Figure 22.
Graph Priming Circuit

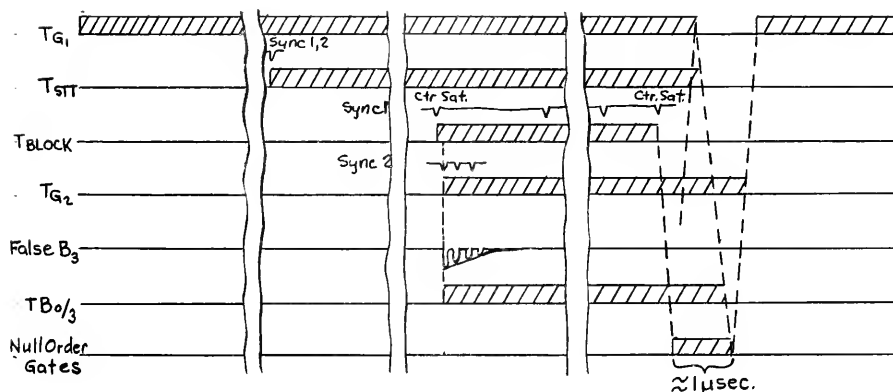


Figure 23.
Graph Timing Diagram

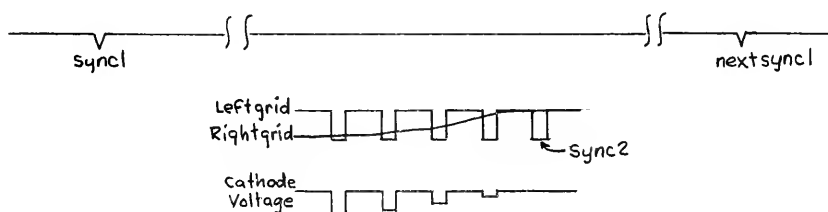
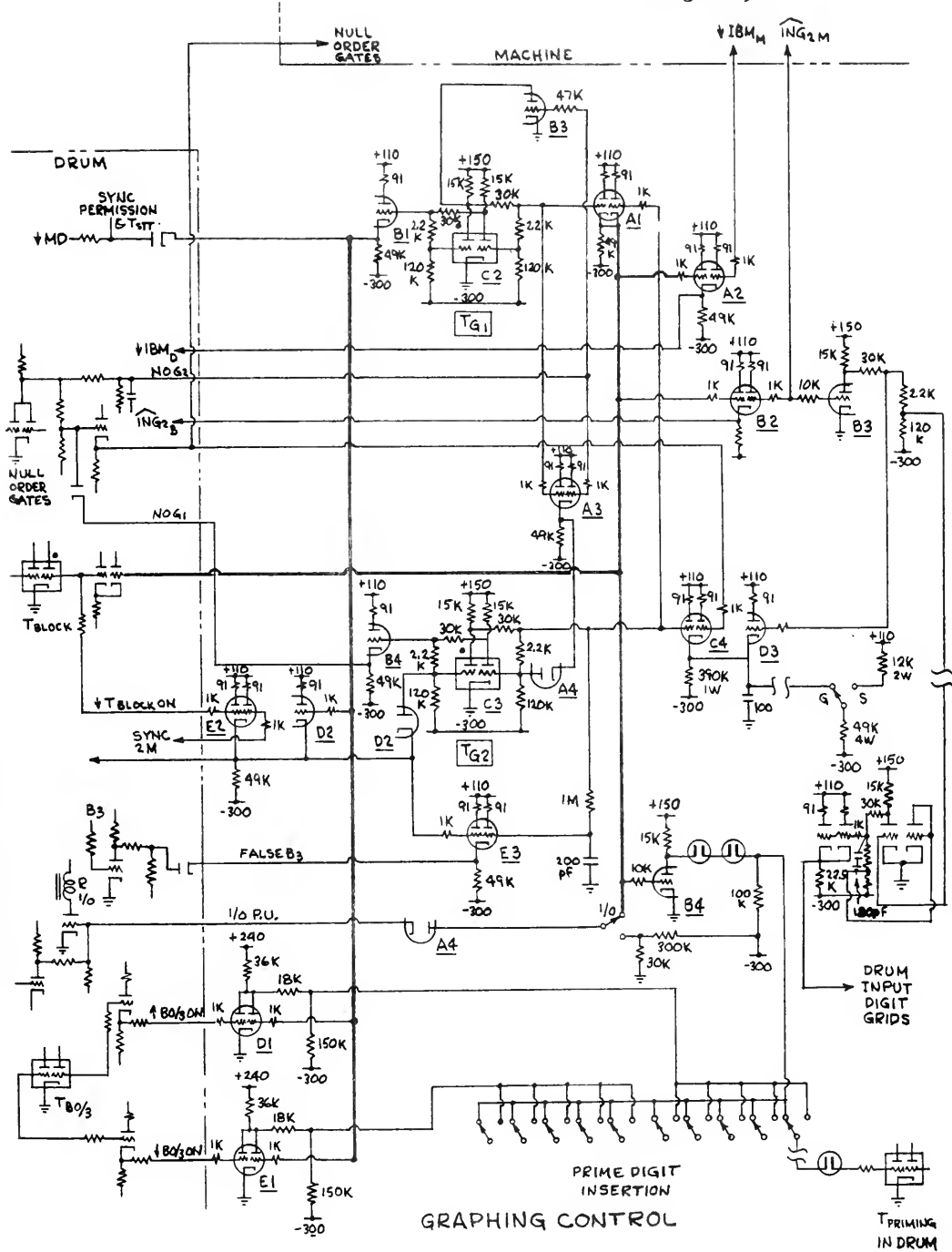


Figure 24.
False B_3 Signal

gating; however, should the digit be switched to the positive potential, the absolute voltage appearing at the left gate grid will not have a guaranteed value (due to variations from one NE-2 to another) and it is conceivable that gating may inadvertently occur prior to the desired gating time. Thus it is necessary to delay the application of the positive potential at the graphing priming switches until the time for the use of that particular group arrives. This is done by utilizing the $T_{BO/3}$ toggle of the drum to apply either of the two positive switching voltages by means of V_{21} and V_{22} shown in the accompanying control circuit schematic, figure (25).

To begin the graphing cycle, let us assume that T_{GL} has just been turned on. It is seen that the two main control lines, line 1 and line 2 are pulled up and down respectively by means of triodes V_6 and V_4 . Consider the functions controlled by line 2: diode V_2 will pull down on the sync permission line, enabling the magnetic drum sync signals to be activated. Diode V_3 pulling down on the T_{STT} control line, conditions the T_{STT} toggle (in the magnetic drum turn on circuits) so that the very next main timing pulse (sync 1, 2) turns on T_{STT} initiating a graphing cycle. The seven digit counter in the drum counts sync 1 pulses and when this count equals the "starting block number" of the priming register a counter satisfy signal turns on the T_{BLOCK} toggle. Meanwhile (via line 1) the normal consequences of T_{BLOCK} being ON in the drum control are inhibited. It should be noted that the coincidence circuit has been referring to the left half of the priming register for this operation since both grids of V_{21} are cut off -- i.e. line 2 of the control is negative and $T_{BO/3}$ is in the OFF state. This supplies a positive neon switching voltage. For any digits requiring a negative neon switching voltage the following

Figure 25 - I-44.



occurs: V_{23} is conducting during this time since line 1 is up, and the current drawn through the two neons in series with the plate load resistor and the 100 K. to - 300 v. develops a neon switching supply voltage of \approx - 100 v. on line C.

Since line 1 is in the up state the cathode of V_7 is held up and ING_{2D} is inhibited; the cathode of V_1 being up for the same reason inhibits IBM_D , and thus normal drum activity is prevented for the duration of the graphing cycle. The choice of selecting drum heads 1 or 0 is made by the switch at the plate of the V_{20} diode. a + or - voltage on this line will set the $R_{1/0}$ control to the desired condition. This switch is prevented from being active during other than graphing times because the positive controlling voltage for the 1/0 line is derived from the #1. main control line, up only for graphing. Since no negative voltage on the plate of the V_{20} diode can affect the 1/0 line, we are assured that the 1/0 function is under normal operating control during computing.

A timing flow diagram is given in figure (23) to facilitate following the remainder of the discussion of the logical process of the control.

With T_{BLOCK} on the left grid of V_{18} is negative. Further, the grid of V_{17} (common cathode with V_{18}) is down due to control line 1 being down. Therefore the first sync 2 pulse will allow the common cathode level to go negative. This is used to turn T_{G2} on (via diode V_{15}) and to create a false B_3 signal, (since the normal one created in the machine is not now available) which is necessary to turn $T_{B0/3}$ on in the drum.

The false B_3 signal is created in the following manner. The left grid of V_{19} is down for the length of time of the sync 2 signals. The right grid has been down while T_{G2} was off, but now will rise at a rate due to the charging of the RC connected to it. During this rise time

several "False B_3 " signals will have time to be initiated. This is shown graphically in figure (24). Note that more than one False B_3 signal is not harmful if they occur in a short enough interval.

Now that T_{BLOCK} is ON (which implies that the counter has already done its first job of recognizing the starting block number) the counter circuitry is free to be cleared in order to start its second job of counting the number of blocks to be handled. The coincidence circuit input must be looking at the right half of the priming register in the drum for this second count. The False B_3 signal is used to clear the counter and also to turn on $T_{BO/3}$ which in turn controls which half of the priming register is inspected.

During the time that T_{BLOCK} is ON the actual graph is being drawn on the cathode ray tube. This condition will continue until the second coincidence signal is obtained indicating that the proper number of blocks of information has been handled. On the receipt of this second counter satisfy signal T_{BLOCK} is turned off. The processes necessary for concluding the graphing cycle and preparing for the next cycle are now initiated.

When T_{G2} was turned on, the cathode of V_{16} sent a down-going signal to the drum's null order gate output line, inhibiting any null order gate signal from being transmitted to the main machine. With T_{BLOCK} OFF (at second counter satisfy time) in coincidence with $T_{BO/3}$ being ON a positive null order gate signal is obtained from the drum circuitry. This causes V_8 to conduct and turn off T_{G1} . The T_{STT} control tube in the drum is then released (via V_3) so that T_{STT} is turned OFF. With T_{STT} OFF, $T_{BO/3}$ is turned off and as a consequence the null order gate request signal is turned off. At this time T_{G2} is turned off via tubes V_9 and V_{13} . Note that it was necessary that T_{G2} remain on until the previous null

order gate signal sequence had finished. That is, the NOG inhibition is used to cover the entire turning off period. This completes the graphing cycle and all elements of the control have been restored to normal or standby condition.

Before starting the next cycle certain conditions must be met. These are incorporated in tubes V_{11} and V_{12} . If an ING_2 signal has been waiting, then T_{G1} is prevented from coming back on to start a new graphing cycle. In this case, ING_2 will initiate the appropriate external order. Note that if an ING_2 request comes during a graphing cycle, the computer will wait until that cycle is completed before the order is executed.

A new graphing cycle may not begin until the completion of the external order (i.e. end of the null order gate signal). At this time the common cathodes of V_{11} and V_{12} will become negative turning T_{G1} on via V_{24} , initiating a new graphing cycle. Note then that graphing operates continually except for interruptions by external machine orders, that is drum or IBM operations.

The remaining functions of the graphing control are to provide proper signals for the deflection and the beam turnon routine. The line marked "Graph Routine", connected to the cathodes of V_{17} and V_{18} , is used for this purpose. It was seen that this line will be down for the simultaneous conditions of:

1. Graphing cycle in progress (T_{G1} on),
2. T_{BLOCK} ON (information being read out of the drum), and
3. Sync 2 pulses being transmitted (timing pulses for each word of information).

Thus a beam turnon signal is available for turning on the cathode ray

tube during each desired word readout.

The Graph Routine line is also used to provide the clear and gate signal for the deflection input circuitry. This signal (during graphing replacing the computer clear signal used during slave operation) acts as a trigger for the clear driver of the graphing deflection circuit. Since each clear and gate action inserts new digit information into the deflection adder, then the total result is that at the time of each word read out for graphing the transfer of that word into the graphing deflection circuit is accomplished. Beam turnon at that time then displays the information in that word as a point at the desired location on the screen of the cathode ray tube. Subsequent words then extend this point to a line or lines, and graphing is accomplished.

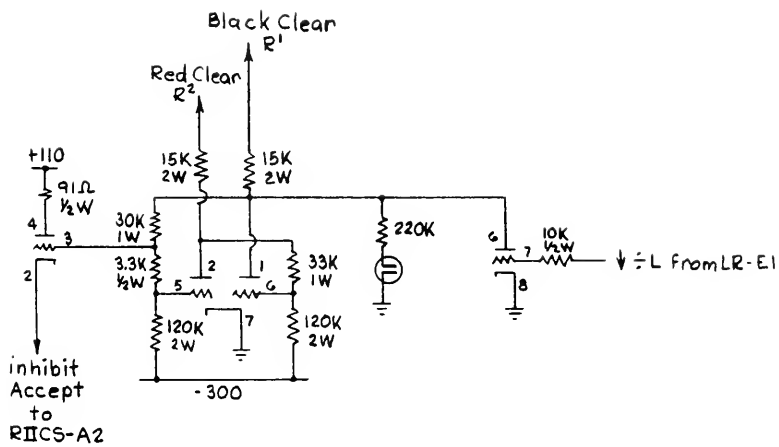
e. Division spill check.

Proper machine numbers must lie in the range $-1 \leq x < 1$ and the division circuitry will give a grossly wrong answer if a proposed quotient $q = x/y$ lies outside this range. A check circuit was added to stop the machine if an improper division is attempted.

The division process used consists of 39 similar steps determining a sign and 38 quotient digits. It is a restoring method in which the adder output is examined for overdraft before it replaces the old remainder. In case of overdraft, the adder output is not used and the old remainder is doubled. The first step of a proper division should always present an overdraft, and this fact is used for the spill check. (See figure (26)).

As the division order is entered, the initial memory sequence which brings the denominator into R^3 sets the division spill toggle to "1" via Red Clear R^2 . Note that this happens for all memory orders

Figure 26 - I-49.



DIVISION SPILL

but that the right hand gate tube will immediately unset the toggle unless a division order is present. The "1" state of this toggle is used to inhibit the "accept" (i.e. adder path) clear and will stop the machine if such a clear is requested. In a proper division, however, the first step is a "reject" (due to the overdraft) and the "reject" clear - Black Clear R^1 - resets the toggle.

At the time of a division spill stop, the original numerator is still in R_1 and the denominator in R^3 so that the operator can judge which is out of scale. The spill inhibition is removed by turning off the order gates (the standby state of the control box).

f. Zero shift order.

In the initial design of the machine it was assumed that if a shift order was entered at least one shift would be done and so the check for shift count satisfaction was placed at the end of the shift cycle. For a number of reasons a zero shift was requested by the users but primarily for routines in which the shift argument is varied by the code.

The zero shift was accomplished by moving the sensing for count satisfaction to the beginning of the shift cycle for all except input-output orders. When executed, a zero shift order leaves the contents of both R_1 and R_2 undisturbed.

g. Memory high voltage change.

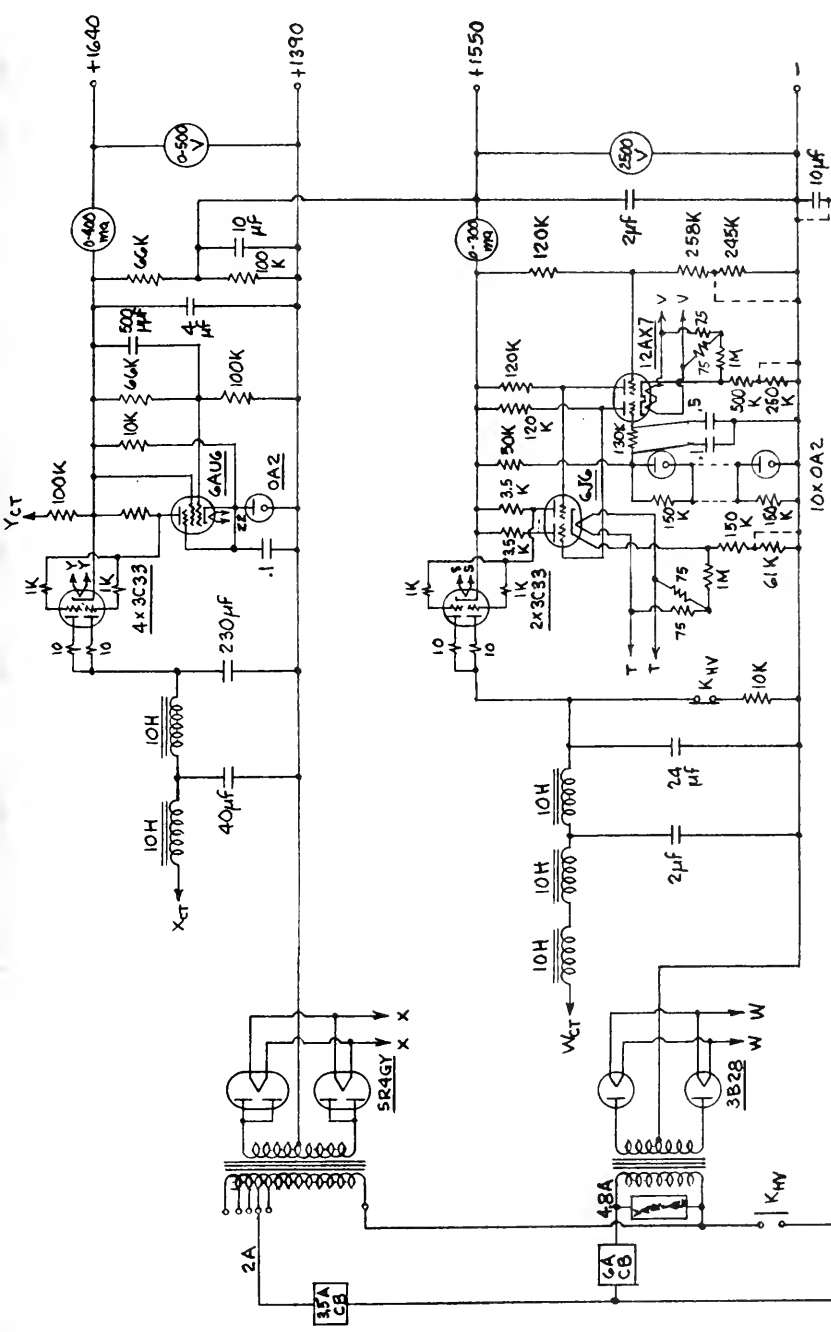
The IAS memory was designed for an accelerating voltage of 1000 volts on both second and third anodes, this being originally a compromise between spot definition (which improves with increasing voltage) and storage flaws (which become worse). As experience was accumulated, both in the machine and in the CRT test rack, it

became evident that the compromise voltage should have been set higher: flaws have not been a problem but read-around has. This is true partly because flaws can be completely evaluated in the test rack whereas read-around cannot; and partly because a flaw-free tube stays so throughout its life while read-around slowly deteriorates.

Unfortunately both grid and deflection plate circuits are direct coupled in the memory and any significant change in cathode to second anode voltage involved a circuit change rather than merely a power supply change. However, preparations were made during the machine move (see C.I., a., i.) for a higher voltage, and all incoming cathode ray tubes were flaw tested at 2000 volts E_b rather than 1000 volts.

In addition since the old high voltage supply was not capable of delivering a higher voltage, a new supply was designed and built (see figure (27)). It does not differ in any important respect from the old one except for the higher voltage, a more easily serviced layout, and an ungrounded negative return. Of some interest may be the use of the gas filled 3B24 rectifiers. These have proved much more reliable than the 8016's previously used and no trouble is caused by the ionization transients of the gas.

Figure 27 - I-49.



ELECTRONIC COMPUTER PROJECT
INSTITUTE FOR ADVANCED STUDY

PRINCETON, N. J.

REGULATED HIGH VOLTAGE SUPPLY
E2P WILLIAMS MEMORY

DRAWN F. FELL DATE 7-29-54 DWG NO. A-2007

REGULATED VOLTAGES

<u>Nominal</u>	<u>Adjustment Range</u>	<u>Set At</u>	<u>M/C Min. ma.</u>	<u>M/C Max. ma.</u>	<u>Normal No-Load Volt</u>	<u>Ref. Volts</u>
+ 86	80- 95	86.0	- 170	10	+100	+ 82
+100	96-108	100.0	0	10	+138	+ 82
+120	111-131	125.0	0	10	+155	+ 82
+136	124-148	136.2	- 200	50	+152	+ 82
+150 D	140-161	151.0	810	1160	+240	+ 82
+150 G	143-164	150.0	150	510	+205	+ 82
+150 M	140-160	152.0	870	1120	+226	+ 82
+161	153-168	163.0	- 35	275	+230	+ 82
+186	174-205	194.1	- 6	20	+239	+ 82
+211	203-216	210.8	0	150	+250	+164
+220	215-228	223.0	510	610	+345	+164
+300 A	293-313	303.5	45	435	+376	+164
+300 D	292-316	303.0	37	45	+362	+164
+300 V	290-312	293.5	1400	1980	+369	+164
+336	330-344	334.0	700	1150	+380	+164
-174	167-177	170.0	595	650	-238	(-300)

REFERENCE AND SCREEN VOLTAGES

<u>Nominal</u>	<u>Load and No-Load Volts</u>	<u>"No-Load" MA</u>	<u>"Loaded" MA</u>	<u>Designed Min. Ma.</u>	<u>Designed Max. Ma.</u>
+ 82	81.9	2	19.0	10	28
+164	164.2	3	10.0	6	15
+232	229.0	0	5.5	3	11
+314	312.0	0	3.5	2	6

Regulated Supplies (16 in all)

27 - 6080
 2 - 6336 (in "300 v")
 16 - 6AU6

Ref. & Screen Volts Chassis

2 - 6AU6
 2 - 12BH7
 2 - OA2
 2 - 5651

Total Internal Watts

Filaments 560
 D.C.Diss. 1100

Figure 28.

Table of Regulated Power Supplies.

3. Machine operation.

a. During the year covered by this report, the machine was operated on a fully scheduled basis except for the four month period in which it was moved. During the eight active months, the machine was run for a total of 3264 hours; of which 10% was spent in routine maintenance, 17% in engineering improvements, 9% in unscheduled maintenance, and 64% in productive operation.

The overall machine efficiency for the year could be expressed as the productive operation time divided by total "on" time with engineering excluded. As a percentage, this "economic" efficiency was 77%. In judging the state of engineering control of the machine, it was perhaps more meaningful to exclude also the routine maintenance time as well as engineering improvement time from the denominator. If this is done, we obtain an "engineering" efficiency of 87% for the year.

b. Weekly time records for the year are given in Table I. For completeness the time records for the previous year are given in Table II. Results for the two years are summarized in Table III, by quarters, the last quarter of 1952 being the first for which these records were kept. With respect to all tables, the time breakdowns are defined as follows:

Routine: All time spent performing a standard set of tests preliminary to each day's operation.

Engineering: All time spent in engineering improvements or additions to the machine.

Unscheduled Maintenance: All time spent in diagnosing and repairing conditions which have interrupted computation or which threaten

to cause errors. Also included is bad operating time which is clearly due to machine trouble.

Operation: All machine "on" time not accounted for by the above.

Table I.

I-56.

BASIC RECORDSDERIVED

Week Of	Routine	Engineering	Unscheduled Maintenance	Operation	Total	(UnM + Op) Available	(Op / Av) % Operation
29 June	7.2	9.3	11.3	125.2	153.0	136.5	92
6 July	12.9	3.5	19.8	99.8	136.0	119.6	83
13 July	13.3	8.6	8.5	103.8	134.2	112.3	92
20 July	8.7	3.4	11.7	124.2	148.0	135.9	91
27 July	8.0	0	3.0	57.2	68.2	60.2	95
3rd Quarter	50.1	24.8	54.3	510.2	639.4	564.5	91

Machine off for moving 1 August 1953 to 10 November 1953.

10 Nov.	0	32.0	0	0	32.0	0	- *
16 Nov.	0	38.7	0	17.1	55.8	17.1	- *
23 Nov.	0	64.0	0	0	64.0	0	- *
30 Nov.	0	67.1	0	12.9	80.0	12.9	- *
7 Dec.	14.9	13.2	7.0	43.6	78.7	50.6	86
14 Dec.	11.9	15.5	6.8	45.8	80.0	52.6	87
21 Dec.	8.4	2.0	2.7	27.8	40.9	30.5	91

4th Quarter	35.2	232.5	16.5	147.2	431.4	163.7	90
-------------	------	-------	------	-------	-------	-------	----

4 Jan.	9.7	9.1	23.3	40.5	82.6	63.8	63
11 Jan.	14.3	1.0	13.0	47.5	75.8	60.5	78
18 Jan.	10.1	2.6	14.2	63.1	90.0	77.3	81
24 Jan.	8.9	16.6	0	65.6	91.1	65.6	100
1 Feb.	7.0	31.7	4.9	40.8	84.4	45.7	89
8 Feb.	9.7	8.7	2.3	63.9	84.6	66.2	96
15 Feb.	11.4	19.1	3.7	43.8	78.0	47.5	92
22 Feb.	6.2	8.3	2.6	59.9	77.0	62.5	96
1 Mar.	13.3	13.2	2.0	52.6	81.1	54.6	96
8 Mar.	11.2	12.7	11.1	54.7	89.7	65.8	83
15 Mar.	7.3	8.0	5.3	68.2	88.8	73.5	93
22 Mar.	6.5	7.3	3.3	65.8	82.9	69.1	95

1st Quarter	115.6	138.3	85.7	666.4	1006.0	752.1	88
-------------	-------	-------	------	-------	--------	-------	----

29 Mar.	6.4	0	27.3	69.2	102.9	96.5	72
5 Apr.	10.1	5.7	7.4	57.7	80.9	65.1	88
12 Apr.	11.5	8.8	4.7	46.1	71.1	50.8	91
19 Apr.	10.4	17.7	20.0	38.3	86.4	58.3	66
26 Apr.	10.5	11.7	22.3	47.2	91.7	69.5	68
3 May	8.8	11.3	0.7	69.5	90.3	70.2	99
10 May	9.7	27.0	12.3	50.3	99.3	62.6	80
17 May	8.9	17.0	3.1	62.8	91.8	65.9	95
24 May	9.9	16.2	7.1	55.0	88.2	62.1	88
31 May	11.1	0.5	10.2	55.2	77.0	65.4	84
7 June	5.5	32.8	16.2	57.4	111.9	73.6	78
14 June	14.7	4.5	10.1	73.2	102.5	83.3	88
21 June	7.1	3.2	9.7	72.8	92.8	82.5	88

2nd Quarter	124.6	156.4	151.1	754.7	1186.8	905.8	83
-------------	-------	-------	-------	-------	--------	-------	----

djustment period after move.

Table III.

Week Ending	<u>BASIC RECORDS</u>			<u>DERIVED</u>			
	Routine	Engineering	Unscheduled Maintenance	Operation	Total	(UnM + Op) Available	(Op / Av) % Operation
31 Oct.	14.5	32.5	6.0	26.0	79.0	32.0	81
7 Nov.	11.0	22.5	6.0	41.0	80.5	47.0	87
14 Nov.	10.5	17.0	37.5	14.5	79.5	52.0	28
21 Nov.	9.5	24.0	27.5	18.0	79.0	45.5	40
28 Nov.	9.5	11.5	10.0	33.0	64.0	43.0	77
5 Dec.	10.5	8.5	9.5	51.5	80.0	61.0	84
12 Dec.	10.0	19.0	9.0	42.0	80.0	51.0	82
19 Dec.	11.0	27.5	5.5	36.0	80.0	41.5	87
26 Dec.	6.5	5.5	1.5	23.0	36.5	24.5	94
2 Jan.	-	-	- (Holiday)	-	-	-	-
Total	93.0	168.0	112.5	285.0	658.5	397.5	73
9 Jan.	9.2	18.1	26.9	25.8	80.0	52.7	49
16 Jan.	8.3	4.8	35.7	31.2	80.0	66.9	47
23 Jan.	10.1	22.5	21.8	25.6	80.0	47.4	54
30 Jan.	9.5	37.0	17.6	17.7	81.8	35.3	50
6 Feb.	8.5	36.3	6.8	28.5	80.1	35.3	81
13 Feb.	7.8	29.7	9.3	34.9	81.7	44.2	79
20 Feb.	7.8	3.9	6.1	62.2	80.0	68.3	91
27 Feb.	8.4	2.5	10.7	58.1	79.7	68.8	84
6 Mar.	8.1	0	18.6	65.6	92.3	84.2	78
13 Mar.	10.5	26.0	10.2	57.3	104.0	67.5	85
20 Mar.	12.5	6.1	0.1	85.1	103.8	85.2	99
27 Mar.	7.8	10.2	9.2	77.0	104.2	86.2	89
Total	108.5	197.1	173.0	569.0	1047.6	742.0	74
2 Apr.	7.4	6.4	4.6	69.4	87.8	74.0	94
12 Apr.	13.1	16.1	4.7	78.7	112.6	83.4	94
17 Apr.	9.1	8.2	21.5	65.1	103.9	86.6	75
24 Apr.	10.8	7.7	3.3	76.0	97.8	79.3	96
1 May	9.2	11.8	3.3	87.7	112.0	91.0	95
8 May	7.3	11.4	39.1	44.1	101.9	83.2	53
15 May	9.2	2.4	44.5	47.9	104.0	92.4	52
22 May	11.9	0	11.6	80.5	104.0	92.1	87
29 May	12.7	2.0	32.9	83.6	131.2	116.5	72
7 June	8.3	8.4	7.8	82.6	107.1	90.4	91
14 June	12.3	15.7	23.9	97.3	149.2	121.2	80
21 June	11.8	9.4	5.4	105.9	132.5	111.3	95
28 June	10.8	7.4	5.5	124.0	147.7	129.5	96
Total	133.9	106.9	208.1	1042.8	1491.7	1250.9	83

Table III.

Quarter	<u>BASIC RECORDS</u>				<u>DERIVED</u>		
	Routine	Eng.	Unsched. Maint.	Operation	Total	(UnM +OP) Available	(Op / Av) % Operation
1952							
4th	93.0	168.0	112.5	285.0	658.5	397.5	73
1953							
1st	108.5	197.1	173.0	569.0	1047.6	742.0	74
2nd	133.9	106.9	208.1	1042.8	1491.7	1250.9	83
3rd	50.1	24.8	54.3	510.2	639.4	564.5	91
4th	35.2	232.5	16.5	147.2	431.4	163.7	90
1954							
1st	115.6	138.3	85.7	666.4	1006.0	752.1	88
2nd	124.6	156.4	151.1	754.7	1186.8	905.8	83
1953-54 totals (3rd and 4th quarters of 1953; 1st and 2nd quarters of 1954)							
	325.5	552.0	307.6	2078.5	3263.6	2386.1	
	10%	17%	9%	64%	100%	87%	



PART II - MATHEMATICS

A. BLAST WAVE CALCULATION*

O. Introduction.

In the succeeding pages we discuss both the numerical analysis and the calculations we performed in connection with a blast wave computation. The problem itself is that of studying the decay and propagation of the shock wave generated by a very strong point-source explosion in an ideal gas under the assumption of spherical symmetry. We additionally were interested in the behavior of the pressure as a functional of radial distance for fixed times and of pressure as a function of time for fixed distances.

The method employed for handling the conditions of Rankine and Hugoniot is an iterative one and is discussed in section 3 below. Recently Brode of the Rand Corporation undertook a blast wave calculation closely paralleling the one described in this paper.[#] His method is, however, quite different.

In the succeeding sections we discuss the physical problem, the numerical algorithm and the computational results. The latter are contained principally in a set of graphs appended at the end of the paper.

1. The differential equations.

It is convenient to let ρ_0 , p_0 be the original density and pressure, i.e. the density and pressure in the undisturbed gas; t is time, r is the Lagrangean radius, R the Eulerian radius, ρ the density, p the pressure, R_s the position of the shock, D the velocity

* This paper has been submitted to a mathematical journal for publication.

Brode, H. L., Results of a Numerical Integration of a Spherical Shock from a Point Source, Rand Report. (This paper contains references to the literature on the subject.)

of the shock, and U the mass-velocity immediately back of the shock.

Then Newton's second law implies at once that behind the shock

$$1.1) \quad \rho \frac{\partial^2 R}{\partial t^2} = - \frac{\partial p}{\partial R}$$

The equation of continuity, i.e. of the conservation of mass, requires that everywhere

$$1.2) \quad \rho \frac{\partial R^3}{\partial r^3} = \rho_0$$

Finally the equation of state requires that

$$1.3) \quad p = k \rho^\gamma ,$$

where k is a function of r but not of t behind the shock, i.e.

$$1.4) \quad k = k(r).$$

These equations describe the conditions behind the shock but do not, as we know, hold across the shock. Instead we must consider the well-known equations of Rankine and Hugoniot. They are these:

$$1.5) \quad \frac{\rho}{\rho_0} = \frac{(\gamma+1)p + (\gamma-1)p_0}{(\gamma-1)p + (\gamma+1)p}$$

$$1.6) \quad U = \sqrt{\frac{2}{\rho_0}} \frac{|p - p_0|}{\sqrt{(\gamma+1)p + (\gamma-1)p_0}}$$

$$1.7) \quad D = \sqrt{\frac{1}{2\rho_0}} \sqrt{(\gamma+1)p + (\gamma-1)p_0}$$

The boundary conditions are two in number, one being at the origin, i.e. at $r = 0$ and the other at the shock, i.e. at $r = R$. They are

$$1.8) \quad R(0, t) = 0 \quad \text{for all } t,$$

$$1.9) \quad R(R, t) = R \quad \text{for all } t,$$

where of course, \mathcal{R} is a function of t ,

$$1.10) \quad \mathcal{R} = \mathcal{R}(t).$$

The initial conditions are discussed in §4 below.

In passing we note that the equations (1.5), (1.6), (1.7), (1.9) are not independent. If we differentiate (1.9) with respect to t , we find

$$1.11) \quad \frac{\partial R}{\partial r} \cdot \frac{d\mathcal{R}}{dt} + \frac{\partial R}{\partial t} = \frac{d\mathcal{R}}{dt};$$

But by (1.2) and (19)

$$\rho \frac{\partial R}{\partial r} = \rho_0$$

at the shock. Thus (1.11) is equivalent to

$$1.12) \quad \left(1 - \frac{\rho_0}{\rho}\right) D = U.$$

It is trivial now to see that this relation plus any two of (1.5), (1.6), (1.7) implies the third.

2. The difference equations.

In what follows we shall show how we replace our original implicitly formulated problem, equations (1.1) - (1.9), by a finitistic, explicit formulation which approximates the original one.

We consider first (1.1), (1.2). We combine them into

$$2.1) \quad \frac{\partial^2 R}{\partial t^2} = - \frac{1}{\rho} \frac{\partial p}{\partial r} = - \frac{R^2}{\rho_0 r^2} \frac{\partial p}{\partial r}$$

Thus our system (1.1) - (1.9) becomes now (2.1), (1.2) - (1.9).

As will be seen later it is convenient to introduce a change of variables. This change is the following:

$$2.2) \quad s = r^2/2$$

In terms of this new variable (2.1) becomes

$$(2.3) \quad \frac{\partial^2 R}{\partial t^2} = - \frac{1}{\rho_0} \frac{R^2}{(2s)^{1/2}} \frac{\partial p}{\partial s},$$

where we now understand R , p to be functions of s , t . We also use the quantity

$$(2.4) \quad \mathcal{S} = \mathcal{R}^{1/2}$$

in what follows.

We now replace our continuous variables r , s , t by discrete ones.

The time variable t is replaced by

$$(2.5) \quad t^h \quad (h = 0, 1, \dots)$$

where

$$(2.6) \quad t^{h+1} = t^h + \Delta t^{h+1/2},$$

with the $\Delta t^{h+1/2}$ determined as indicated in (3.35) below. We note that the t^h ($h = 0, 1, \dots$) are not necessarily equidistant. The spatial variables are defined for each t^h in this fashion. The distance from 0 to $\mathcal{S}^h = \mathcal{S}(t^h)$ is divided into L equal parts, thus:

$$(2.7) \quad ds^h = \mathcal{S}^h/L \quad (L \text{ a positive integer}).$$

Then s_j is given with the help of the relation

$$(2.8) \quad s_j = jds^h \quad (j = 0, 1, \dots, L);$$

note that the s_j are functions both of j and h . We suppress the dependence on h when no ambiguity can arise.

By this means our spatial scales cover just the relevant portions of space, namely, a gradually expanding region about the center. In order to compare results at two different time levels it is, of course, necessary to take into account the dependence of the s_j on h .

These things being understood we discuss the difference equations to be used in place of (2.3), (1.2) - (1.9).

Consider the formula

$$(2.9) \quad \bar{R}_j^{h+1} = \hat{R}_j^{h+1} + \frac{1}{\rho_0} \frac{\mathcal{R}^h}{2L^{1/2}} (P_{j-1/2}^h - P_{j+1/2}^h) \frac{(R_j^h)^2}{j^{1/2}} \frac{dt^{h+1/2}}{ds^h} \frac{dt^{h+1/2} + dt^{h-1/2}}{2ds^h}$$

$$(j = 1, 2, \dots, L-1).$$

In this \bar{R}_j^{h+1} corresponds to R_j^{h+1} except that the readjustment of the spatial scale to the change from s^h to s^{h+1} is not contained in it, i.e. it corresponds to the same Lagrangean position. To understand this recall that

$$(2.10) \quad \bar{R}_j^{h+1} = R(jds^h, t^{h+1})$$

whereas

$$(2.11) \quad R_j^{h+1} = R(jds^{h+1}, t^{h+1}).$$

Further \hat{R}_j^{h+1} is the estimate of R_j^{h+1} obtained by extrapolating linearly in t from R_j^{h-1} , R_j^h , taking all three quantities in the spatial scale at time t^h . If

$$\bar{R}_j^{h-1} = R(jds^h, t^{h-1}),$$

then

$$(2.12) \quad \hat{R}_j^{h+1} = R_j^h + \frac{dt^{h+1/2}}{dt^{h-1/2}} (R_j^h - \bar{R}_j^{h-1}) \quad , \quad (j = 1, 2, \dots, L-1).$$

It is thus clear that

$$\begin{aligned} \bar{R}_j^{h+1} - \hat{R}_j^{h+1} &= R(jds^h, t^{h+1}) - R(jds^h, t^h) \\ &= - \frac{dt^{h+1/2}}{dt^{h-1/2}} [R(jds^h, t^h) - R(jds^h, t^{h-1})] \\ &= \frac{\partial^2 R}{\partial t^2} (dt^{h+1/2}) \left(\frac{dt^{h+1/2} + dt^{h-1/2}}{2} \right) + \dots \end{aligned}$$

We consider next the remaining terms in (2.9). With the help of (2.4) and (2.7) we find that

$$\begin{aligned} & \frac{1}{\rho_0} \frac{\mathcal{R}^h}{2L^{1/2}} (p_{j-1/2}^h - p_{j+1/2}^h) \frac{(R_d^h)^{24}}{j^{1/2}} \frac{dt^{h+1/2}}{ds^h} - \frac{dt^{h+1/2} + dt^{h-1/2}}{2ds^h} \\ &= - \frac{1}{\rho_0} \frac{R^2}{(2s)^k} dt^{h+1/2} \left(\frac{dt^{h+1/2} + dt^{h-1/2}}{2} \right) \frac{\partial p}{\partial s} + \dots . \end{aligned}$$

Thus through second order terms formula (2.9) is an approximation to (2.3).

We turn attention now to relations (1.2), (1.3). Since k is independent of t^h , we see that

$$2.13) \quad \frac{\bar{p}_{j+1/2}^{h+1}}{p_{j+1/2}^h} = \left(\frac{\bar{p}_{j+1/2}^{h+1}}{p_{j+1/2}^h} \right)^s$$

where the bars over p and ρ have the significance explained earlier in connection with R , i.e.

$$2.14) \quad \bar{p}_{j+1/2}^{h+1} = p[(j+1/2)ds^h, t^{h+1}] \quad , \quad \bar{p}_{j+1/2}^{h+1} = [(j+1/2)ds^h, t^{h+1}]$$

We find with the help of (1.2) that (2.11) becomes

$$2.15) \quad \bar{p}_{j+1/2}^{h+1} = p_{j+1/2}^h \left[\frac{(R_{j+1}^h)^3 - (R_j^h)^3}{(\bar{R}_{j+1}^{h+1})^3 - (\bar{R}_j^{h+1})^3} \right]^s \quad (j = 0, 1, \dots, L-1).$$

The remaining relations (1.5) - (1.9) are already finitistic in character and require no emendation.

Our new system is thus (2.9), (2.15), (1.5) - (1.9) together with the definitions (2.10), (2.11), (2.12), (2.14). It remains only to describe the computational algorithm based on these equations and the process used for obtaining the initial values.

3. The computational algorithm.

We assume as given the following quantities:

$$3.1) \quad R_j^h, p_{j-1/2}^h \quad (j = 0, 1, \dots, L), \quad \hat{R}_j^{h+1} \quad (j = 1, 2, \dots, L-1);$$

$$3.2) \quad \mathcal{R}^h, D^{h-1/2}, D^{h-3/2}, t^h, dt^{h+1/2}, dt^{h-3/2}.$$

We describe in this section how to calculate the corresponding quantities at time t^{h+1} .

First we notice that formula (2.9) enables us immediately to define

$$3.3) \quad \bar{R}_j^{h+1} \quad (j = 1, 2, \dots, L-1);$$

(1.8) yields

$$3.4) \quad \bar{R}_0^{h+1} = 0.$$

Thus only \bar{R}_L^{h+1} is lacking -- this value will be determined with the help of the, as yet unused, relations (1.5) (1.7), (1.9).

Next formula (2.15) permits us to calculate easily

$$3.5) \quad \bar{p}_{j+1/2}^{h+1} \quad (j = 0, 1, \dots, L-2)$$

from the sequence (3.3), (3.4) above. Given \bar{R}_L^{h+1} we can also form

$$3.6) \quad \bar{p}_{L-1/2}^{h+1}$$

directly from (2.15). Finally by the spherical symmetry of the problem

$$3.7) \quad \bar{p}_{-1/2}^{h+1} = \bar{p}_{1/2}^{h+1}.$$

We turn attention now to the determination of \bar{R}_L^{h+1} , i.e. to the utilization of the shock conditions (1.5) - (1.7), (1.9). The procedure to be described is an inductive one, as will be seen. It is due to R. Peierls originally. The induction insofar as the shock velocity is concerned yields a value $_{k+1}\mathcal{D}$ for this velocity given $_k\mathcal{D}$ and $_{k-1}\mathcal{D}$. Thus initially one requires estimates $_0\mathcal{D}$, $_1\mathcal{D}$.

It starts in this manner: Given the quantities (3.1), (3.2) it is desired to find first approximations \mathcal{D}_0 , \mathcal{D}_1 to $D^{h+1/2}$. This is done with the help of the relations

$$3.8) \quad \mathcal{D}_0 = \mathcal{D}^{h-1/2}, \quad \mathcal{D}_1 = \mathcal{D}^{h-1/2} + \frac{dt^{h+1/2}}{dt^{h-1/2}} (\mathcal{D}^{h-1/2} - \mathcal{D}^{h-3/2}) = \mathcal{D}_0 + \frac{dt^{h+1/2}}{dt^{h-1/2}} (\mathcal{D}_0 - \mathcal{D}^{h-3/2})$$

We thus have first approximations \mathcal{D}_0 , \mathcal{D}_1 to the shock velocity at time $t^{h+1/2} = t^h + dt^{h+1/2}$.

The general step in the induction can now be described. Given an approximation \mathcal{D}_k to $D^{h+1/2}$ we find from (1.7) a value p_k of the shock pressure at $t^{h+1/2}$; it is this

$$3.9) \quad p_k = \frac{2}{\gamma + 1} \rho_0 D^2 - \frac{\gamma - 1}{\gamma + 1} p_0 .$$

Given this estimate for the shock pressure (1.6) combined with (1.7) yields a value U_k of the mass-velocity at the shock; it is this

$$3.10) \quad U_k = \frac{p_k - p_0}{\rho_0 D} .$$

Finally relation (1.12) implies that

$$3.11) \quad \frac{\rho_0}{\rho_k} = 1 - \frac{U_k}{D} .$$

Thus an estimate ρ_k for the shock density can be obtained.

We describe now how these quantities

$$3.12) \quad k^D, k^p, k^U, k\rho ,$$

are used. From what has preceded we know the values of

$$\bar{R}_{L-2}^{h+1}, \bar{R}_{L-1}^{h+1}$$

and thus we know

$$(3.13) \quad \delta_{L-2} = U_{L-2}^{h+1/2} dt^{h+1/2} = \bar{R}_{L-2}^{h+1} - R_{L-2}^h, \quad \delta_{L-1} = U_{L-1}^{h+1/2} dt^{h+1/2} = \bar{R}_{L-1}^{h+1} - R_{L-1}^h,$$

i.e. we have U , the mass velocity, at $(L-2)$ ds^h , $(L-1)$ ds^h and at the shock $\mathcal{S}^{h+1/2}$. From these we can by quadratic interpolation find U at Lds^h . This is the purpose of the formula

$$(3.14) \quad \delta_L = \frac{8\delta + 2u(u+4)\delta_{L-1} - u(u+2)\delta_{L-2}}{(u+2)(u+4)}, \quad \delta = {}_k U dt^{h+1/2}$$

$$(3.15) \quad u = L(2\rho + \frac{\rho^2}{2}), \quad \rho = {}_k D dt^{h+1/2} / \mathcal{R}^h$$

(Notice in these formulas that ρ , u , δ and thus δ_L depend upon the inductive index k .) With the help of ${}_k \delta_L$ we now define an estimate for \bar{R}_L^{h+1} by means of the formula

$$(3.16) \quad {}_k \bar{R}_L^{h+1} = R_L^h + {}_k \delta_L.$$

With this quantity we can form

$$\frac{{}_k \bar{p}_{L-1/2}^{h+1}}{k^p}$$

from (2.15). But we already know

$$\frac{{}_k \bar{p}_{L-5/2}^{h+1}}{k^p}, \quad \frac{{}_k \bar{p}_{L-3/2}^{h+1}}{k^p};$$

thus by a quadratic extrapolation we can find an estimate

$$(3.17) \quad k^p(h+1/2)$$

for the pressure at

$$(3.18) \quad s = \mathcal{S}^{h+1/2}, \quad t = t^{h+1}.$$

This quantity is obtained from the formula

$$(3.19) \quad f_u = f_j + \frac{u}{2}(f_{j+1} - f_{j-1}) + \frac{u^2}{2}(f_{j+1} - 2f_j + f_{j-1}),$$

with

$$3.20) \quad f_i = \bar{P}_{i+\frac{1}{2}}^{h+1} (i = L - \frac{3}{2}), \quad u = \frac{1}{2} (3 + L(2\nu + \frac{\nu^2}{2}))$$

To see this value for u is correct we note that the s -distance in question is from $s = (L - 3/2)$ ds^h to $s = \mathcal{S}^{h+1/2}$. This is

$$\begin{aligned} ds^h + \dot{s}s^h/2 + \mathcal{S}^{h+1/2} - L ds^h &= \\ = 3ds^h/2 + (\mathcal{R}^h + D^{h+1/2} ds^{h+1/2}/2)^2/2 - (\mathcal{R}^h)^2/2 &= \\ = \frac{1}{2}(3 + L(2\nu + \nu^2/2)) ds^h. \end{aligned}$$

The reader is referred to Figure I below.

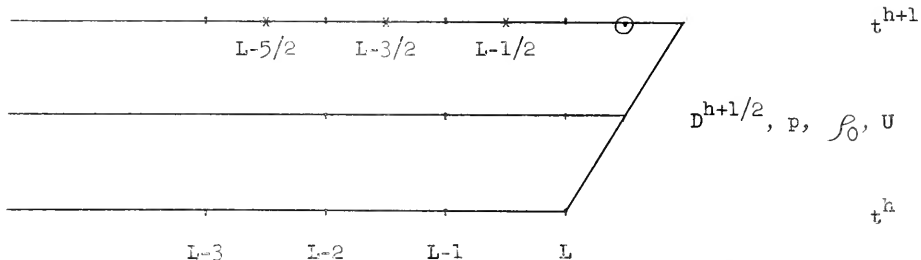


Figure I.

We go now to obtain another estimation

$$3.21) \quad k^p(h+1/2)$$

for the pressure at the (s, t) -point (3.18). We do this with the help of the adiabatic law. The value of p in question may be obtained as

$$3.22) \quad k^p(h+1/2) = k^p \left[\zeta \frac{(\mathcal{R}^{h+1})^3 - (\mathcal{R}^h)^3}{(\mathcal{R}^{h+1})^3 - (k \mathcal{R}_L^{h+1})^3} \right]^\gamma,$$

where

$$(3.23) \quad \zeta = \rho_0/\rho = 1 - k^U/k^D, \quad R^{h+1} = R^h + k^D \cdot dt^{h+1/2} .$$

(Note that both ζ and R^{h+1} are functions of k , the inductive index.)

Given these two not necessarily equal values of $p(R^{h+1/2}, t^{h+1})$

we are able to form an "error indicator"

$$(3.24) \quad k^\Delta = k^p[h+1/2] - k^p(h-1/2)$$

and to use it as a means of obtaining a new, improved value k_{+1}^D for the shock velocity. This is done with the help of the formulae

$$(3.25) \quad k_{+1}^D = k^D + \frac{k^\Delta}{k_{-1}^\Delta - k^\Delta} (k^D - k_{-1}^D), \quad -1^D = D^{h-1/2} ,$$

and (3.8).

The procedure is iterated until for some pre-assigned ϵ we have

$$(3.26) \quad |k^D - k_{-1}^D| < \epsilon (k_{-1}^D - (\rho_0/\rho_0)^{1/2}) .$$

When this point is reached, by definition

$$(3.27) \quad D^{h+1/2} = k^D, \quad R^{h+1} = R^h + D^{h+1/2} \cdot dt^{h+1/2}, \quad \bar{R}_L^{h+1} = \bar{R}_L^h, \quad t^{h+1} = t^h + dt^{h+1/2} .$$

In (3.3), (3.4) we saw how \bar{R}_j^{h+1} ($j = 0, 1, \dots, L-1$) were obtained.

We now have the complete sequence

$$(3.28) \quad \bar{R}_j^{h+1} \quad (j = 0, 1, \dots, L)$$

and also from (3.5), (3.6), (3.7)

$$(3.29) \quad \bar{p}_{j-1/2}^{h+1} \quad (j = 0, 1, \dots, L) .$$

We describe next how to obtain R_j^{h+1} , $R_{j-1/2}^{h+1}$ ($j = 0, 1, \dots, L$) out of

these sequences. This is done with the aid of interpolation formula

(3.19).

To form

$$(3.30) \quad R_j^{h+1} \quad (j = 1, 2, \dots, L-1)$$

we use (3.19) with

$$3.31) \quad f_j = \bar{R}_j^{h+1}, \quad u = j(2\nu + \nu^2), \quad = D^{h+1/2} \cdot dt^{h+1/2}/\mathcal{R}^h \quad .$$

$$3.32) \quad R_0^{h+1} = 0, \quad R_L^{h+1} = \mathcal{R}^{h+1} \quad .$$

Thus we have obtained, as desired, the sequence

$$3.33) \quad R_j^{h+1} \quad (j = 0, 1, \dots, L) \quad .$$

Similarly we find the $p_{j-1/2}^{h+1}$. Specifically by setting

$$f_j = \bar{p}_{j-1/2}^{h+1}, \quad c = (j - 1/2)(2\nu + \nu^2)$$

we obtain $p_{j-1/2}^{h+1}$ ($j = 1, 2, \dots, L-1$) from (3.5), (3.6), (3.7). Then

we set

$$p_{-1/2}^{h+1} = p_{1/2}^{h+1} \quad .$$

The final value $p_{L-1/2}^{h+1}$ is obtained by setting $u = 1 + (L - 1/2)(2\nu + \nu^2)$, i.e. by an extrapolation. Thus we obtain

$$3.34) \quad p_{j-1/2}^{h+1} \quad (j = 0, 1, \dots, L) \quad .$$

It remains now to describe the formation of \hat{R}_j^{h+2} and of $dt^{h+3/2}$.

To calculate the former quantities with relations (2.12) we need first $dt^{h+3/2}$. According to the usual stability arguments we must have

$$3.35) \quad \frac{\Delta R}{\Delta t} > \left(\frac{\gamma p}{\rho}\right)^{1/2} \quad ;$$

this is equivalent to

$$3.36) \quad \Delta t < \left(\frac{\gamma p}{\rho}\right)^{-1/2} \cdot \frac{\partial R}{\partial s} \Delta s \quad .$$

It turns out that the right-hand member of (3.36) has its smallest value at the shock. Thus p , ρ , $\partial R / \partial s$ may be evaluated there. This yields our condition

$$\begin{aligned} dt &= \Gamma \left(\frac{\rho}{\gamma p} \right)^{1/2} \cdot \frac{1}{R} \cdot \frac{\partial R}{\partial r} \cdot \Delta s = \\ &= \Gamma \left(\frac{\rho}{\gamma p} \right)^{1/2} \frac{\rho_0}{P} \cdot \frac{\Delta s}{R}, \end{aligned}$$

where Γ is a constant < 1 . Our formula is then this:

$$3.37) \quad dt^{h+3/2} = \Gamma \left(\frac{\rho_c}{\gamma p} \left(1 - \frac{u}{D} \right) \right)^{1/2} \cdot \frac{ds^{h+1}}{R^{h+1}}.$$

Given this $dt^{h+3/2}$ we now proceed to the calculation of \hat{R}_j^{h+2} with the help of (2.12). To this end it is necessary first to calculate R_j^h , i.e.

$$\hat{R}_j^h = R(jds^{h+1}, t^h).$$

This is accomplished by the use of the quadratic interpolation formula (3.19) with

$$3.38) \quad f_j = R_j^h, \quad u = j(2\nu + \nu^2).$$

Then (2.12) yields directly

$$3.39) \quad \hat{R}_j^{h+2} \quad (j = 1, 2, \dots, L-1).$$

This completes the induction. R_j^{h+1} are given by (3.31), (3.32); p_j^{h+1} by (3.34); \hat{R}_j^{h+2} by (3.27); R^{h+1} by (3.27); $D^{h+1/2}$ by (3.27); $D^{h-1/2}$ by (3.2); t^{h+1} by (3.27); $dt^{h+3/2}$ by (3.37) and $dt^{h+1/2}$ by (3.2).

In relation (3.26) we adopted what may at first seem to be a quite arbitrary definition for when two approximants to $D^{h+1/2}$ are near enough to each other. We say a few words now in explanation of this formulation.

Relation (3.9) implies that if δD is an error in D , $\delta(p - p_0)$, the corresponding error in $p - p_0$, is

$$\delta(p - p_0) = \frac{2}{\gamma + 1} \rho_0 \cdot 2D \delta D$$

and

$$3.40) \quad \frac{\delta(p - p_0)}{p - p_0} = \frac{2D}{D^2 - \frac{\gamma p_0}{\rho_0}} \quad \delta_D.$$

With the help of (3.26) this becomes

$$3.41) \quad \frac{\delta(p - p_0)}{p - p_0} < \frac{2D}{D + (\frac{\gamma p_0}{\rho_0})^{1/2}}.$$

At the beginning of the calculation the ratio

$$D / (\gamma p_0 / \rho_0)^{1/2}$$

is about 7 and it approaches, as we know, asymptotically to 1. In the former case we see that

$$3.42) \quad \frac{\delta(p - p_0)}{p - p_0} < 2\varepsilon$$

and in the latter

$$3.43) \quad \frac{\delta(p - p_0)}{p - p_0} < \varepsilon.$$

Thus relation (3.26) guarantees that the relative error in the shock over-pressure determined by κ_D does not exceed 2ε for large D and ε for D near $(\gamma p_0 / \rho_0)^{1/2}$; and therefore in all cases the relative error in the determination of the shock over-pressure is about 2ε . It is important to notice that the relations (3.42) and (3.43) are concerned with over-pressure since they are the relevant quantities in the computation. As will be seen the calculation starts with this over-pressure being about 100 atmospheres and continues until it is about 0.02

atmospheres. Evidently it is the relative precision of this quantity which is of interest.

We close this section with a discussion of the meaning of the iterative relation (3.25). As we saw, for each given D there are determined two pressures $p_{(h+1/2)}$, $p_{(h+1/2)}$ which are equal if and only if the D is the correct value. Thus we desire to solve iteratively the functional equation

$$3.44) \quad \Delta(D) = p_{[h+1/2]}(D) - p_{(h+1/2)}(D) = 0$$

for D . As is well-known an error-squaring technique for solving such relations is that of Newton-Raphson. According to this method if D is an approximant to the solution of (3.44), then

$$3.45) \quad D^1 = D - \frac{\Delta(D)}{\Delta'(D)} \quad (\Delta'(D) = d\Delta/dD)$$

is a better one. In fact if D_0 is the exact solution, i.e. if

$$\Delta(D_0) = 0,$$

then

$$3.46) \quad D' - D_0 = ((D - D_0) \Delta'(D) - (\Delta(D) - \Delta(D_0))) / \Delta'(D) \sim \frac{\Delta''(D)}{2\Delta'(D)} (D - D_0)^2.$$

Thus the error $(D' - D_0)$ is proportional to the square of the previous error $(D - D_0)$, the factor of proportionality being $\Delta''/2\Delta'$.

The exact evaluation of Δ' is quite difficult and thus instead of using precisely (3.45) we have used (3.25). In that formula the expression

$$({}_k D - {}_{k-1} D) / ({}_{k-1} \Delta - {}_k \Delta)$$

is introduced as an approximation to $-1/\Delta'({}_k D)$.

4. The initial values.

If the pressure ratio p/p_0 at the shock is infinite, it is known that the original problem (1.1) - (1.9) has an exact analytic solution. This has been shown by the senior one of us. (Cf. Brode, Op. Cit.) The solution is a similarity one in the sense that p and $w = R/\mathcal{R}$ are expressible as functions of the variable

$$4.1) \quad Z = r/\mathcal{R} .$$

It is not difficult to show that

$$4.2) \quad \mathcal{R} = a t^{2/5}.$$

To express p and R it is convenient to introduce a parametric representation for r , R , p .

$$r = \mathcal{R} \chi^{\frac{r}{2\delta+1}} \left(\frac{1+\chi}{2} \right)^{-\frac{2}{5}} \left(\frac{3(2-\delta)\chi + (2\delta+1)}{7-\delta} \right)^{\frac{13\delta^2-7\delta+12}{15(2-\delta)(2\delta+1)}} ,$$

$$4.3) \quad R = \mathcal{R} \chi^{\frac{r-1}{2\delta+1}} \left(\frac{1+\chi}{2} \right)^{-\frac{2}{5}} \left(\frac{r+\chi}{\delta+1} \right)^{\frac{5\delta+1}{3\delta-1}} \left[\frac{3(2-\delta)\chi + (2\delta+1)}{7-\delta} \right]^{-\frac{13\delta^2-7\delta+12}{5(2-\delta)(3\delta-1)}} ,$$

$$p = \frac{8}{25(\delta+1)} p_0 a^2 t^{-\frac{48}{5}} \left(\frac{1+\chi}{2} \right)^{\frac{6}{5}} \left(\frac{r+\chi}{\delta+1} \right)^{\frac{48}{3\delta-1}} \left[\frac{3(2-\delta)\chi + (2\delta+1)}{7-\delta} \right]^{\frac{13\delta^2-7\delta+12}{5(2-\delta)(3\delta-1)}} ,$$

With the help of the equations we can calculate initial values. It is known that for

$$p/p_0 \sim 100 \text{ atmos.}$$

the equations (4.3) yield a quite good description of the situation.

These equations are somewhat cumbersome to handle in a machine calculation so we have replaced them with the following equivalent differential system. In this system r has been replaced by s .

$$\begin{aligned}
 4.4) \quad \frac{dR}{ds} &= -\frac{R}{2s} \left(\frac{1-\gamma}{\gamma+x} \right) \\
 \frac{dx}{ds} &= \frac{x(1+\gamma)[3(2-\gamma)x + (2\gamma+1)]}{2s(\gamma x^2 + 2x + \gamma)}, \\
 \frac{dp}{ds} &= \frac{p}{\gamma+x} [3(\gamma-1)x + 2\gamma s \frac{dx}{ds}] \cdot \frac{1}{2s}
 \end{aligned}$$

are the differential equations and

$$\begin{aligned}
 R(\mathcal{S}) &= R_0, \\
 x(\mathcal{S}) &= 1, \\
 p(\mathcal{S}) &= \frac{\delta p_0}{25(\gamma+1)} \cdot \frac{R^2}{t^2}
 \end{aligned}$$

are the initial conditions. The integration proceeds from $s = \mathcal{S}$ to $s = 0$.

5. Preliminary remarks on the calculation.

In this section we discuss some of the relevant details of the calculation.

As we mentioned in the introductory section it is known that the analytical results (4.3) give a close approximation to the actual physical situation for shocks whose pressure ratios are in the neighborhood of 100 atmospheres. Accordingly it was decided to start the computation with the initial shock pressure-ratio as 100 atmospheres and quite arbitrarily with the initial shock radius as 1/2 unit; also arbitrarily the pressure and density of the undisturbed gas as unity. We have taken

$$\gamma = 1.4. \text{ Hence}$$

$$p_0 = 1, \rho_0 = 1, R^0 = \frac{1}{2}, p(\mathcal{S}, t^0) = 100$$

The conditions (5.1) in conjunction with (4.2) determine the time t^0 .

With these initial values the equations (4.4), (4.5) were integrated from the shock inward to yield R , p at the time

$$(5.2) \quad t^0 = 0.0182575$$

as functions of jds^0 , where

$$(5.3) \quad ds^0 = 1/800.$$

Thus

$$(5.4) \quad R_j^0, p_{j-1/2}^0 \quad (j = 1, 2, \dots, L)$$

are formed. By definition

$$R_0^0 = 0, p_{-1/2}^0 = p_{1/2}^0.$$

The first two of equations (4.4) were then integrated with

$$(5.6) \quad R(S') = R^{-1} = R^0 - D^{-1/2} dt^{-1/2}, \quad x(S') = 1$$

where

$$dt^{-1/2} = dt^{1/2} = 0.000086,$$

$$(5.7) \quad D = 2 R / 5t.$$

In order to tabulate the resulting function against jds^0 the equations were first integrated from S^{-1} to $S^0 - ds^0$. This provides starting values for R , p at lds^0 . From this point inward to $1 ds^0$ the calculation proceeds normally. Thus \hat{R}_j^{-1} is obtained and from this and R_j^0 , we find

$$\hat{R}'_j.$$

This procedure yields the starting values of

$$(5.9) \quad R_j^0, p_{j-1/2}^0, \hat{R}'_j, t^0, dt^{-1/2}, dt^{1/2}, D^{-3/2}, D^{-1/2} \quad (j=0, 1, \dots, L);$$

they arise from equations (5.1) - (5.8).

The numerical procedure used to carry out the integration was the well-known one of Runge-Kutta. Three different intervals of integration were used. They were

$$-\Delta s = 1/32,000, 1/16,000, 1/8,000.$$

We compared the values of $R_1^0, p_{1/2}^0, R_1^1$ as obtained by the three integrations and give below the relative errors. Let the quantities with "bars" over them refer to those obtained with the interval of integration $|\Delta s| = 1/32,000$; with "tildes" over them the interval $|\Delta s| = 1/16,000$ and with no symbol the interval $|\Delta s| = 1/8,000$. Then

$$\frac{\tilde{R}_1^0 - R_1^0}{R_1^0} = 2.54 \times 10^{-10}, \quad \frac{\tilde{P}_{1/2}^0 - P_{1/2}^0}{P_{1/2}^0} = 7.24 \times 10^{-6}, \quad \frac{\tilde{R}_1' - \hat{R}_1'}{\hat{R}_1'} = 4.22 \times 10^{-7};$$

$$\frac{\tilde{R}_1^0 - R_1^0}{R_1^0} = 7.01 \times 10^{-8}, \quad \frac{\tilde{P}_{1/2}^0 - P_{1/2}^0}{P_{1/2}^0} = 5.62 \times 10^{-6}, \quad \frac{\tilde{R}_1' - \hat{R}_1'}{\hat{R}_1'} = 4.27 \times 10^{-7}$$

The data corresponding to $|\Delta s| = 1/8,000$ were accepted as the initial values for R, p, \hat{R} .

To completely characterize the problem we need the initial data (5.1), (5.3), (5.9) together with values for the Γ of (3.37) and L. We carried out three different calculations determined by

$$5.10) \quad p_0 = 0, L = 100, \quad \Gamma = 1/2,$$

$$5.11) \quad p_0 = 1, L = 100, \quad \Gamma = 1/2,$$

$$5.12) \quad p_0 = 1, L = 80, \quad \Gamma = 2/5.$$

The results of these caluclations are discussed in more detail in what follows.

The actual algorithm can best be described inductively. Suppose given

$$p_0, p_0, ds^h, dt^{h-1/2}, dt^{h+1/2}, D^{h-3/2}, D^{h-1/2}, L, \Gamma, \mathcal{R}^h, R_j^h, p_{j-1/2}^h, \hat{R}_j^{h+1}.$$

The modus procedendi is then this. We first seek the value $D^{h+1/2}$. This is obtained by the iterative procedure outlined in §3 above. The approximant $-_1^D$ is given by

$$-_1^D = D^{h-1/2}$$

and $_0^D$ by relation (3.8). The iteration then proceeds as described in §3; the principal formula being (3.25). This iteration terminates when the relation (3.26) is satisfied. The value

$$\varepsilon = 2^{-18}$$

(5.13)

was used throughout almost all calculations. Near the end of the problem (5.11) it was altered to

$$\varepsilon = 2^{-16}.$$

(5.13')

The number of iterations of (3.25) required to satisfy (3.26) with ε determined by (5.13) was about three independent of the shock over-pressure. To test "noise level" of this scheme, i.e. to measure the accumulation of rounding errors, we evaluated the D corresponding to the shock over-pressure of 50, starting with two quite dissimilar sets of initial estimates. The relative disagreement was about one part in a million. For smaller over-pressures this disagreement was even smaller. Thus our choices (5.13), (5.13') yield results above the "noise level".

Having calculated $D^{h+1/2}$, we next form

$$\mathcal{R}^{h+1} = \mathcal{R}^h + D^{h+1/2} dt^{h+1/2},$$

$$ds^{h+1} = \frac{\mathcal{R}^{h+1}}{L} = \frac{(\mathcal{R}^{h+1})^2}{2L},$$

and then with the help of (3.37)

(5.14)

(5.15)

$$dt^{h+3/2}.$$

It is interesting to notice that the ratio

$$dt^{h+3/2}/ds^{h+1}$$

varies only by a small amount throughout the entire calculation. For an over-pressure of about 49, it is .04, for an over-pressure of 1.04, it is .08, and for an over-pressure of .02 it is .03. The three corresponding values of ds^{h+1} are

$$.002, \quad .04, \quad 2.92.$$

These quantities having been determined, we are enabled to calculate with the help of formulae (2.9), (2.15) the

$$\bar{R}_j^{h+1}, \quad \bar{p}_{j-1/2}^{h+1}.$$

Then with the help of the interpolation formula (3.19) we form

$$R_j^{h+1}, \quad p_{j-1/2}^{h+1}, \quad \hat{R}_j^{h+2} \quad (j = 0, 1, \dots, L),$$

and this completes the induction since

$$t^{h+1} = t^h + dt^{h+1/2}.$$

The details have already been discussed in §3 above.

There is one important deviation from this program we must describe at this time. The functions R , \hat{R} are not adequately representable by quadratic approximations near $s = 0$ to permit of the interpolation procedure just discussed. In the table below we give the values $R_0^0, R_1^0, \dots, R_6^0$ to show this. We tried to run the problem (5.10) as just described and found that quite soon it reached a point where $R_{j-1}^{h+1} > R_j^{h+1}$ for j near 2. This physical absurdity stopped the calculation.

To rectify this situation without resorting to elaborate methods we recalled that R , \bar{R} are nearly proportional to $s^{1/7}$ near $s = 0$, as

can be seen from formulae (4.3) and thus that R^7 , \bar{R}^7 are nearly linear. This is shown in the following table. Accordingly, we first raised to the power 7 the functions R_j , \bar{R}_j and then performed the interpolation for $j = 0, 1, \dots, 5$. For $j > 5$ the functions R , \bar{R} are sufficiently slowly changing to permit local quadratic approximations.

	ΔR	$\Delta^2 R$
R_0^0	0	
R_1^0	.27494	.27494
R_2^0	.30349	.02855
R_3^0	.32149	.01800
R_4^0	.33486	.01337
R_5^0	.34558	.01072

	ΔR^7	$\Delta^2 R^7$
$(R_0^0)^7$	0	
$(R_1^0)^7$	1.1877×10^{-4}	1.1877×10^{-4}
$(R_2^0)^7$	2.3712×10^{-4}	1.1835×10^{-4}
$(R_3^0)^7$	3.5494×10^{-4}	1.1782×10^{-4}
$(R_4^0)^7$	4.7214×10^{-4}	1.1720×10^{-4}
$(R_5^0)^7$	5.8865×10^{-4}	1.1651×10^{-4}

In a typical time step there are 2746 multiplications and 1790 divisions. Since the only variable length portion of the code is the iteration at the shock, and since the number of these iterations is virtually a constant, this count of the multiplications and divisions is quite accurate. Assuming that a multiplication requires $720 \mu s$ and a division $1100 \mu s$ on our machine, we find that 3.95 seconds are

spent in each time step on multiplications and divisions. An actual "clocking" of the time spent on such a step gives 10.17. Thus the solution time is 2.57 times the time spent in multiplying and dividing.

An examination of the solutions (4.3) shows that problem (5.10) is such that

$$5.16) \quad R_j^h / R^h, p_{j-1/2}^h / p_{L-1/2}^h$$

are independent of h , i.e. of t^h . To test the accuracy of the code and of our numerical procedure we accordingly undertook the solution of problem (5.10) and printed out the data (5.16). The calculation started with a shock-pressure of 100 atmospheres and stopped with a shock-pressure of about 48. To measure the accuracy of the results notice in formulae (4.3) or (4.5) that the shock pressure is

$$P = \frac{8\rho_0}{25(\gamma+1)} \frac{R^2}{t^2} = \frac{8\rho_0 \alpha^6}{25(\gamma+1)} R^{-3} ;$$

and thus that

$$p R^3 = \text{const.}$$

We used the relative change in this quantity $p R^3$ as an overall figure of merit for our code. We found in our calculation this relative error to be about 5.25×10^{-4} .

The results $R_j^h, p_{j-1/2}^h, \hat{R}_j^{h+1}$ ($j = 0, 1, \dots, L$) were printed out periodically. It was arranged that for

$$p > 2.04$$

this took place whenever a 12.5% change in the shock pressure occurred and in the contrary case whenever a 12.5% change in the shock over-pressure occurred. For the entire problem between 45 and 47 time steps made up such a group.

The problem (5.11) was then undertaken, and to obtain some evaluation of the overall accuracy of the results, we carried out (5.12). This yielded an estimation for the overall error including that arising from the interpolation process. To compare the results of the two calculations we used the results of the problem (5.11) to obtain the values of the shock over-pressure at the shock radii obtained in the problem (5.12) and then compared these over-pressure to those actually obtained in (5.12). This yielded a set of relative errors in the over-pressure which increase slowly as indicated below.

<u>p - 1</u>	<u>relative error</u>
50.00	1.8×10^{-4}
10.00	4.8×10^{-4}
5.00	8.2×10^{-4}
2.00	4.6×10^{-4}
1.00	5.9×10^{-4}
.60	1.3×10^{-3}
.30	1.8×10^{-3}
.05	4.9×10^{-3}
.02	7.9×10^{-3}

The comparisons were made in this manner. It is known -- Cf. Figure I and Table I below -- that the shock over-pressure and shock radius are related by a relation of the form

$$(5.17) \quad p - 1 = A R^{-n}$$

where n is a slowly varying function of R . Further, as we indicated above, the tabulations we obtained from the machine computation occur at 12.5% changes in the shock over-pressure. Thus, it seems reasonable to perform the comparisons discussed above logarithmically. If $p_1 - 1$,

R_1 ; $p_2 - 1$, R_2 are two consecutive points on the $p - 1$, R curve as determined by the solution of problem (5.11) and $\bar{p} - 1$, \bar{R} is a point on the corresponding curve for (5.12) with

$$\mathcal{R}_1 < \bar{\mathcal{R}} < \mathcal{R}_2,$$

then our interpolation procedure is this. Form

$$\tilde{\log} (p - 1)/(p_2 - 1) = -n \log \bar{\mathcal{R}} / \mathcal{R}_2,$$

where

$$5.18) \quad n = -\frac{\log (p_1 - 1)/(p_2 - 1)}{\log \mathcal{R}_1 / \mathcal{R}_2}.$$

Then

$$\delta \sim \log(1 + \delta) = \log \frac{\bar{p} - 1}{\tilde{p} - 1} = \log \frac{\bar{p} - 1}{p_2 - 1} - \log \frac{\tilde{p} - 1}{p_2 - 1}$$

where

$$\delta = \frac{(\bar{p} - 1) - (\tilde{p} - 1)}{\tilde{p} - 1}$$

and we have accordingly an estimate for the relative error in question.

After having obtained tabulations of the functions

$$R(r, t) \quad p(r, t),$$

we required tabulations of the function

$$p = P(R, t).$$

To do this, we needed to invert for each t^h the function
 $r = R(r, t^h)$

and substitute the resulting function of R into $p(r, t^h)$. This was accomplished by choosing a unit dR and then solving the equation

$$5.19) \quad k dR = R_i + \frac{u}{2}(R_{i+1} - R_{i-1}) + \frac{u^2}{2}(R_{i+1} - 2R_i + R_{i-1})$$

for u as a function of k ; with this u the corresponding p can be found as

$$P_{k-\frac{1}{2}} = p_{i-\frac{1}{2}} + \frac{u}{2}(p_{i+\frac{1}{2}} - p_{i-\frac{1}{2}}) + \frac{u^2}{2}(p_{i+\frac{1}{2}} - 2p_{i-\frac{1}{2}} + p_{i-\frac{3}{2}})$$

To solve (5.18) for us we used a Newton-Raphson type formula. If u' is an approximation to the solution of (5.18), then

$$u' = \frac{1}{2} \left(u - \frac{bu+c}{au+b} \right),$$

where

$$a = \frac{1}{2}(R_{i+1} - 2R_i + R_{i-1}), \quad b = \frac{1}{4}(R_{i+1} - R_{i-1}), \quad c = R_i - k dR$$

A starting approximant is, of course

$$u_0 = -c/2b$$

To avoid obtaining too many values P_k for a given t^h , several choices were made for the unit dR . In fact, it was chosen in accordance with the relation

$$dR = 1/2^n \text{ for } 50/2^{n-1} \geq R > 50/2^n .$$

6. The results.

We have arranged the results of our calculations in a number of Tables and Figures which are appended hereto.

In Figure I we have displayed the shock over-pressure as a function of the shock radius. Since the relation between these quantities is as indicated in (5.17) above it was found convenient to plot the curve on log-log paper.

In Figure II the time of the arrival of the shock at a given radius is plotted against that radius. This plot is also on log-log paper.

In Table I following Figure II we have displayed the shock

radius, the exponent n of (5.18), the dynamic over-pressure, and the over-pressure for a number of values of the overpressure, spaced roughly 12% apart. (The dynamic over-pressure is the ordinary one plus $(1/2) \rho u^2$, i.e.

$$P - 1 = p - 1 + (1/2) \rho u^2$$

where p , ρ , u are the pressure, density and velocity at the shock.) In Table II the shock velocity and time of arrival are displayed at the same over-pressure as in Table I.

Figures III-VII, inclusive, are graphs of the over-pressure as a function of Eulerian radius at various typical times.

Figures VIII-XVI, inclusive, are graphs of the over-pressure as a function of the time for various values of the radius.

Figure XVII is a graph of the length of the positive phase as a function of the shock radius.

Figure I - II-28.

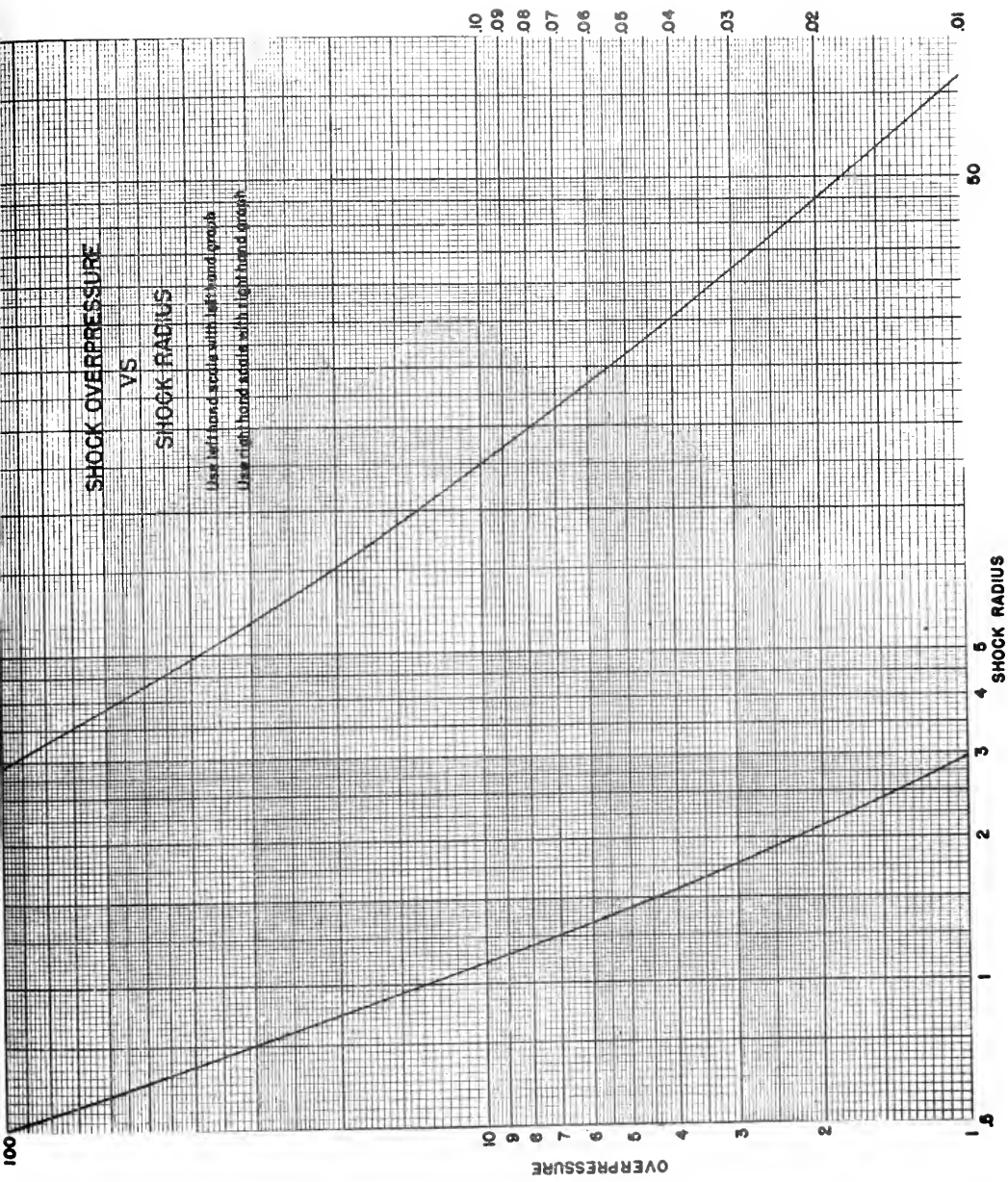
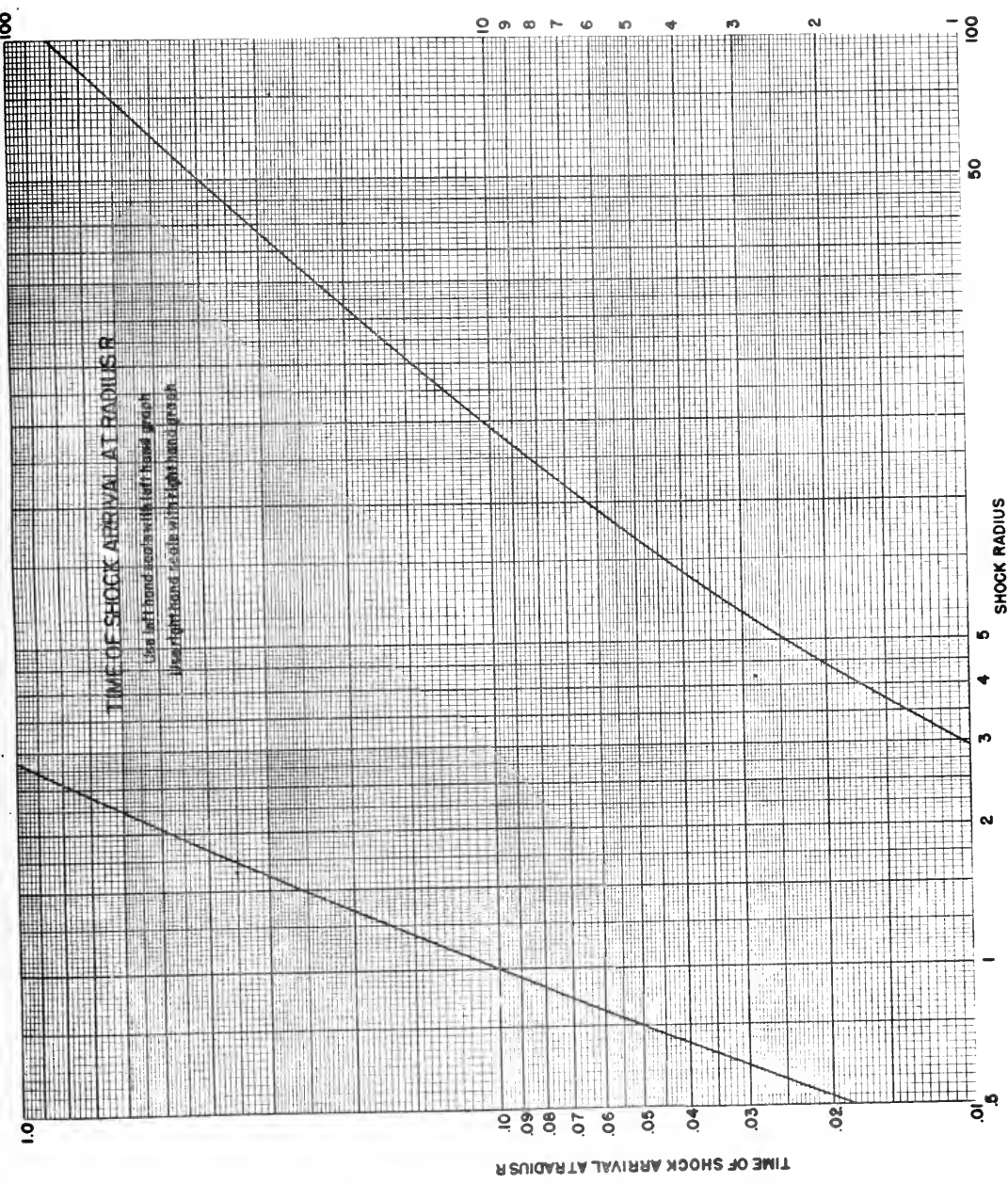


Figure II - II-29.



Shock Radius	Exponent	Dynamic Overpressure	Overpressure
0 . 5 0 0 4 7 4	0 . 0 0 0 0 0 0 0	1 0 7 . 2 6 7 0 6 7	1 0 0 . 0 0 6 4 5 4
0 . 5 2 5 7 6 0	2 . 9 7 6 1 0 2 8 8	9 2 . 6 7 3 4 1 2	8 6 . 3 6 1 6 4 8
0 . 5 5 0 5 6 7	2 . 9 5 9 5 3 5 2 1	8 0 . 8 9 1 9 3 7	7 5 . 3 4 6 4 9 2
0 . 5 7 6 6 7 5	2 . 9 5 4 1 8 9 7 1	7 0 . 5 8 3 0 0 3	6 5 . 7 0 8 4 4 0
0 . 6 0 4 1 7 8	2 . 9 4 8 4 1 4 5 5	6 1 . 5 6 1 9 8 0	5 7 . 2 7 4 8 7 9
0 . 6 3 3 1 7 9	2 . 9 4 1 7 8 5 9 0	5 3 . 6 6 8 4 9 2	4 9 . 8 9 5 8 7 5
0 . 6 6 3 7 9 5	2 . 9 3 3 8 3 0 9 4	4 6 . 7 6 2 9 4 0	4 3 . 4 4 0 9 2 8
0 . 6 9 6 1 5 8	2 . 9 2 5 2 1 0 4 1	4 0 . 7 2 1 3 2 8	3 7 . 7 9 4 1 3 3
0 . 7 3 0 4 1 6	2 . 9 1 5 0 0 1 5 3	3 5 . 4 3 6 8 0 5	3 2 . 8 5 5 6 1 9
0 . 7 6 5 9 4 4	2 . 9 0 3 9 5 5 2 0	3 0 . 9 0 6 5 1 2	2 8 . 6 2 2 6 8 7
0 . 8 0 3 6 3 2	2 . 8 9 1 5 7 2 0 9	2 6 . 9 3 3 2 2 1	2 4 . 9 1 0 2 6
0 . 8 4 3 6 8 8	2 . 8 7 7 2 5 9 3 7	2 3 . 4 4 9 4 9 9	2 1 . 6 5 7 6 3 6
0 . 8 8 6 3 5 0	2 . 8 6 1 2 2 5 0 5	2 0 . 3 9 5 6 4 6	1 8 . 8 0 6 7 5 7
0 . 9 3 1 8 9 4	2 . 8 4 3 5 7 0 7 6	1 7 . 7 1 9 0 6 9	1 6 . 3 0 9 2 7 9
0 . 9 8 0 6 3 7	2 . 8 2 3 6 1 1 8 6	1 5 . 3 7 4 1 2 2	1 4 . 1 2 2 5 9 4
1 . 0 3 2 9 5 0	2 . 8 0 1 3 5 9 9 0	1 3 . 3 2 0 5 6 1	1 2 . 2 0 9 1 4 7
1 . 0 8 9 2 6 1	2 . 7 7 5 2 9 2 4 3	1 1 . 5 2 3 9 0 0	1 0 . 5 3 6 7 6 8
1 . 1 5 0 0 7 0	2 . 7 4 6 2 9 9 8 6	9 . 9 5 3 0 2 6	9 . 0 7 6 4 3 9
1 . 2 1 5 9 6 1	2 . 7 1 7 4 5 0 7 1	8 . 5 7 9 0 9 9	7 . 8 0 1 2 7 3
1 . 2 8 7 6 1 6	2 . 6 8 3 1 1 6 7 1	7 . 3 7 9 6 3 9	6 . 6 9 0 3 0 2
1 . 3 6 5 8 3 1	2 . 6 4 5 9 5 5 6 2	6 . 3 3 3 4 6 3	5 . 7 2 3 7 5 3
1 . 4 5 1 5 4 3	2 . 6 1 5 9 3 5 8 9	5 . 4 1 8 7 5 6	4 . 8 8 1 2 8 8
1 . 5 5 2 2 7 0	2 . 4 4 9 2 6 9 0 5	4 . 6 1 2 6 0 5	4 . 1 4 1 6 0 9
1 . 6 6 1 7 0 5	2 . 4 7 8 5 6 5 8 3	3 . 9 0 8 1 1 0	3 . 4 9 8 1 3 5
1 . 7 8 8 8 6 3	2 . 4 0 6 1 1 7 4 8	3 . 2 8 2 1 3 1	2 . 9 2 9 4 4 4
1 . 9 3 7 6 4 9	2 . 3 3 9 6 3 2 4 8	2 . 7 2 8 9 1 4	2 . 4 2 9 9 9 0
2 . 0 8 2 1 4 8	2 . 2 7 4 7 6 6 8 2	2 . 3 2 0 0 6 0	2 . 0 6 3 2 3 4
2 . 2 4 3 4 3 3	2 . 2 1 2 0 4 4 7 4	1 . 9 6 8 0 1 1	1 . 7 4 9 3 4 3
2 . 4 2 8 0 9 5	2 . 1 4 6 1 1 3 4 5	1 . 6 5 9 8 6 6	1 . 4 7 6 2 1 8
2 . 6 3 5 5 6 2	2 . 0 7 9 8 2 2 4 2	1 . 3 9 7 3 4 4	1 . 2 4 4 7 8 2
2 . 8 6 8 9 8 4	2 . 0 1 4 1 2 0 6 1	1 . 1 7 4 5 3 3	1 . 0 4 9 2 1 1
3 . 1 3 7 9 4 3	1 . 9 4 8 8 2 1 0 7	0 . 9 8 2 4 1 4	0 . 8 8 1 0 9 1
3 . 4 4 8 7 1 5	1 . 8 8 4 2 0 0 5 2	0 . 8 1 8 0 7 1	0 . 7 3 7 4 7 2
3 . 8 0 8 6 9 3	1 . 8 2 0 5 0 1 1 7	0 . 6 7 8 6 1 3	0 . 6 1 5 5 2 8
4 . 1 1 2 6 5 2	1 . 7 6 7 7 0 8 5 7	0 . 5 8 9 4 6 3	0 . 5 3 7 4 0 5
4 . 4 4 7 3 4 1	1 . 7 2 4 4 3 2 1 2	0 . 5 1 2 3 0 1	0 . 4 6 9 5 7 9
4 . 8 1 5 8 0 5	1 . 6 8 3 0 8 5 3 3	0 . 4 4 5 5 9 1	0 . 4 1 0 7 0 2
5 . 2 2 1 3 5 9	1 . 6 4 4 0 6 0 8 4	0 . 3 8 7 9 4 9	0 . 3 5 9 5 8 0
5 . 6 8 0 2 8 8	1 . 6 0 6 8 2 8 9 2	0 . 3 3 6 9 0 5	0 . 3 1 4 0 5 6
6 . 1 8 6 4 5 0	1 . 5 7 1 4 3 3 1 5	0 . 2 9 2 9 7 5	0 . 2 7 4 6 3 3
6 . 7 4 4 5 4 6	1 . 5 3 8 3 8 0 8 2	0 . 2 5 5 1 4 5	0 . 2 4 0 4 6 2
7 . 3 7 6 7 4 4	1 . 5 0 7 1 0 2 7 8	0 . 2 2 1 7 4 7	0 . 2 1 0 0 8 8
8 . 0 7 5 2 0 4	1 . 4 7 7 6 3 0 1 2	0 . 1 9 3 0 4 2	0 . 1 8 3 8 0 1
8 . 8 6 7 4 7 7	1 . 4 4 9 8 8 1 6 7	0 . 1 6 7 7 4 8	0 . 1 6 0 4 7 8
9 . 7 4 4 5 7 6	1 . 4 2 3 7 6 6 9 3	0 . 1 4 6 0 2 6	0 . 1 4 0 3 1 1
1 0 . 7 1 5 3 6 2	1 . 3 9 9 5 6 0 9 4	0 . 1 2 7 3 3 8	0 . 1 2 2 8 4 8
1 1 . 8 1 7 8 9 8	1 . 3 7 6 8 0 5 1 9	0 . 1 1 0 8 5 6	0 . 1 0 7 3 5 2
1 3 . 0 4 0 8 1 8	1 . 3 5 5 4 1 0 0 3	0 . 0 9 6 6 7 5	0 . 0 9 3 9 3 9
1 4 . 3 9 7 0 4 1	1 . 3 3 5 4 4 9 0 4	0 . 0 8 4 4 4 8	0 . 0 8 2 3 1 2
1 5 . 9 3 9 5 3 8	1 . 3 1 6 9 1 4 7 0	0 . 0 7 3 6 4 6	0 . 0 7 1 9 8 7
1 7 . 6 5 4 0 2 0	1 . 2 9 9 1 9 4 8 5	0 . 0 6 4 3 2 8	0 . 0 6 3 0 3 9
1 9 . 5 5 9 4 4 9	1 . 2 8 2 5 2 4 4 6	0 . 0 5 0 2 7 7	0 . 0 5 5 2 7 4
2 1 . 7 3 0 0 7 4	1 . 2 6 6 9 9 1 8 3	0 . 0 4 9 1 5 0	0 . 0 4 8 3 7 4
2 4 . 1 4 8 0 7 2	1 . 2 5 2 3 8 9 2 5	0 . 0 4 2 9 8 8	0 . 0 4 2 3 8 7
2 6 . 8 4 1 4 3 4	1 . 2 3 8 4 4 9 4 0	0 . 0 3 7 6 5 0	0 . 0 3 7 1 8 4
2 9 . 9 1 5 0 1 3	1 . 2 2 5 0 9 2 7 4	0 . 0 3 2 9 1 9	0 . 0 3 2 5 5 9
3 3 . 3 4 6 7 9 7	1 . 2 1 1 8 8 6 8 0	0 . 0 2 8 8 2 2	0 . 0 2 8 5 4 4
3 7 . 1 7 8 3 4 8	1 . 2 0 0 2 9 9 3 4	0 . 0 2 5 2 6 6	0 . 0 2 5 0 5 1
4 1 . 4 5 6 0 6 0	1 . 1 8 8 9 3 5 4 0	0 . 0 2 2 1 7 5	0 . 0 2 2 0 0 8
4 6 . 3 4 6 4 8 9	1 . 1 7 0 9 2 5 2 1	0 . 0 1 9 4 4 3	0 . 0 1 9 3 1 4
5 1 . 8 1 9 7 2 0	1 . 1 5 1 1 3 3 8 4	0 . 0 1 7 0 8 6	0 . 0 1 6 9 8 5

Overpressure	Shock Velocity	Time of Shock Arrival
1 0 0 . 0 0 6 4 5 4	0 . 1 1 0 1 8 5 1 8	0 . 0 1 8 3 0 0
8 6 . 3 6 1 6 4 8	0 . 1 0 2 4 8 6 0 9	0 . 0 2 0 6 8 2
7 5 . 3 4 6 4 9 2	0 . 0 9 5 8 2 0 5 6	0 . 0 2 3 1 8 6
6 5 . 7 0 8 4 4 0	0 . 0 8 9 5 8 2 4 4	0 . 0 2 6 0 0 5
5 7 . 2 7 4 8 7 9	0 . 0 8 3 7 4 3 5 7	0 . 0 2 9 1 8 2
4 9 . 8 9 5 8 7 5	0 . 0 7 8 2 7 8 3 8	0 . 0 3 2 7 6 6
4 3 . 4 4 0 9 2 8	0 . 0 7 3 1 6 3 5 9	0 . 0 3 6 8 1 4
3 7 . 7 9 4 1 3 3	0 . 0 6 8 3 7 6 1 4	0 . 0 4 1 3 9 1
3 2 . 8 5 5 6 1 9	0 . 0 6 3 8 9 5 8 1	0 . 0 4 6 5 7 7
2 8 . 6 2 2 6 8 7	0 . 0 5 9 7 8 8 9 8	0 . 0 5 2 3 2 8
2 4 . 9 1 1 0 2 6	0 . 0 5 5 9 4 0 3 5	0 . 0 5 8 8 4 8
2 1 . 6 5 7 6 3 6	0 . 0 5 2 3 3 4 6 6	0 . 0 6 6 2 5 5
1 8 . 8 0 6 7 5 7	0 . 0 4 8 9 5 7 2 3	0 . 0 7 4 6 8 8
1 6 . 3 0 9 2 7 9	0 . 0 4 5 7 9 4 2 5	0 . 0 8 4 3 1 2
1 4 . 1 2 2 5 9 4	0 . 0 4 2 8 3 3 5 3	0 . 0 9 5 3 2 4
1 2 . 2 0 9 1 4 7	0 . 0 4 0 0 6 3 6 7	0 . 1 0 7 9 5 9
1 0 . 5 3 6 7 6 8	0 . 0 3 7 4 7 5 4 9	0 . 1 2 2 5 0 1
9 . 0 7 6 4 3 9	0 . 0 3 5 0 5 9 5 6	0 . 1 3 9 2 8 8
7 . 8 0 1 2 7 3	0 . 0 3 2 8 0 4 7 7	0 . 1 5 8 7 2 9
6 . 6 9 0 3 0 2	0 . 0 3 0 7 0 5 6 4	0 . 1 8 1 3 2 1
5 . 7 2 3 7 5 3	0 . 0 2 8 7 5 5 0 1	0 . 2 0 7 6 6 0
4 . 8 8 1 2 8 8	0 . 0 2 6 9 3 9 8 3	0 . 2 3 8 4 7 4
4 . 1 4 1 6 0 9	0 . 0 2 5 2 3 8 7 2	0 . 2 7 7 1 6 8
3 . 4 9 8 1 3 5	0 . 0 2 3 6 5 9 5 9	0 . 3 2 2 0 0 1
2 . 9 2 9 4 4 4	0 . 0 2 2 1 7 0 5 5	0 . 3 7 7 5 7 6
2 . 4 2 9 9 9 0	0 . 0 2 0 7 7 4 9 6	0 . 4 4 6 9 7 8
2 . 0 6 3 2 3 4	0 . 0 1 9 6 8 7 2 6	0 . 5 1 8 4 8 8
1 . 7 4 9 3 4 3	0 . 0 1 8 7 0 6 1 8	0 . 6 0 2 6 0 2
1 . 4 7 6 2 1 8	0 . 0 1 7 8 0 8 6 0	0 . 7 0 3 8 6 1
1 . 2 4 4 7 8 2	0 . 0 1 7 0 1 0 9 9	0 . 8 2 3 1 5 8
1 . 0 4 9 2 1 1	0 . 0 1 6 3 0 6 6 1	0 . 9 6 3 4 2 0
0 . 8 8 1 0 9 1	0 . 0 1 5 6 7 5 8 1	1 . 1 3 1 7 7 7
0 . 7 3 7 4 7 2	0 . 0 1 5 1 1 6 1 0	1 . 3 3 3 8 1 7
0 . 6 1 5 5 2 8	0 . 0 1 4 6 2 4 0 7	1 . 5 7 6 1 1 0
0 . 5 3 7 4 0 5	0 . 0 1 4 2 9 9 9 5	1 . 7 8 6 3 8 0
0 . 4 6 9 5 7 9	0 . 0 1 4 0 1 2 4 7	2 . 0 2 2 9 0 1
0 . 4 1 0 7 0 2	0 . 0 1 3 7 5 8 0 6	2 . 2 8 8 3 6 0
0 . 3 5 9 5 8 0	0 . 0 1 3 5 3 3 2 8	2 . 5 8 5 6 6 1
0 . 3 1 4 0 5 6	0 . 0 1 3 3 2 9 9 2	2 . 9 2 7 4 4 4
0 . 2 7 4 6 3 3	0 . 0 1 3 1 5 1 2 7	3 . 3 0 9 8 2 8
0 . 2 4 0 4 6 2	0 . 0 1 2 9 9 4 4 4	3 . 7 3 6 8 4 2
0 . 2 1 0 0 8 8	0 . 0 1 2 8 5 3 4 3	4 . 2 2 6 1 1 9
0 . 1 8 3 8 0 1	0 . 0 1 2 7 3 0 1 2	4 . 7 7 2 2 4 9
0 . 1 6 0 4 7 8	0 . 0 1 2 6 1 9 7 2	5 . 3 9 7 4 3 3
0 . 1 4 0 3 1 1	0 . 0 1 2 5 2 3 4 7	6 . 0 9 5 2 2 6
0 . 1 2 2 8 4 8	0 . 0 1 2 4 3 9 5 3	6 . 8 7 3 1 1 2
0 . 1 0 7 3 5 2	0 . 0 1 2 3 6 4 5 5	7 . 7 6 2 2 1 9
0 . 0 9 3 9 3 9	0 . 0 1 2 2 9 9 3 0	8 . 7 3 1 1 0 1
0 . 0 8 2 3 1 2	0 . 0 1 2 2 4 2 4 4	9 . 8 3 6 4 4 4
0 . 0 7 1 9 8 7	0 . 0 1 2 1 9 1 7 4	1 1 . 0 9 9 1 2 5
0 . 0 6 3 0 3 9	0 . 0 1 2 1 4 7 6 2	1 2 . 5 0 8 0 4 5
0 . 0 5 5 2 7 4	0 . 0 1 2 1 0 9 2 1	1 4 . 0 7 9 1 9 3
0 . 0 4 8 3 7 4	0 . 0 1 2 0 7 4 9 7	1 5 . 8 7 4 3 7 7
0 . 0 4 2 3 8 7	0 . 0 1 2 0 4 5 1 8	1 7 . 8 7 9 4 4 0
0 . 0 3 7 1 8 4	0 . 0 1 2 0 1 9 2 4	2 0 . 1 1 8 0 0 0
0 . 0 3 2 5 5 9	0 . 0 1 1 9 9 6 1 3	2 2 . 6 7 7 7 8 0
0 . 0 2 8 5 4 4	0 . 0 1 1 9 7 6 0 3	2 5 . 5 4 1 0 2 2
0 . 0 2 5 0 5 1	0 . 0 1 1 9 5 8 5 1	2 8 . 7 4 2 8 1 0
0 . 0 2 2 0 0 8	0 . 0 1 1 9 4 3 2 4	3 2 . 3 2 2 3 1 7
0 . 0 1 9 3 1 4	0 . 0 1 1 9 2 9 7 0	3 6 . 4 1 9 4 6 6
0 . 0 1 6 9 8 5	0 . 0 1 1 9 1 7 9 8	4 1 . 0 0 9 7 1 9

Figure III - II-32.

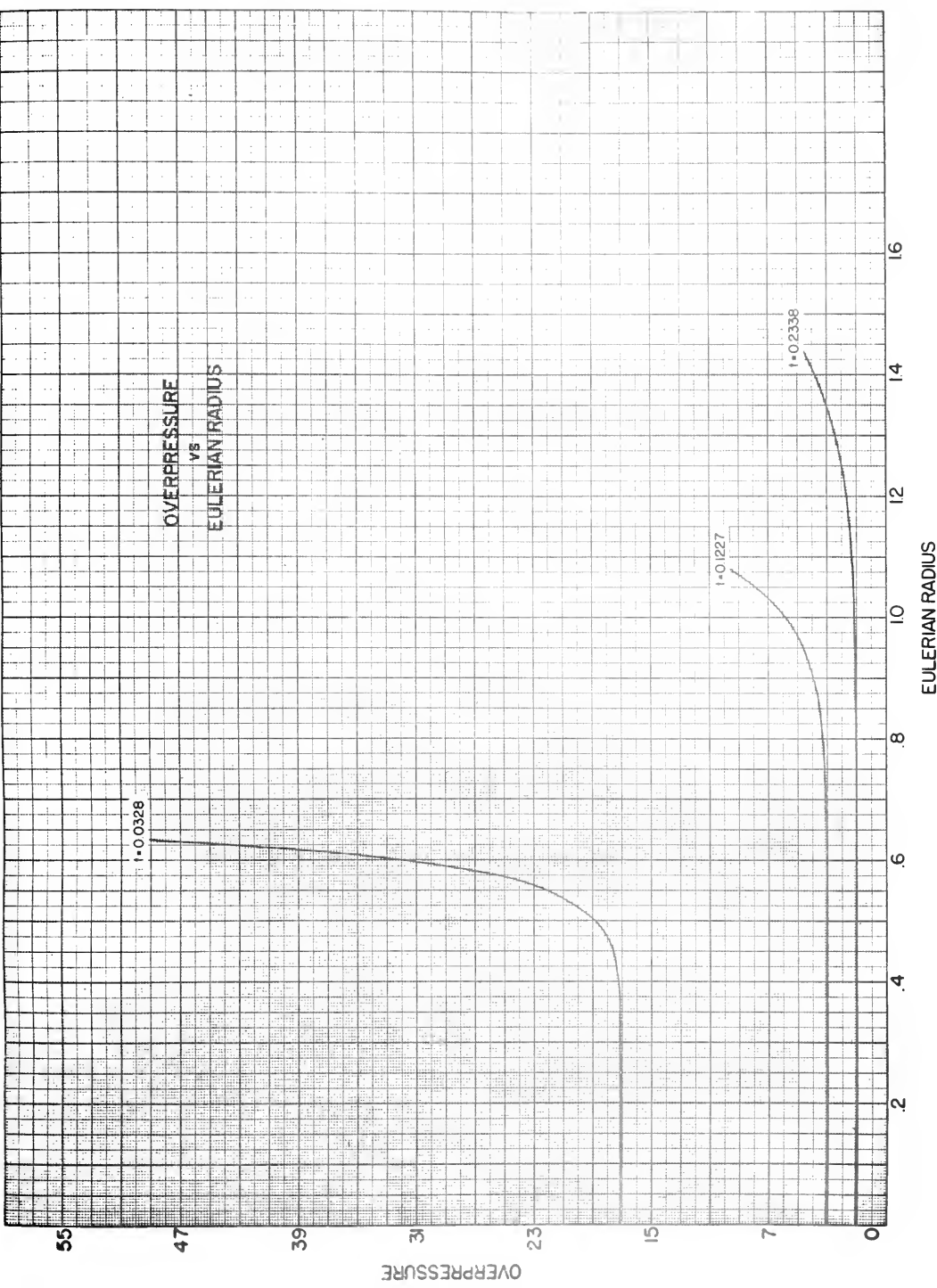


Figure IV - II-33

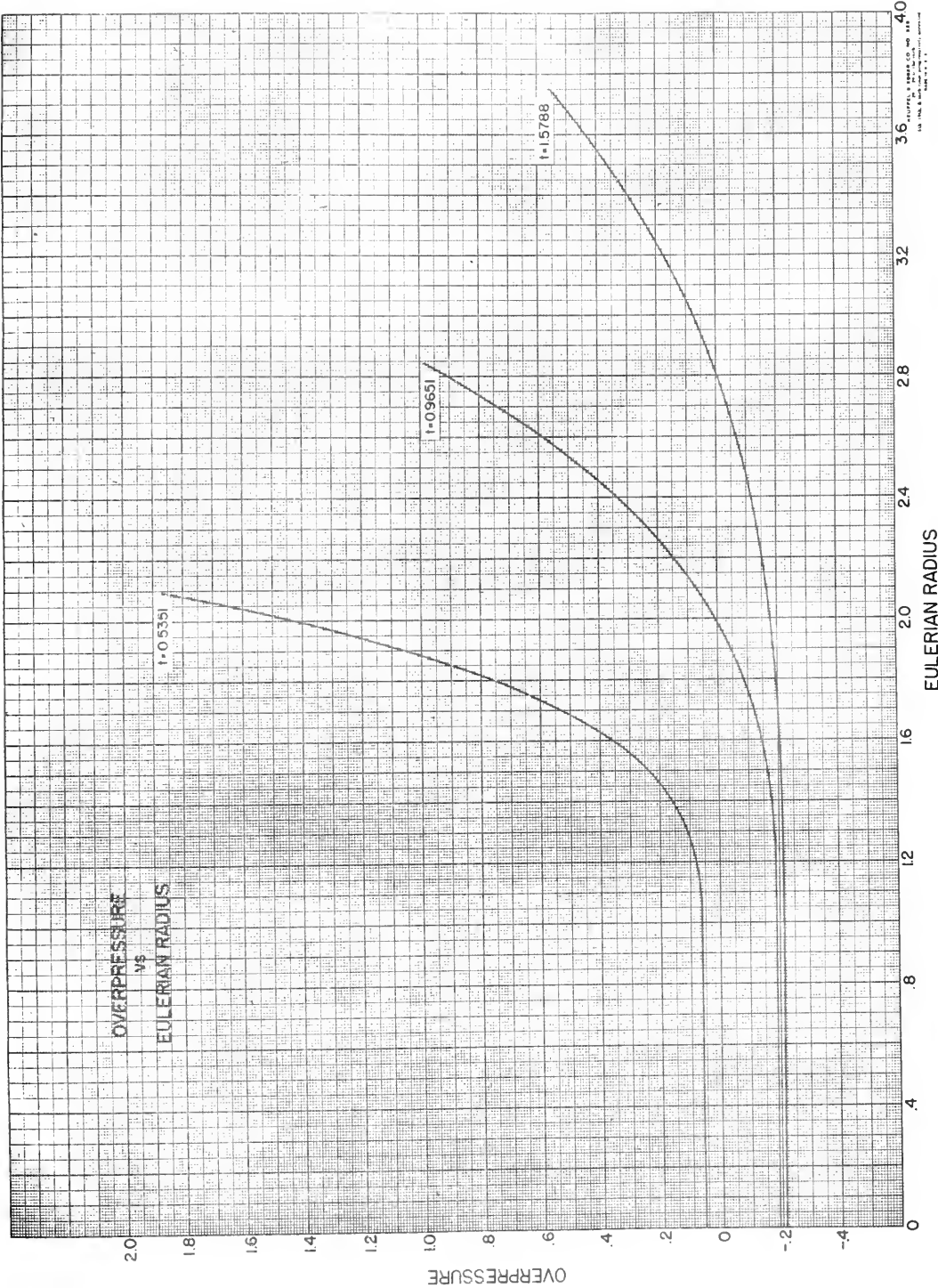


Figure V - II-34.

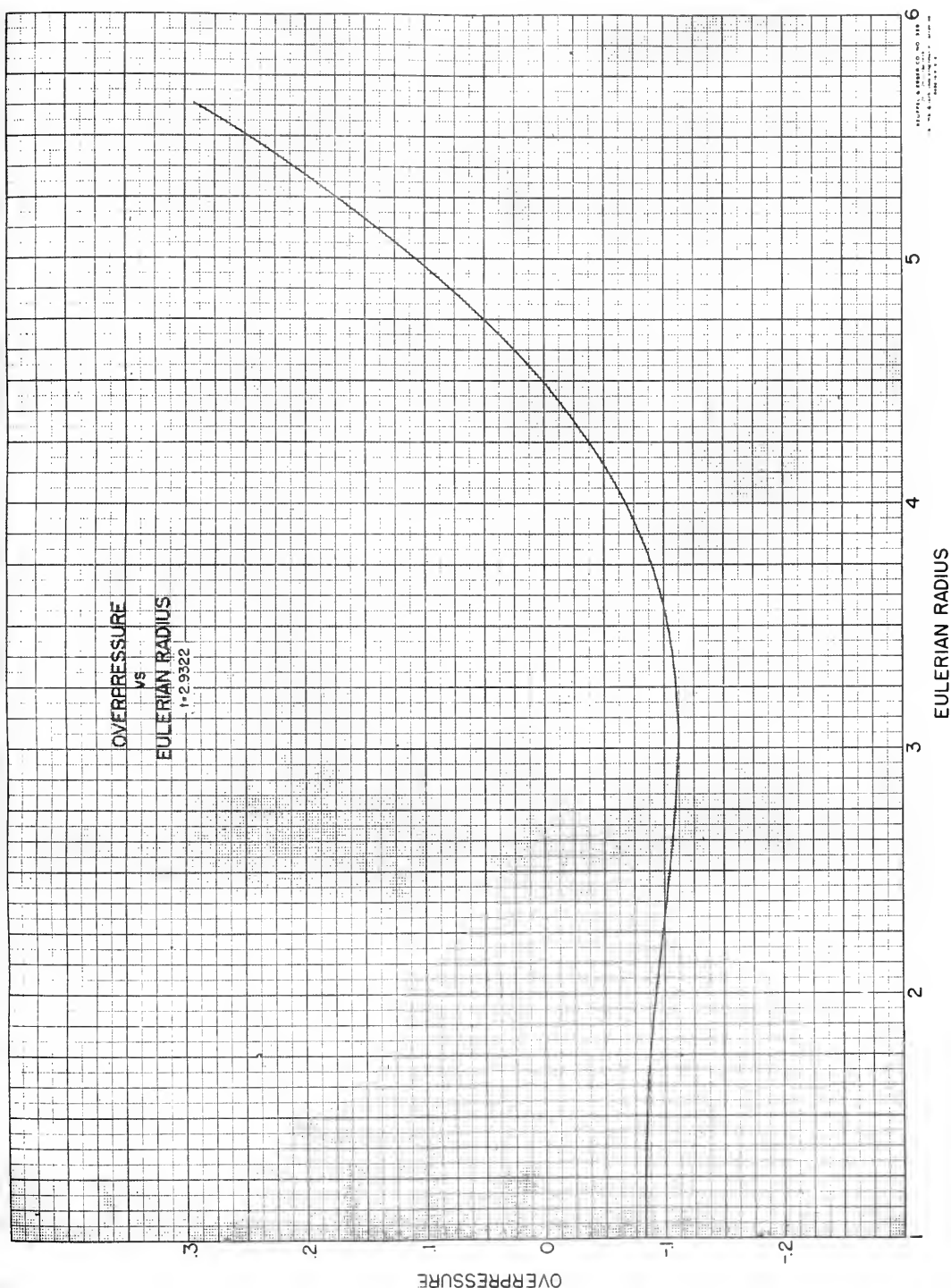


Figure VI - II-35.

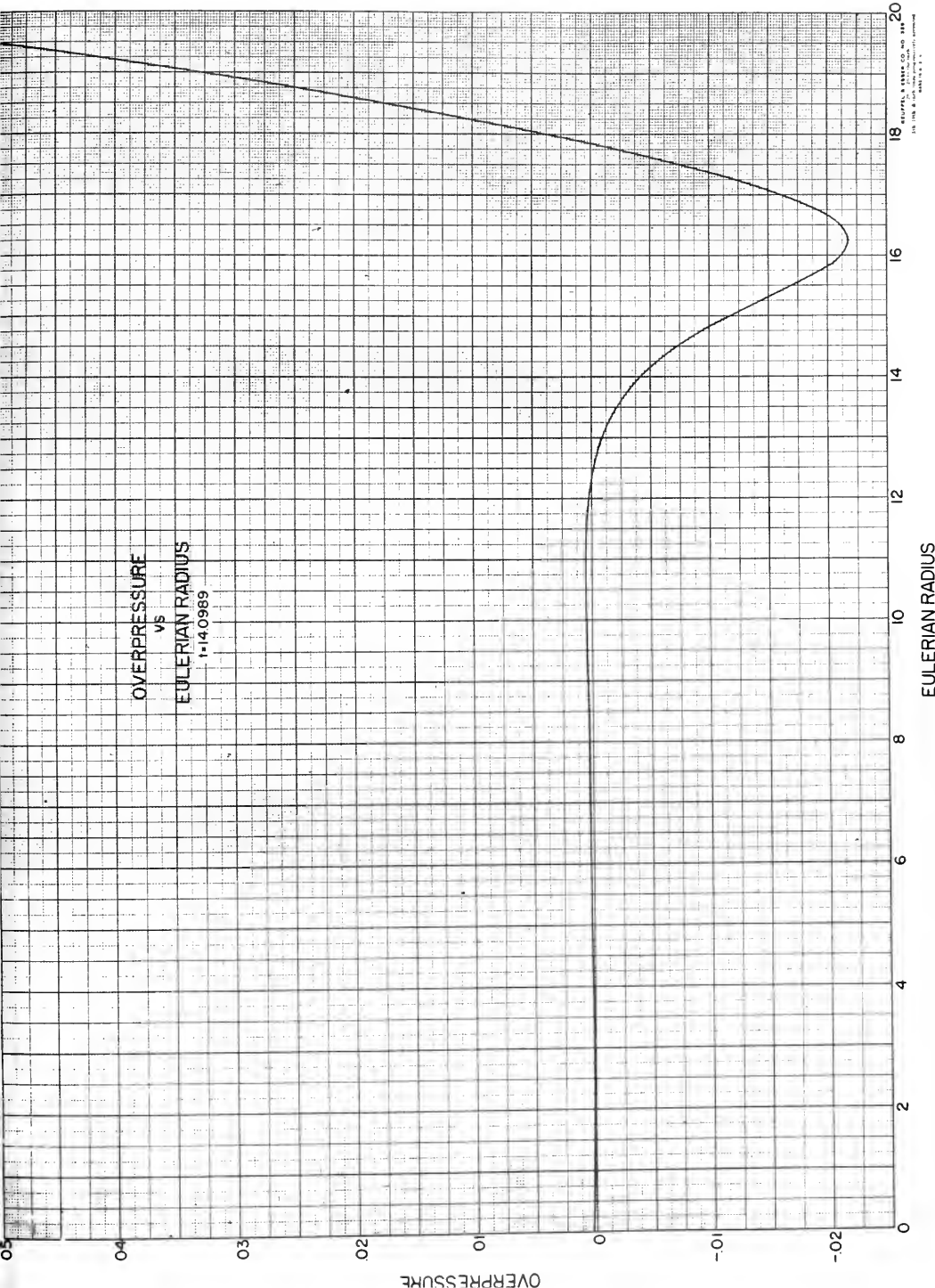


Figure VII - II-36.

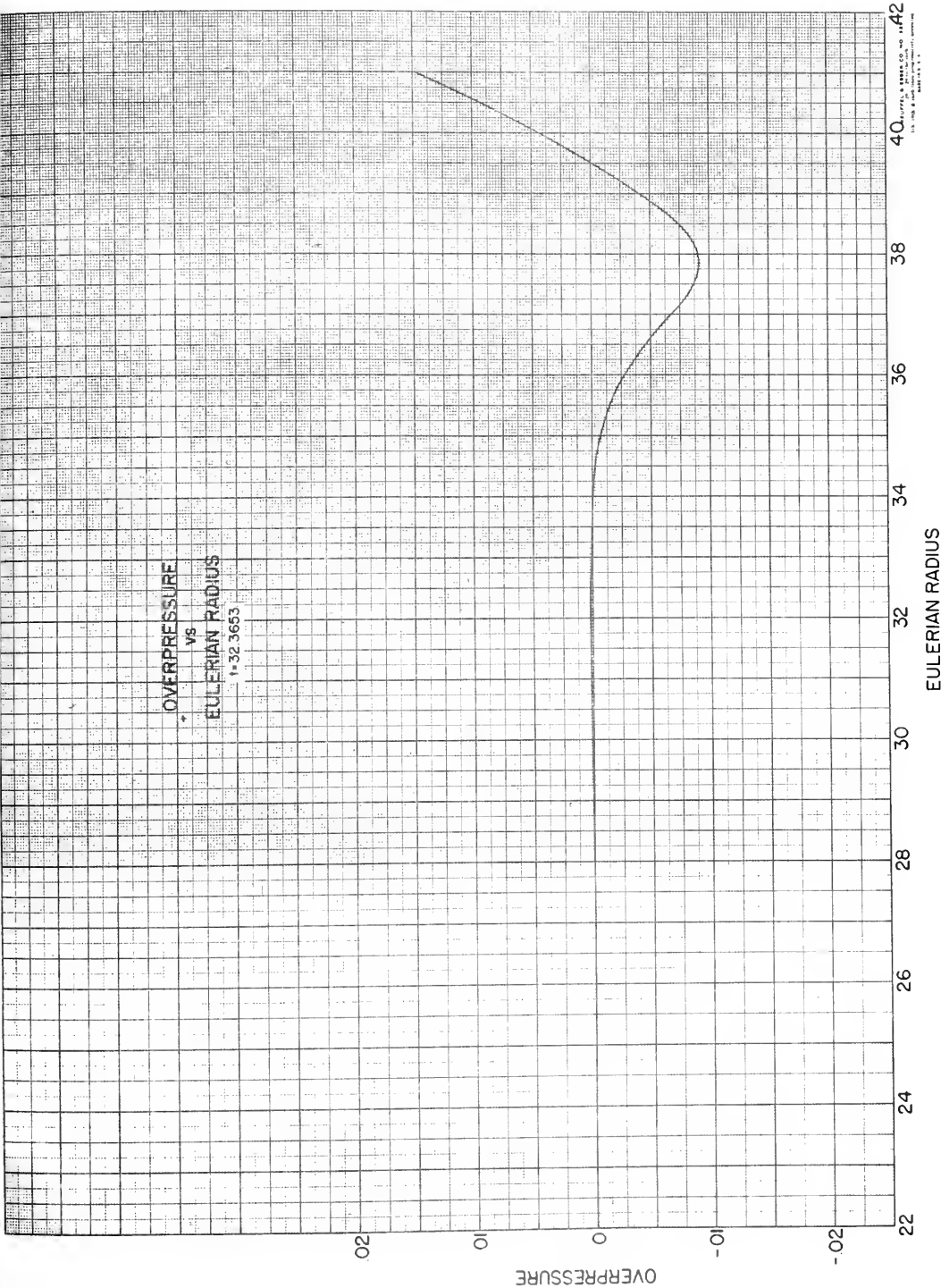




Figure VIII - II-37.

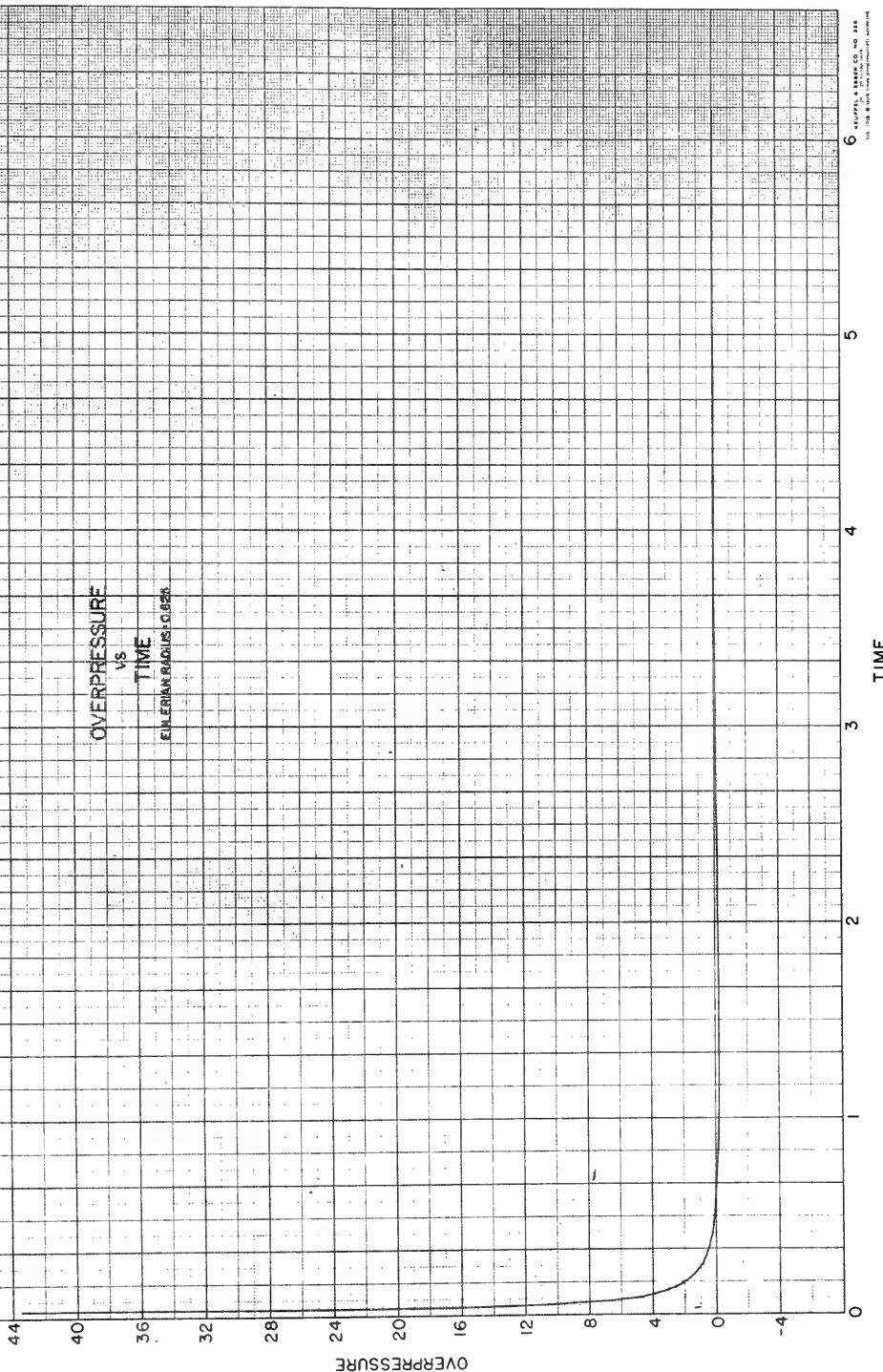
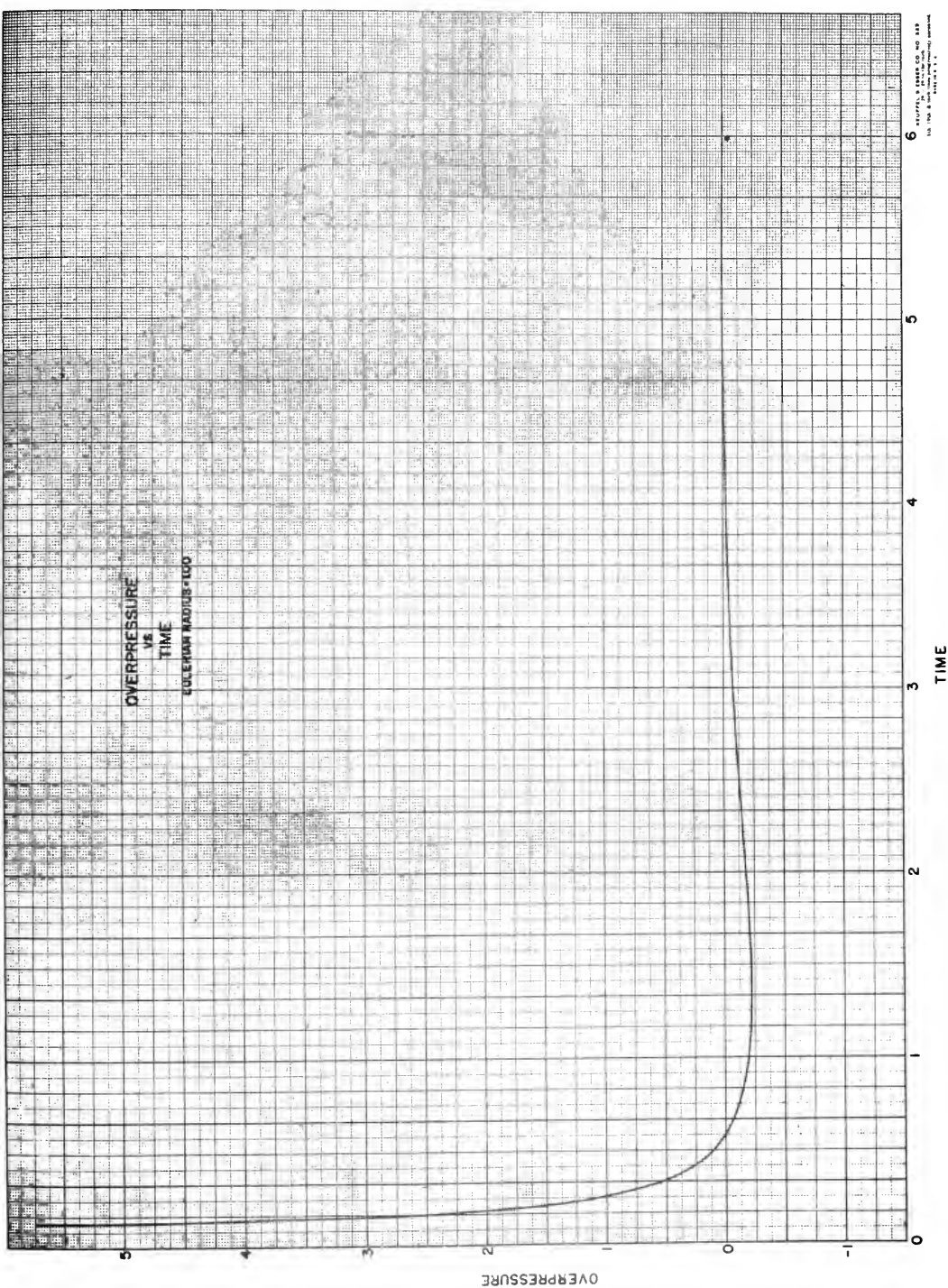


Figure IX - II-38.



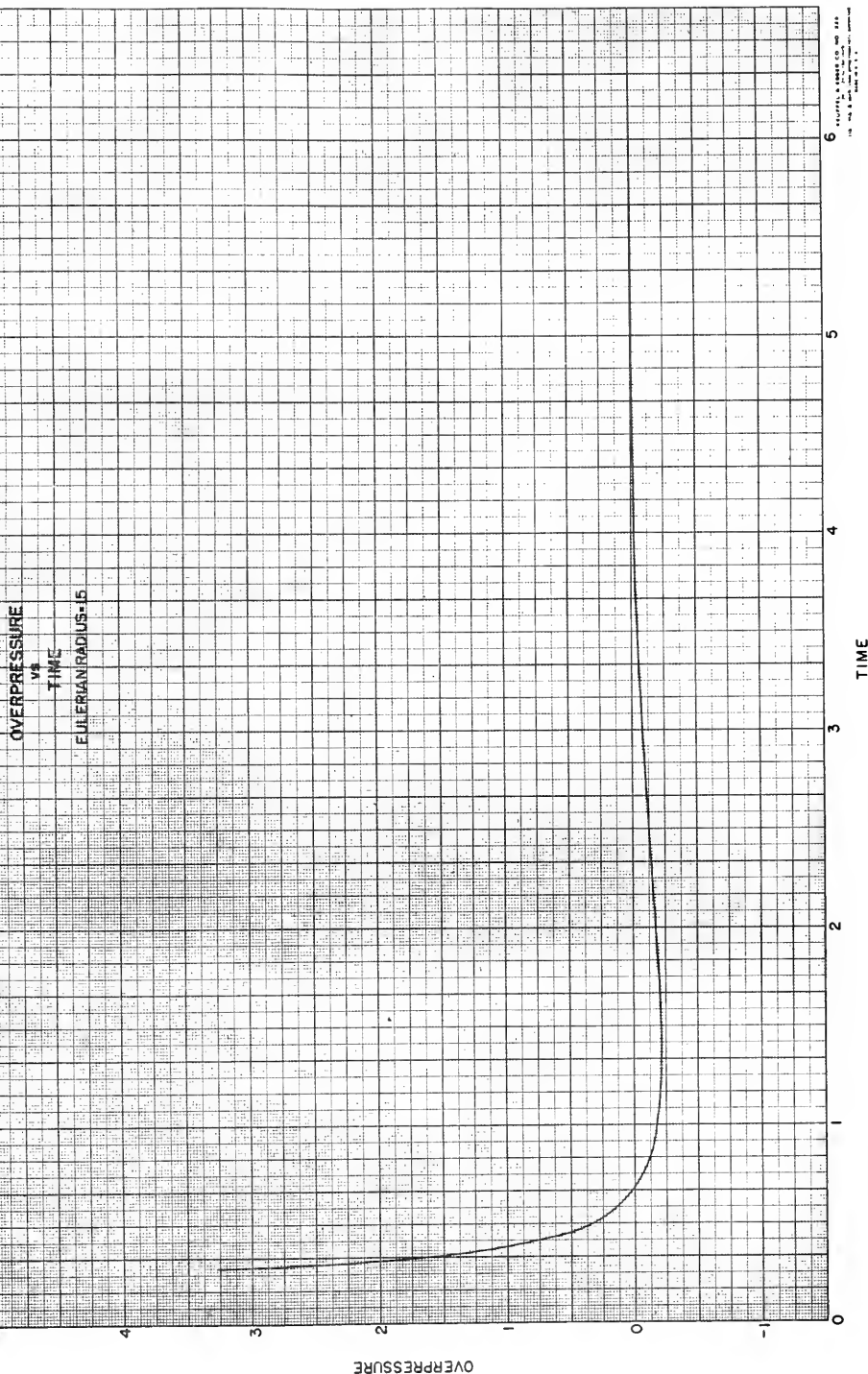


Figure XI - II-40.

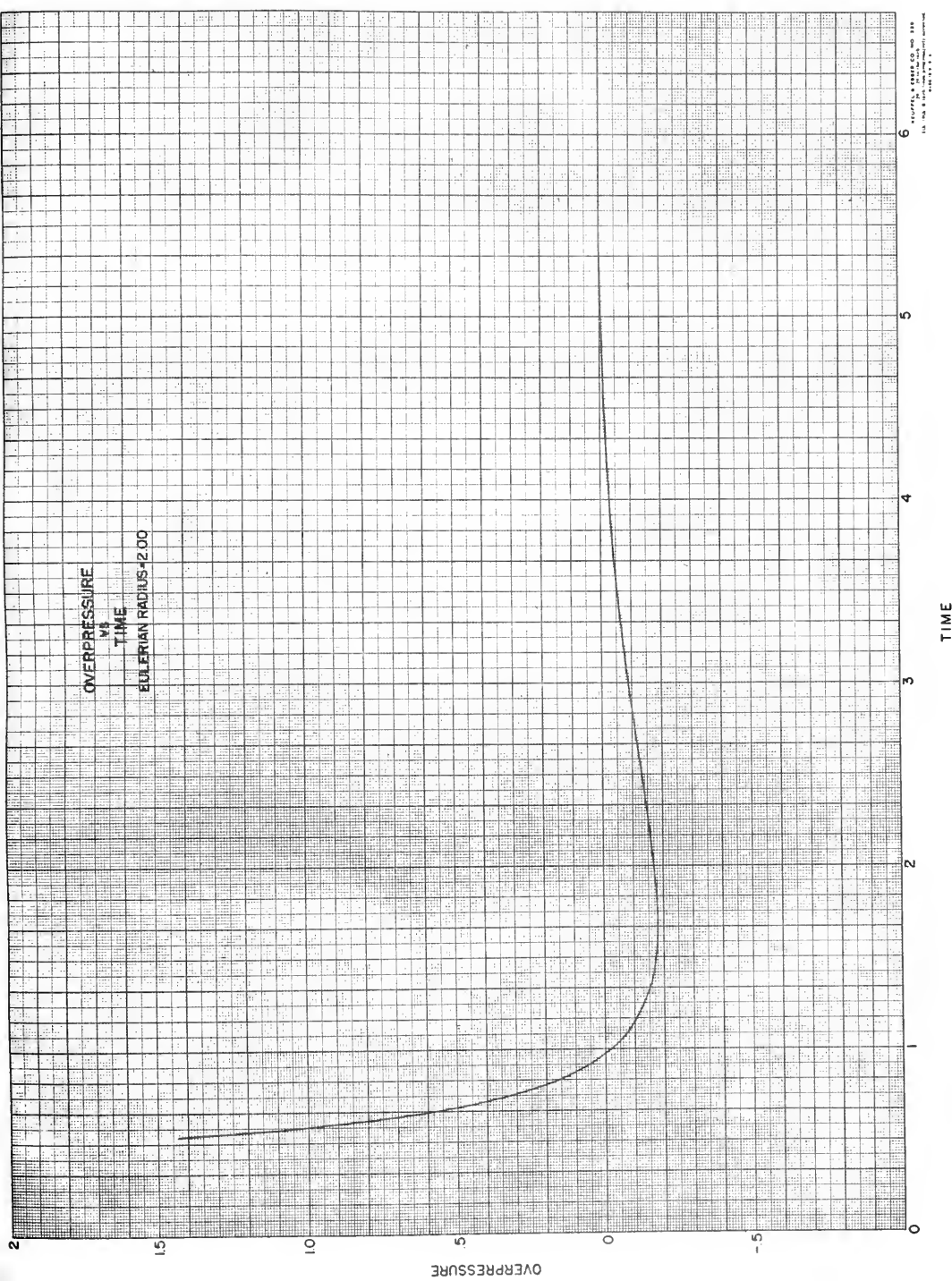


Figure XII - II-41.

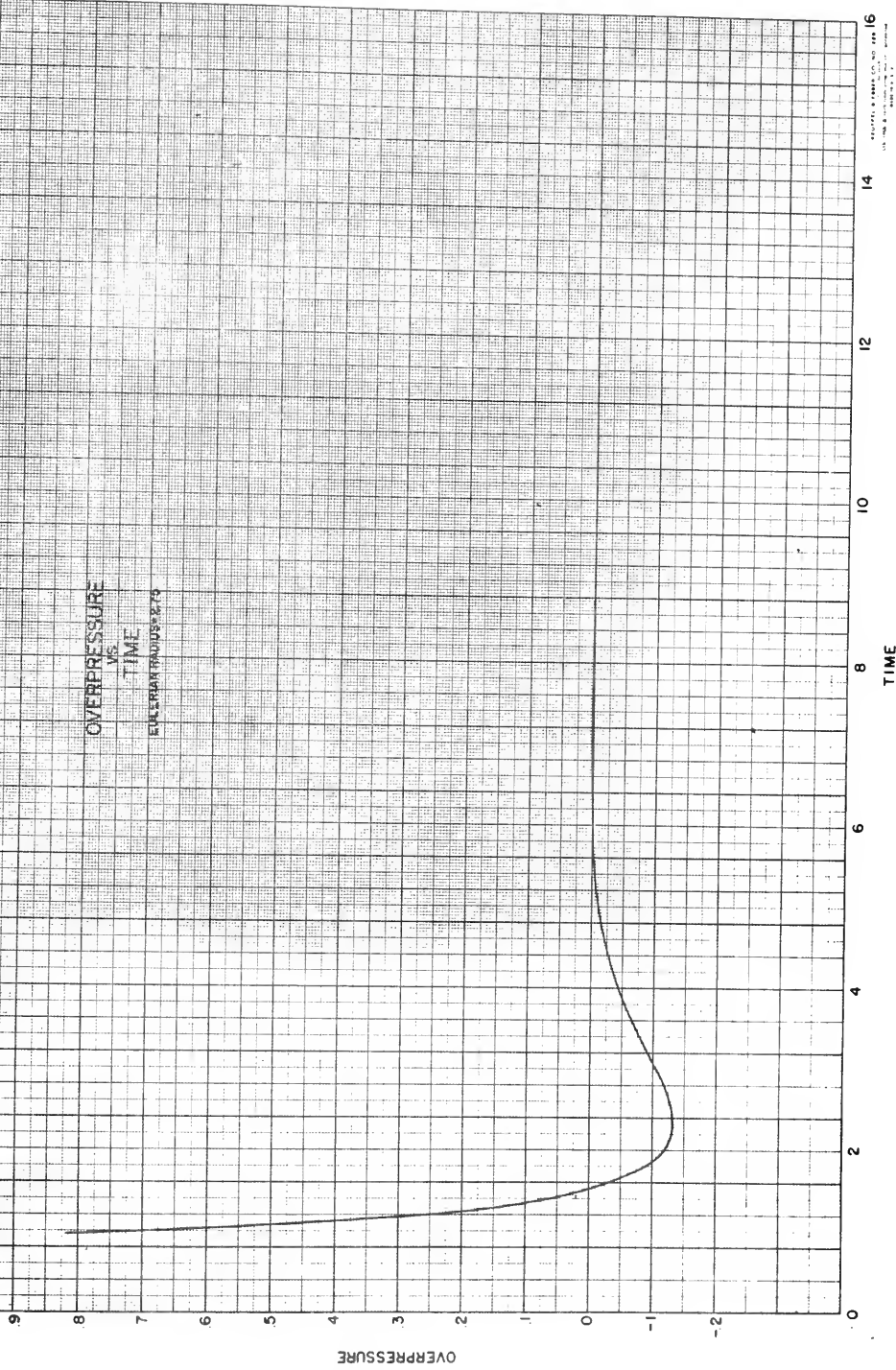


Figure XIII - II-42.

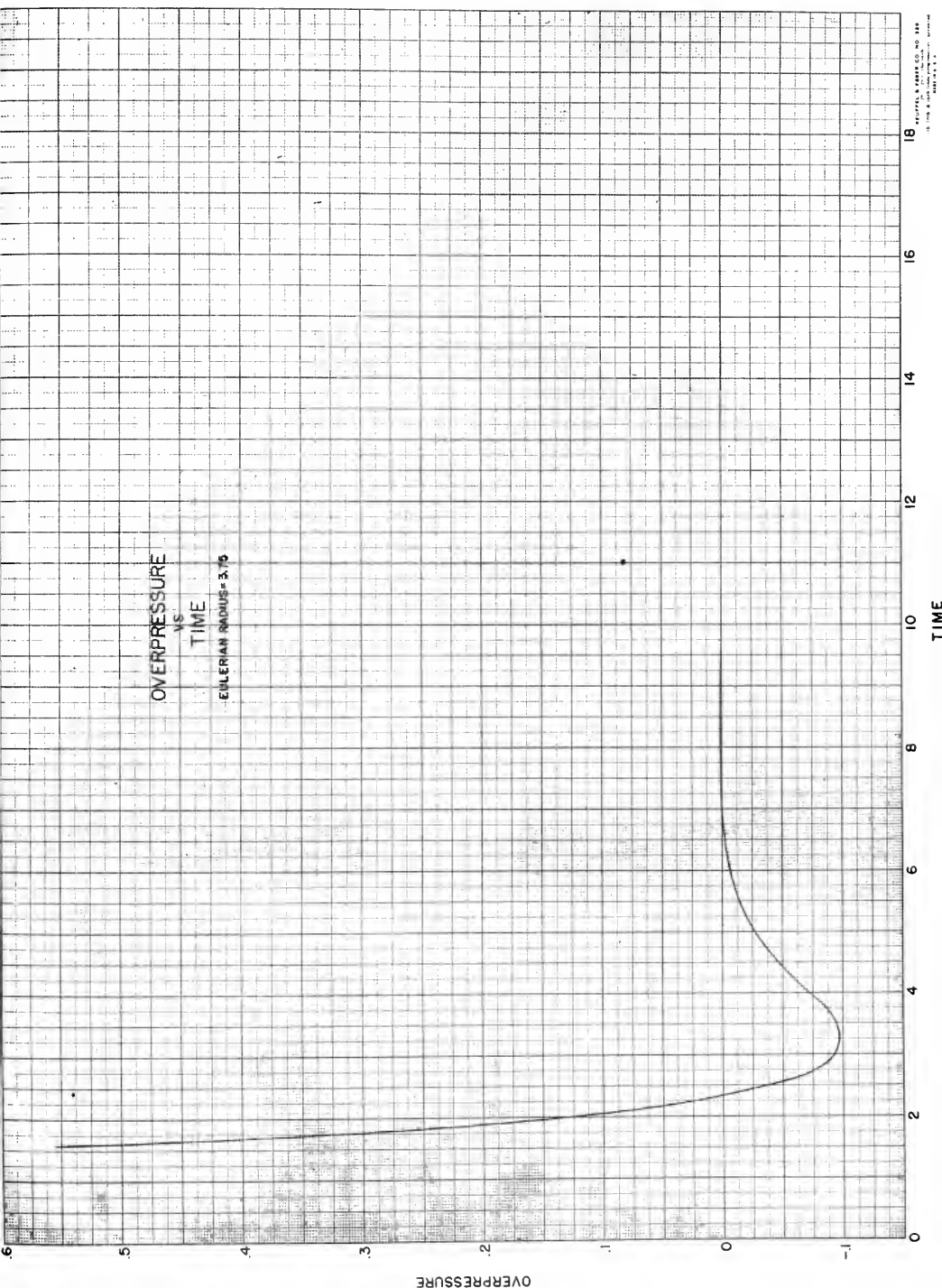


Figure XIV - II-43.

OVERPRESSURE
vs
TIME
EUERIAN RATIO=1.00

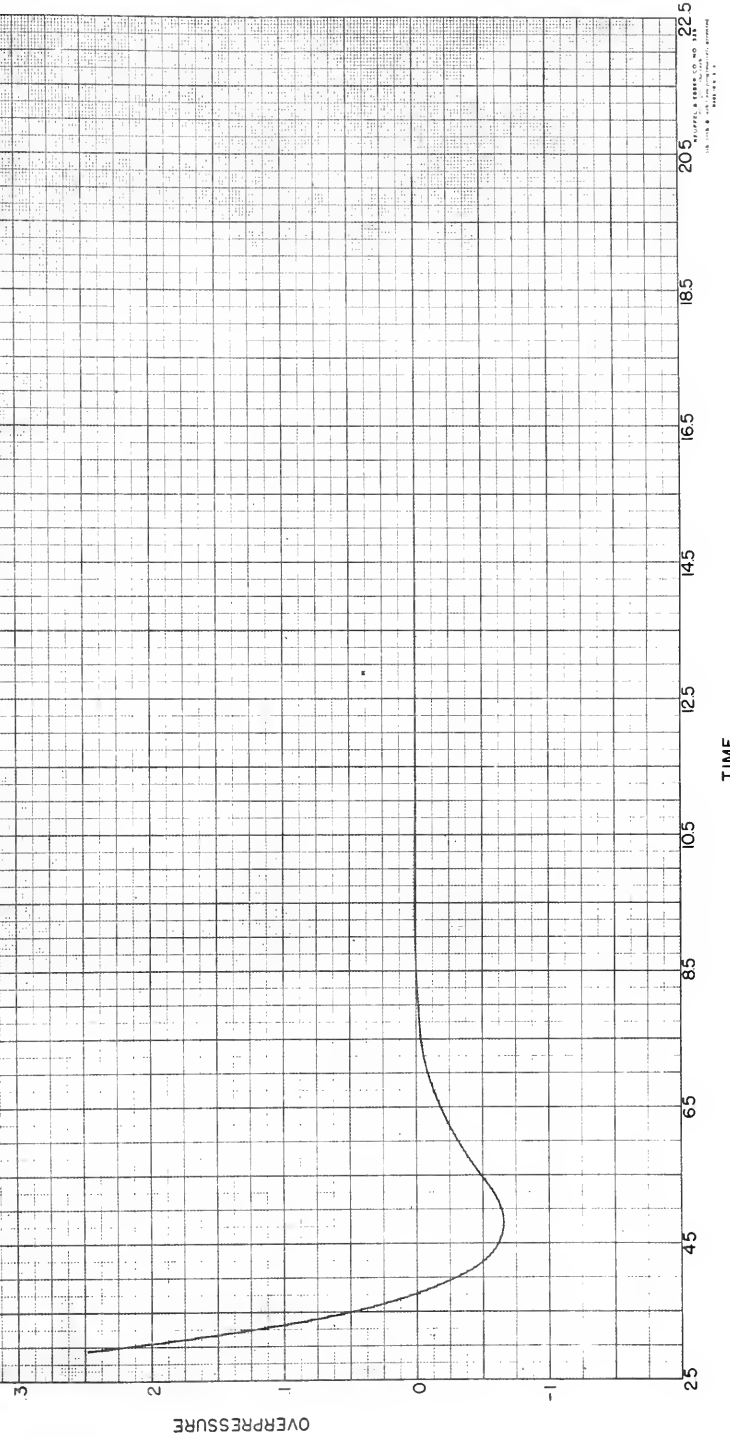


Figure XV - II-44.

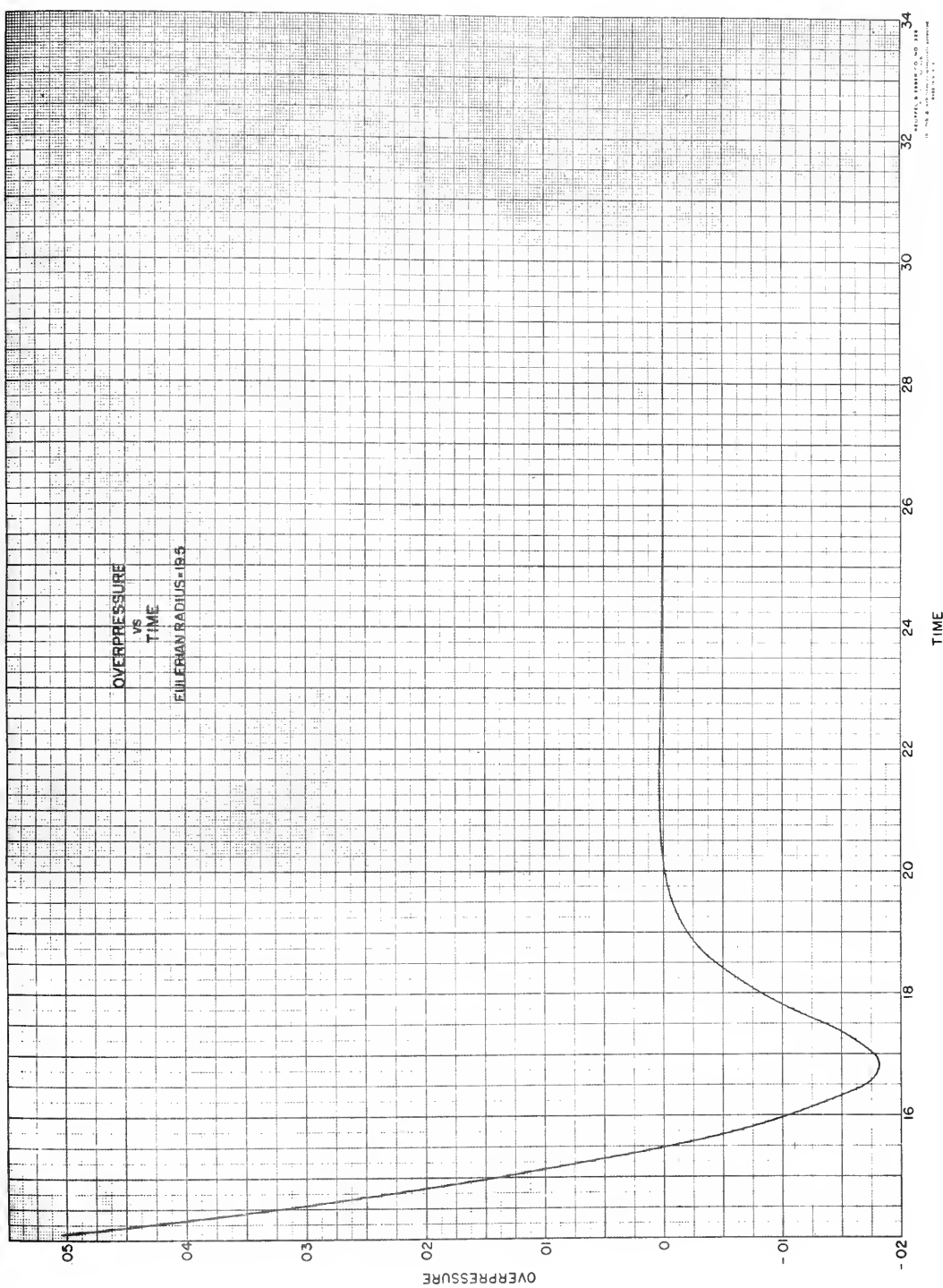


Figure XVI - II-45.

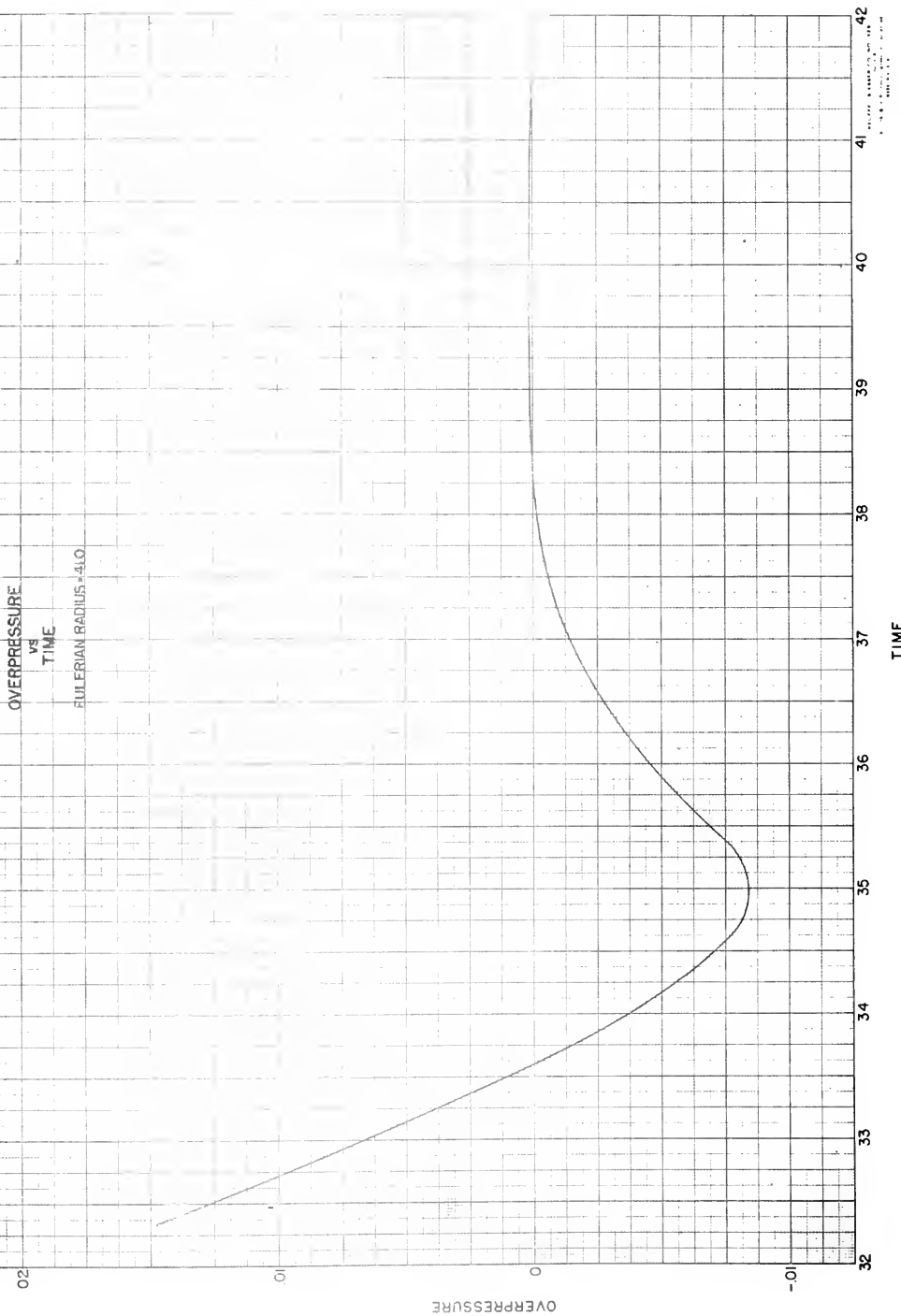


Figure XVII - II-46.

LENGTH OF POSITIVE PHASE
vs.
SHOCK RADIUS

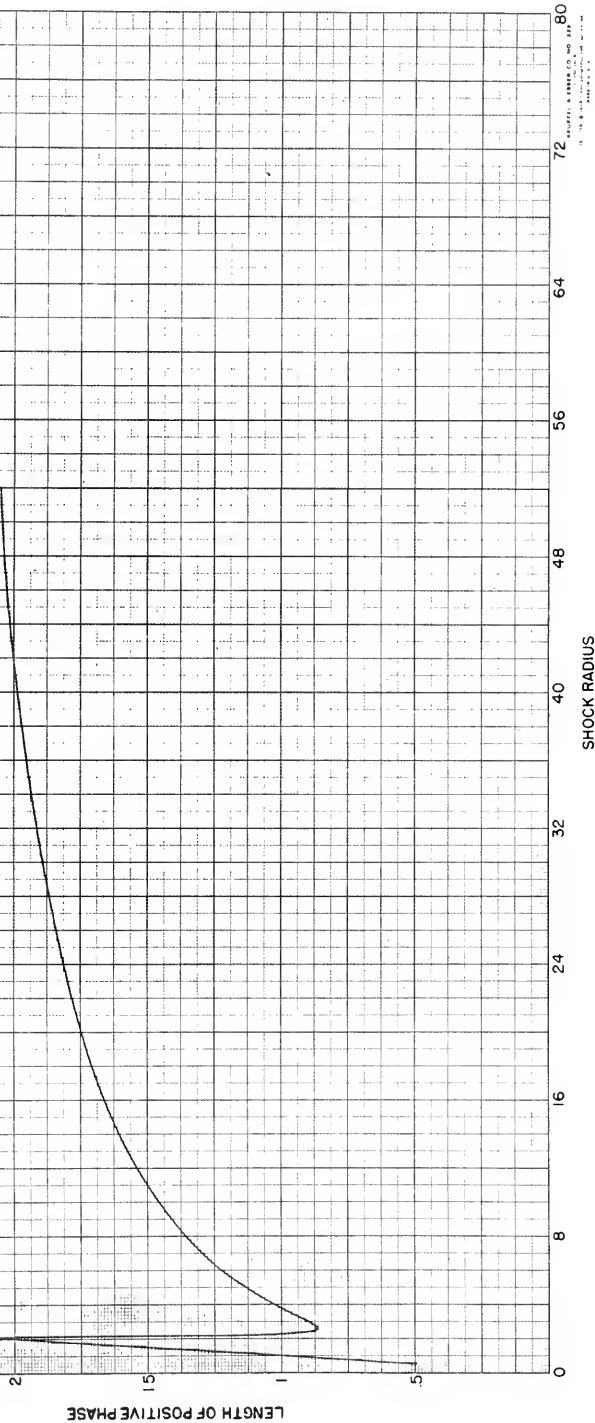
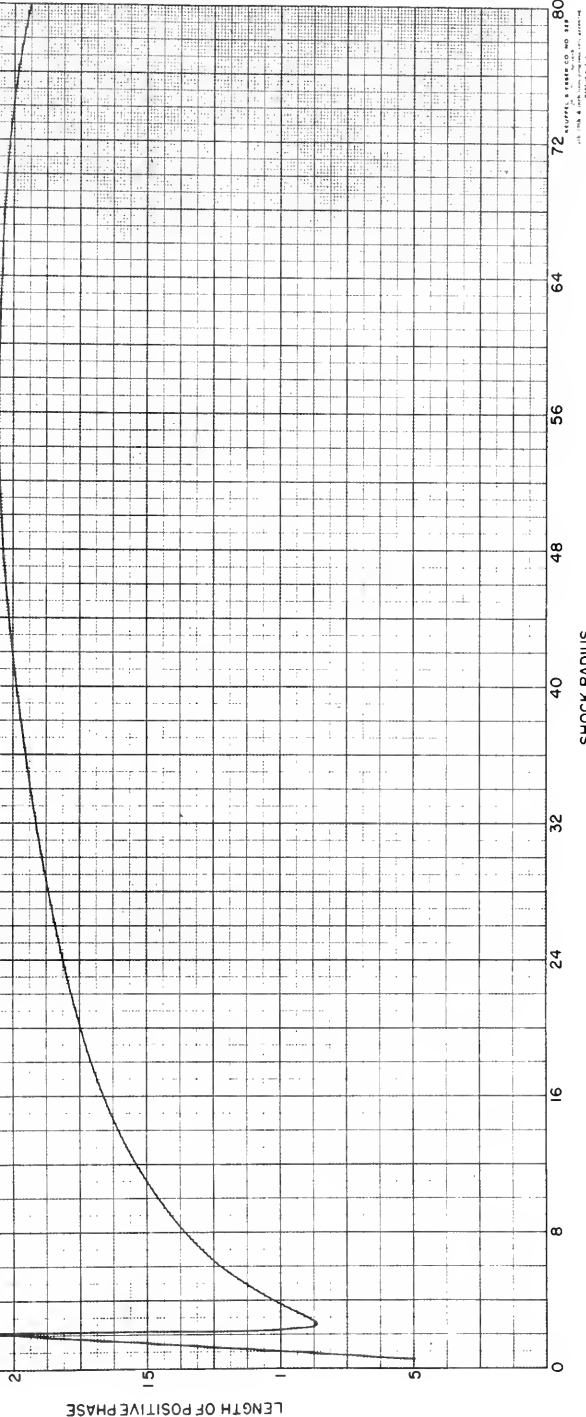


Figure XVIII - II-47.

LENGTH OF POSITIVE PHASE
vs
SHOCK RADIUS



B. CONTINUED FRACTION EXPANSIONS OF ALGEBRAIC NUMBERS*

0. Summary.

Every real irrational number x has a unique infinite simple continued fraction expansion

$$\begin{aligned} x = a_1 + \cfrac{1}{a_2 + \cfrac{1}{a_3 + \dots}} &\equiv a_1 + \cfrac{1}{a_2 + \cfrac{1}{a_2 + a_3 + \dots}} \\ &= [a_1, a_2, a_3, \dots] \end{aligned}$$

where the a_i are integers, positive for $i > 1$; conversely every such infinite simple continued fraction represents a unique real number. (A rational number has two trivially different finite simple continued fraction expansions.)

Among the irrational numbers the quadratic surds are distinguished as those whose simple continued fraction expansions are eventually periodic -- for example, $\sqrt{3} = [1, 1, 2, 1, 2, \dots] = [1, \overline{1, 2}]$.

The question naturally arises as to whether there are any evident peculiarities in the simple continued fraction expansions of other algebraic numbers. As material for such an inquiry, extensive expansions of given algebraic numbers were desired. Codes for producing them have been written and used on the IAS computer, and work is in progress on additional codes.

The first code written dealt with the case next beyond the quadratic, that is, with cubic irrationalities. With modifications of this code, the continued fraction expansions of $\sqrt[3]{2}$ to 2232 terms and of

* A portion of this problem has been submitted in a preliminary note to MATHEMATICAL TABLES AND OTHER AIDS TO COMPUTATION for publication.

$3^{1/3}$ to 500 terms were obtained. (The modifications chiefly involved methods of checking the computations in the face of memory difficulties related to the high memory reference repetition rates characteristic of this code.)

A code is now being written which generalizes, from 3 to n , the degree D of the polynomial defining the algebraic irrationality, and which also incorporates error-detecting-and-correcting facilities. Additional production of results is planned when this more general code is available.

The results so far obtained have been examined, without any obvious peculiarities being noticed. In addition, certain statistics have been tabulated, such as the frequency distribution, sum, and geometric mean of the first 2000 partial quotients of $2^{1/3}$.

Khintchine and Levy have given some probabilistic results on the distributions of the sum $S_n(x)$ and of the geometric mean $G_n(x)$ of the first n partial quotients, and of the n th root of the denominator of the n th convergent, of random numbers x uniformly distributed between 0 and 1. The results for the sum are of an essentially weaker type than those for the two other variables mentioned.

For example, for almost all x -- i.e., except on an exceptional set of measure zero -- $G_n(x)$ approaches an absolute constant K . One may ask whether or not a given number belongs to this exceptional set (evidently most if not all quadratic surds do belong to it). However, the theorems do not in themselves provide numerical estimates of the distribution functions of $G_n(x)$, so that the interpretation of a $G_n(x)$, computed from a finite number of partial quotients of a given x , is still open.

1. The continued fraction algorithm for real algebraic irrationalities.

It is desired to find the simple continued fraction expansion of a real irrational x defined as a root $y = x$ of an integral polynomial $P(y)$ of degree D . We will suppose that x is > 1 and is the largest root of $P(y)$ (if not, the first step of the algorithm would need a small modification).

Suppose that the property, "there is given an integral polynomial $P_n(y_n)$, of degree D in the indeterminate y_n , having $y_n = x_n = [a_n, a_{n+1}, \dots]$ as its sole root > 1 ," holds for $n = h$. Then the integral part of x_h is the desired h -th partial quotient, a_h , characterized as the largest integer a for which $\operatorname{sgn} F(a) \neq \operatorname{sgn} F(+\infty)$. Let $y_h = a_h + 1/y_{h+1}$. Then it is easily shown (since $x_h = a_h + 1/x_{h+1}$) that if

$$P_{h+1}(y_{h+1}) = y_{h+1}^D \cdot P_h(a_h + 1/y_{h+1})$$

then the above property holds for $n = h + 1$. Letting $P_1(y_1)$ be $P(y)$, all the a_n and P_n are then defined inductively. The above procedure is the algorithm used for determining the partial quotients.

2. Outline of the basic code.

Each step of the algorithm is seen to consist of three types of operations with polynomials F of degree D :

- (1) determination of the largest a ($= a_h$) for which $\operatorname{sgn} F_h(a) \neq \operatorname{sgn} F_h(+\infty)$
- (2) translation of the independent variable by a_h ,
- (3) inversion of the independent variable.

The computer must be coded to accomplish a sequence of these steps.

As the induction index h increases, the coefficients of the polynomials tend to increase, and quickly exceed the 40-binary-digit word

length of the computer. Hence it is necessary to define a representation of large numbers as p -tuples of computer words. At any stage of the computations for an irrationality of degree D , we need $D+1$ such multiple-word length numbers, and it may be useful, but is not essential, to have an additional one as a working space. It is convenient to represent these $D+1$ or $D+2$ numbers with a common multiplicity p ; to avoid waste of machine time in the early part of the computations (since computation time is nearly proportional to p), p is made variable, starting at 1 and increased only as necessary, as the coefficients grow. (Eventually the coefficients grow to occupy all the storage available for them. This limits the length to which any particular non-periodic expansion can be computed, since the computer has a finite memory.)

A chief requisite for the continued fraction code is the provision of subroutines for doing the necessary arithmetic on multiple word-length (MWL) numbers. Since MWL arithmetic demands codewise lengthy methods of accomplishing mathematically simple operations, it pays in the present codes to keep the basic multiple-word-length-arithmetic subroutines (MWL SRs) free of multiplication orders (for time economy), and limited in variety and complexity of purpose (for coding and memory-space economy), relying on controlling subroutines to call the MWL SRs as needed to synthesize less simple operations.

The operations chosen for realization as MWL SRs are: left shift and right shift (i.e., multiplication by specified positive or negative -- or zero -- powers of 2), and addition. Each MWL SR is entered with a three-parameter word specifying the MWL operands -- or operand and number of shifts -- and the location of the MWL result.

The determination of a_n (≥ 1) is effected binary-digit-wise, by

ascertaining first the position of the most significant digit (1) of x_h , and then the presence or absence of 1 in each successively less significant position (down through the units position); or stated differently, by successively determining and subtracting from x_h the highest remaining power of 2 (down through 2^0). The translation by a_h , from $P_h(x_h)$ as a polynomial in x_h to $P_h(a_h + z_h)$ as a polynomial in z_h ($= x_h - a_h$) is made stepwise, by powers of 2, as the corresponding digits of a_h are determined.

Each test of a polynomial $F(u)$ to determine whether $\operatorname{sgn} F(2^k) \neq \operatorname{sgn} F(+\infty)$, followed by a translation by 2^k in case the inequality holds, is in practice carried out by testing a polynomial $F^*(v) \equiv F(2^k v)$ to determine whether $\operatorname{sgn} F^*(1) \neq \operatorname{sgn} F^*(+\infty)$, followed by a translation by 1 in case the inequality holds. Starting from a P_h , the exponent k of the scale factor 2^k is first increased (from 0) until the highest power of 2 in a_h is found, then decreased to 0 while the remaining powers of 2 are found.

The inversion, converting $P_h(a_h + z_h)$ into $P_{h+1}(y_{h+1}) \equiv y_{h+1}^D \cdot P_h(a_h + 1/y_{h+1})$, where $z_h = 1/y_{h+1}$, consists merely in interchanging the coefficients of each two terms whose degrees in z_h add to D .

In this manner the inductive step, of determining a_h and P_{h+1} from P_h , is reduced to a combination of the elementary polynomial operations:

- (a) replacing $F(u)$ by $F^*(v) = F(2v)$
- (b) replacing $F(u)$ by $F^*(v) = F(v/2)$
- (c) replacing $F(u)$ by $F^*(v) = F(1+v)$
- (d) replacing $F(u)$ by $F^*(v) = v^D \cdot F(1/v)$
- (e) testing whether $F(1) \neq F(+\infty)$.

These operations on polynomials can in turn be broken down into operations,

by the three MWL SRs, on their coefficients. (In the original code these breakdowns were made in extenso for the case $D = 3$. In the more general code in progress, and in an intermediate check-code already written and used, they are done inductively, and are valid for arbitrary D .)

Thus the inductive step of the algorithm is constructed. With its incorporation into a repetitive process, and the addition of input, output, and other peripheral facilities (such as the periodic read-out of the coefficients, from which the code could be re-started at a later time), the basic program is complete.

3. Checking facilities.

For results to be reliable it is essential to have methods of checking them. At first with a new code the concern is with the correctness of the coding; then in production the concern is with the accuracy of the machine calculations. Among the possible methods of checking are the following:

- (1) Duplication: that is, making supposedly the same computation twice, and examining whether the results are identical;
- (2) Using two somewhat different methods which should give the same results, and examining whether the results are identical;
- (3) Using a redundancy check; that is, some property (not used directly in performing the codes) which should hold among the intermediate or final results.

In the continued fraction codes, a large fraction of the computation time is spent in the inner loops of the MWL SRs, where corresponding operations are performed on one segment after another of the two or three MWL numbers involved. These loops have few orders, with no multiplications

or divisions, and therefore have a high memory-reference repetition rate. A well-known hazard ("read-around") of cathode-ray tube memories is that frequent reference to the same memory locations may endanger the contents of nearby locations which are not concurrently referred to; one way of conventionally avoiding this danger is to isolate the high-reference-rate locations, by a buffer zone of unused locations.

In spite of such isolation of the inner loops of the MWL SRs, the continued fraction code has at times been more than usually subject to machine errors, some of which have even been duplicated. The evidence strongly suggests that the errors occur in the memory, and are related to the high memory-reference repetition rate, but their nature remains obscure; they are not of the type usually designated as read-around, and have not been so troublesome with other codes.

In the continued fraction code (more than in some other codes) a certain type of machine error is propagated with increasing effect through all later calculations; so that no errors can be tolerated.

As a check on machine operation, method (1), while wasteful of time, is simple, and is an effective detector of certain machine errors. No results have been accepted without at least this check. Against the above-mentioned errors, which repeated in identical circumstances (even though the overall error rate was low), duplication offers no protection. It is no check at all on the coding.

Method (2) is also wasteful of time; but by imposing a different pattern of computations or of digits, or a restated logic, it could show up some types of coding errors, and in the detection of machine errors is safer than duplication. In this problem it was early applied, primarily as a code check, by slightly changing the basic code so that

instead of the polynomials P_h , there were produced in one case $3^h \cdot P_h$, in another case $k \cdot P_h$. The agreement or proper relationship between results was a partial confirmation of the correctness of the MWL SRs (which were also checked by cases), since compensating errors would be unlikely to occur in such different numbers.

A method of type (3), which is appropriate for the continued fraction codes, is to check the arithmetic on the MWL numbers by performing analogous arithmetic on their residues to some modulus, which for convenience has been taken as $(2^{39} - 1)$, and comparing the results. This process is fast, compared to the main computation, since it deals with single-word-length, instead of MWL, coefficients. Although it does not check all phases of a computation, it does give positive protection against the greatest hazard, the change of a single binary digit in some coefficient (it could also show up some types of coding errors). A check code using this process (for general degree D) was written, and used to check the results already produced. The generalized main code now being written incorporates the check, concurrent with the main computation, so that if an error is detected, the computation may be restarted immediately from a just previous point; this will be more efficient than a post-mortem method.

Additional results will be produced when this more general and efficient code is available.

C. MAGNETOHYDRODYNAMIC THEORY OF SOLAR SPICULES

This problem is being computed for Dr. Schlüter, Dr. Schwarzschild, and Mr. Lautman of the Princeton University Observatory.

Spicules or jets are relatively small (6" of arc) disturbances of the solar chromosphere which are characterized by an increasing rate of outward propagation and a short lifetime of the order of two minutes. Knowledge is urgently needed on the nature of spicules since it is now thought that they transport energy to the corona.

In this theory the spicule begins as a pressure variation at the base of the chromosphere. In the absence of a magnetic field this would create an ordinary spherical sound wave in the isothermal chromosphere. However, the effect of a magnetic field on a disturbance in the highly conductive gas gives rise to the phenomenon known as magnetohydrodynamic waves (see Alfven, Cosmical Electrodynamics, Oxford, 1950). The velocity of propagation of these waves is inversely proportional to the square root of the density, hence in the very high density gradient of the chromosphere the propagation velocity of the wave will increase greatly as it progresses.

The basic equations of this problem are:

$$1. \quad \vec{E} = -\vec{v} \times \vec{H} \quad (\vec{I} = \sigma (\vec{E} + \vec{v} \times \vec{H}) \text{ with } \sigma = \infty)$$

$$2. \quad \nabla \times \vec{E} = -\frac{\partial \vec{H}}{\partial t}$$

$$3. \quad \nabla \times \vec{H} = 4\pi \vec{j} \quad \left(\frac{\partial \vec{v}}{\partial t} \ll \vec{j} \right)$$

$$4. \quad \rho \frac{d\vec{v}}{dt} = \vec{j} \times \vec{H} - \nabla P - \rho \nabla \phi \quad (\text{equation of motion})$$

$$5. \frac{\partial \rho}{\partial t} = - \nabla \cdot (\rho \vec{v}) \quad (\text{equation of continuity})$$

The assumptions made are:

1. Plane-parallel chromosphere.
2. Barometric density gradient ($\rho \sim e^{-cz}$).
3. Small vertical extent ($\nabla \Phi = g = \text{const.}$).
4. Axial symmetry ($E_\phi = v_\phi = 0, E_z = E_s = J_z = J_s = 0$).
5. Homogeneous vertical magnetic field of value H_0 .
6. All changes adiabatic.

Assumption 6. leads to another basic equation, the adiabatic equation:

$$6. \frac{dP}{dt} = \gamma \frac{P}{\rho} \frac{d\rho}{dt}$$

Under these assumptions the basic equations are expanded and linearized, and the following non-dimensional variables defined:

$$r = \frac{g}{c^2} s, \quad y = \frac{g}{c^2} z, \quad \tau = \frac{g}{c} t, \quad c^2 = \frac{P_0}{\rho_0} = \text{const.}$$

$$w = \frac{c^2}{sg} \rho_0 v_s, \quad v = \rho_0 v_z, \quad B = \frac{H_0^2}{c^2 \rho_0} = B_0 e^y$$

P_0 = undisturbed pressure

ρ_0 = undisturbed density

The linearized equations then take the form:

$$7. \frac{\partial^2 w}{\partial \tau^2} = B \left[\frac{\partial^2 w}{\partial r^2} + \frac{3}{r} \frac{\partial w}{\partial r} \right] + \frac{\partial^2}{\partial y^2} (Bw) - \frac{1}{r} \frac{\partial}{\partial r} (\frac{\dot{P}}{g})$$

$$8. \frac{\partial^2 v}{\partial \tau^2} = - \frac{\partial}{\partial y} (\frac{\dot{P}}{g}) - \frac{c^2}{g} \dot{\rho}$$

$$9. - \frac{c^2}{g} \dot{\phi} = r \frac{\partial W}{\partial r} + 2W + \frac{\partial v}{\partial y}$$

$$10. - \frac{\dot{P}}{g} = -v \frac{c^2}{g} \dot{\phi} + (\gamma - 1) v$$

Equations 7-10 may be combined to yield the final differential equations of the problem:

$$11. \frac{\partial^2 W}{\partial r^2} = (B + v) \left[\frac{\partial^2 W}{\partial r^2} + \frac{3}{r} \frac{\partial W}{\partial r} \right] + \frac{\partial^2}{\partial y^2} (BW) + \frac{v}{r} \frac{\partial^2 v}{\partial r \partial y} \\ + (\gamma - 1) \frac{1}{r} \frac{\partial v}{\partial r}$$

$$12. \frac{\partial^2 v}{\partial r^2} = v \frac{\partial}{\partial y} (r \frac{\partial W}{\partial r} + 2W) + v \left(\frac{\partial^2 v}{\partial r^2} + \frac{\partial v}{\partial y} \right) + r \frac{\partial W}{\partial r} + 2W .$$

The right-hand sides of (11) and (12) are converted to finite-difference relations by the equations $r = R \Delta r$ ($0 \leq R \leq 15$) and $y = Y \Delta y$ ($0 \leq Y \leq 17$) by means of the usual definitions of the space-derivatives. B becomes $B_0 e^{Y \Delta y}$. $e^{\Delta y}$ is computed at the beginning of the problem, and with each succeeding vertical increment is multiplied by $e^{\Delta y}$ to give its proper value. The computation of $e^{\Delta y}$ is simplified by means of the following expansion

$$e^{\Delta y} = (((\frac{\Delta y}{4} + 1) \frac{\Delta y}{3} + 1) \frac{\Delta y}{2} + 1) \Delta y + 1 .$$

The initial conditions are:

$$P = P_0 e^{-\alpha(r^2+y^2)} \quad (\text{pressure "hump"})$$

$$W = V = 0 \quad (\text{all velocities equal zero})$$

Therefore initially 7. becomes

$$\frac{\partial W}{\partial r} = - \frac{1}{gr} \frac{\partial P}{\partial r}$$

and 8. with the aid of 9. becomes

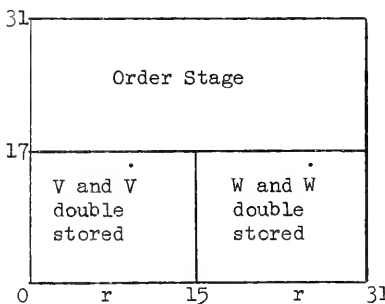


$$\frac{\partial V}{\partial \tau} = - \frac{1}{g} \frac{\partial P}{\partial y} .$$

We are now able to compute the initial values of W and V at all points in the field. To simplify the boundary conditions the wave is put in a "box", i.e. horizontal velocities vanish at vertical boundaries and vertical velocities vanish at horizontal boundaries. The singularities in W at $r = 0$ are removed by means of an expansion valid in this region.

W and V for each time step are computed from the formulae $\dot{X}^{T+1/2} = \dot{X}^{T-1/2} + \Delta \tau \dot{X}^T$ and $X^{T+1} = X^T + \Delta \tau \dot{X}^{T+1/2}$. Since in the final equations the only time-dependent term is \dot{X} and $\dot{X}^{T=0}$ is known from the initial conditions, it is a very simple matter to compute each succeeding time step from the one before.

The 32×32 place memory of the computer is divided for the purpose of this problem into three fields as shown in the following diagram.

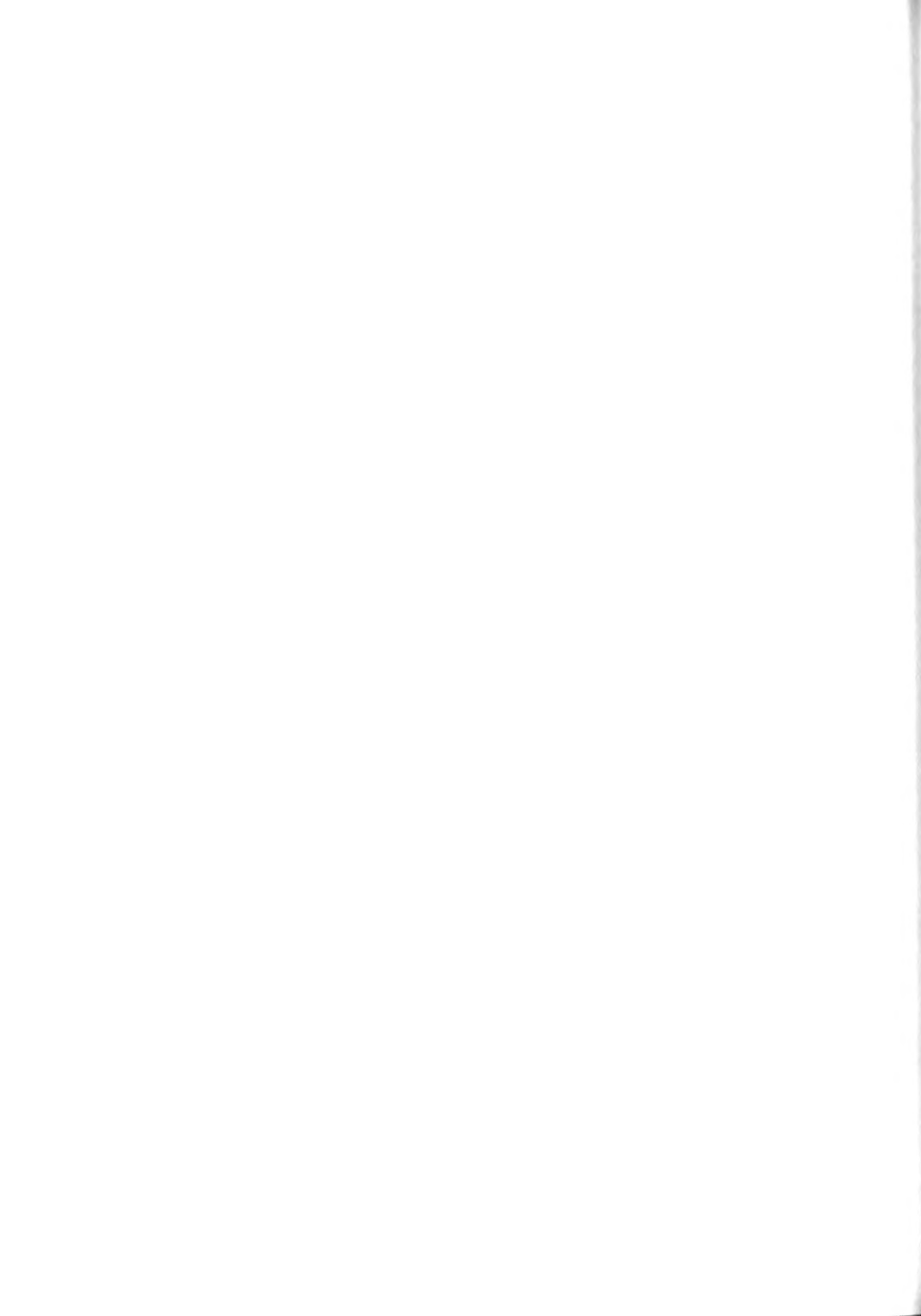


At each point in the field $\Delta \tau \dot{W}$ and $\Delta \tau \dot{V}$ are computed and added to W^T and V^T to give W^{T+1} and V^{T+1} , these quantities being stored in the second half of each word. After all points have been computed we have W^T in the first phase and W^{T+1} in the second phase. The same is true for V . The computer is then made to sweep through the whole

bottom part of the memory, multiplying the second phase of each word by ΔT and adding the result to the first phase. This then gives us the new W and V at all points. This two-step procedure is more efficient than a single scan over the field giving an immediate computation of the new W's and V's, the second method requiring complicated shift procedures.

Since there is not enough room in the memory (the magnetic drum was not in operation at the time this problem was coded), a conversion code was not incorporated, the results being punched out in binary form. The results are then converted in a separate operation. Five quantities are required at each point, W, \dot{W} , V, \dot{V} , and $\dot{\phi}$, however, we are only able to store the first four for all points. It would be very time-consuming to place the five quantities in temporary storage and punch out point-by-point as the computation proceeds. Therefore, the computation of $\dot{\phi}$ by 9. is incorporated in the conversion code. Thus it is only necessary to punch out 48 cards containing 1152 quantities as against 288 cards containing 1440 quantities. Punchouts are made every twelfth time step. In addition, a supplementary one-card-punchout is made containing the volume integrals of $\dot{\phi}$ for each of the 12 time steps. This is a check to see that the enclosed mass remains constant.

Two integrations have been performed and others are pending. One integration was performed with $B = 0$ (no magnetic field) and the expected spherical wave resulted. Another integration was performed with a magnetic field, but the results have not been analyzed as yet. The pending integrations will test the coarseness of the time increments for the second integration above as well as observe the effect of different magnetic field strengths both on the above density gradient field and on a homogeneous density field.



D. CALCULATION OF THE ENERGY BAND STRUCTURE OF IRON WITH APPLICATION
TO THE THEORY OF FERROMAGNETISM.

The fundamental problem of solid state physics is the calculation of the energy values and wave functions of electrons in a solid. On this basis it should be, in principle, possible to explain all the observed electronic behavior of solids. But because a solid contains so very many electrons, a rigorous calculation, which would have to consider some 10^{23} mutually interacting particles for a sample of ordinary size, is utterly out of the question.

The most common approximation which is made in order to reduce the problem to tractable dimensions is that the wave function for the solid can be written as some simple combination of "one-electron" functions -- functions which depend only on the co-ordinates and the spin of one particle. This wave function has to satisfy the requirements of anti-symmetry imposed by the Pauli exclusion principle; the wave function of the system must be anti-symmetric under the interchange of the coordinates and spin of any two electrons. A form of the wave function which satisfies this requirement is the determinantal; the wave function is written as a determinant of one-electron functions, one for each energy state:

$$\Psi(x_1, \dots, x_n, s_1, \dots, s_n) = \frac{1}{\sqrt{n!}} \begin{vmatrix} u_1(x_1, s_1) & \dots & u_1(x_n, s_n) \\ \vdots & & \vdots \\ u_n(x_1, s_1) & \dots & u_n(x_n, s_n) \end{vmatrix}$$

The quantities $x_1 \dots x_n$ are the coordinates of the n electrons, and the quantities $s_1 \dots s_n$ are their spin.



According to the minimum theorem of quantum mechanics the best possible wave function of the system will be obtained by minimizing the expectation value of the energy with respect to small variations of the one-electron function $u_j(x_i, s_i)$ (providing these functions remain normalized and orthogonal). This variation procedure leads to an equation for the one-electron functions:

The Hamiltonian operator can be written as

$$H = \sum_{i=1}^M \left(-\frac{\hbar^2}{2m} \nabla_i^2 + \sum_{\ell=1}^N V_\ell(r_i) + \frac{e^2}{2} \sum_{j \neq i} \frac{1}{r_{ij}} \right)$$

in which i and j refer to the position of the electrons, and ℓ refers to the atoms. $V_\ell(r_i)$ is the potential energy for electron i in the field of atom ℓ , nucleus plus core, (if there are low lying states which are not altered by presence of other atoms). The equations obtained by the minimization are the Hartree-Fock equations

$$H(x_i) u_i(x_i) + e^2 \left(\sum_j \int |u_j(x_2)|^2 \frac{1}{r_{12}} dx_2 \right) u_i(x_i) - e^2 \sum_j \left(\int u_j^*(x_2) u_i(x_2) \frac{1}{r_{12}} dx_2 \right) u_j(x_i) = \epsilon_i u_i(x_i)$$

$H(x_i)$ contains the kinetic energy for electron i plus its potential energy in the field of all the nuclei. The quantity (ϵ_i) is the one-electron energy. The last term on the left, or exchange term vanishes unless the spin i = spin j .

It has been shown that the Hartree-Fock equations can be regarded as ordinary Schroedinger equations for the motion of electrons, each electron moving in a slightly different potential field, which is computed by electrostatics from all the changes of the system, positive and negative, corrected by the removal of an exchange charge, equal in magnitude to one electron, surrounding the electron whose motion is being investigated. In a solid, the periodic arrangement of the atoms causes,

by Bloch's theorem, a like periodicity of the one-electron functions which are solutions of the Hartree-Fock equations. To each wave function corresponds an energy level, and these levels are grouped in the energy bands.

The Hartree-Fock equations can be used as a basis for the theory of Ferromagnetism. Consider an unmagnetized crystal in which we reverse the spin of one electron, from - to +. Since there are now more pairs of electrons of positive spin than of negative spin, the exchange term, which reduces the coulomb repulsion of the electrons, tends to lower the energy of the crystal. On the other hand, it is necessary to place the electron whose spin is changed into a higher energy state, for all the lower states of that spin are filled. Ferromagnetism will occur when the decrease in exchange energy is greater than the increase caused by the operation of the exclusion principle: the Fermi energy.

In principle, the Hartree-Fock equations should be solved by the method of the self-consistent field. This has so far proved impossible for the following reason; assuming a starting potential, the Hartree-Fock equations yield a set of wave functions. It is necessary to compute a new potential and compare and average it with the first, and repeat the process until the potentials from the n-l and the n-th stages agree with an allowed error. But the calculation of the second potential requires a summation over all the occupied states, and our methods of solving the differential equations in a solid are not sufficiently good so as to give accurate solutions except for states of special symmetry.

One has to use his physical intuition as to what corresponds to a reasonable crystal potential, including the effect of exchange terms, and try to solve the differential equation for as many states as possible

using this potential. One common way to obtain a starting potential is to superpose the charge densities from Hartree fields for free atoms placed at the proper points in the crystal lattice. An approximate exchange potential can be obtained in the same way using Slater's free electron approximation in which the exchange potential is proportional to the cube root of the charge density. If it is desired to examine the possibility of Ferromagnetism for the system it is necessary to prepare exchange potentials for the magnetized and unmagnetized states.

Given a starting potential, one way of solving the Hartree-Fock equation is through the orthogonalized plane wave method. This approach expands the wave function in terms of a complete set of functions periodic in the crystal; plane waves which have been made orthogonal by the Schmidt process to the (assumed known) low lying states of the atomic core. An orthogonalized plane wave is defined as:

$$X_k = \frac{e^{i\vec{k} \cdot \vec{n}}}{\Omega_0^{1/2}} - \sum_r e^{i\vec{k} \cdot \vec{n}_r} \sum_j \varphi_j(n - n_r) u_{kj}$$

where Ω_0 is the volume of a unit cell of the crystal, \vec{n}_r runs over all atomic sites, $\varphi_j(n - n_r)$ is the j-th core function on the site r and

$$u_{jk} = \int \frac{e^{i\vec{k} \cdot \vec{n}} \varphi_j^*(\vec{n}) d\vec{n}}{\Omega_0^{1/2}}$$

The wave function u_k^i which is classified as belonging to the i-th irreducible representation of the wave vector \vec{k} , is written as:

$$u_k^i = \sum_h' a_{k,h}^i X_{\vec{k} + \vec{h}}$$

We must form

$$(u_k^i, Hu_k^i) = E_k^i (u_k^i, u_k^i)$$

where H is the appropriate Hamiltonian from the (simplified) Hartree-Fock equations. The symbol (\cdot) represents scalar product. From (7) we obtain a set of linear equations for the coefficients a_k^i , which must lead to a secular equation of the form:

$$\det [(X_h, HX_k) - E_k^i (X_h, X_k)] = 0$$

We will include, of course, only a finite number of terms in the series (4), hoping that the series will essentially have converged. The process of solving this secular equation is greatly simplified by group theoretical considerations according to the symmetry of the function u_k^i .

This work has involved a calculation of the energy values and wave functions for the body-centered form of iron, according to the method whose principles have been sketched. The greatest part of the work consists in the calculation of the matrix elements (X_h, HX_k) and (X_h, X_k) , and the solution of the equation (8) for 16 different states of high symmetry. Equation (8) is equivalent to a problem of simultaneous diagonalization of two Hermitian matrices, and it is in this form that the solutions have been found. Since it is desired to investigate the ferromagnetism of iron, exchange potentials have been prepared for three different spin arrangements, corresponding to a magnetized and an unmagnetized state. The solution of (8) for the 16 states has to be repeated for each exchange potential. This problem would be completely impossible without the use of a high speed computer.

After the energy values are available for certain states of high symmetry, it is necessary to interpolate to find the energies of more general states according to some procedure and then to compute a density

of states-curve (number of states per unit energy as a function of energy) for each exchange potential. The comparison of the density of states-curves should reveal the tendency toward Ferromagnetism, in that a decrease in the energy of the system should result on passing to the ferromagnetic from the unmagnetized state.

We give in the following paragraphs a brief description of the mathematical method used to effect the calculations carried out on this problem. It is clear that one desires to find the proper values and the corresponding functions of the matrix $A - \lambda B$ where A is symmetric and B is positive Hermitian. In a prior report (Final Report on Contract No. DA-36-034-ORD-1023) we discussed a method for the case in which B is the identity matrix. From the mathematical side our interest in the present problem lies in examining the situation where B is a quite general Hermitian matrix. To handle the present problem we replace the matrix A by a new symmetric matrix C such that the proper values of $C - \lambda I$ are the same as those for $A - \lambda B$ and we also establish a procedure for finding the corresponding proper functions. We proceed in this fashion.

By means of our procedure for handling symmetric matrices we express B in the form

$$B = U^* D U$$

where U is a unitary matrix, D is a diagonal one, and U^* is the transpose of U (we assume all quantities to be real; this is not a fundamental restriction; everything that is being done is still valid if one replaces symmetric by Hermitian and makes the obvious emendations in the text). We now extract a reciprocal square root of B in this manner

$$B^{-1/2} = U^* D^{-1/2} U$$

and express a matrix C in the following fashion

$$C = D^{-1/2} UAU^*D^{1/2} = (U*D^{-1/2}) * A (U*D^{-1/2}).$$

Consider now a proper value λ and a corresponding proper function x. By definition

$$(A - \lambda B)x = 0.$$

In what follows it is convenient to define a new matrix V for which

$$V = U*D^{-1/2}$$

and a vector y for which

$$y = V^{-1}x = D^{1/2}Ux.$$

Then we have

$$\begin{aligned} (C - \lambda I)y &= (V^*AV - \lambda I)y = V*(A - \lambda (V^{-1})V^{-1})Vy = \\ &= V*(A - \lambda U*D^{1/2}D^{1/2}U)Vy = V*(A - \lambda B)Vy = \\ &= V*(A - \lambda B)x = 0. \end{aligned}$$

Thus every proper value λ of the matrix $A - \lambda B$ is also a proper value for the matrix $C - \lambda I$ and the corresponding proper vectors are related as indicated in the relation (#). The converse, of course, is equally clear.

Thus the procedure for handling the matrix $A - \lambda B$ has been reduced to that of handling the matrix $C - \lambda I$. First the matrix B is diagonalized, then C is. The procedure indicates a quite convenient method for inverting a matrix. Although it involves somewhat more work than the Gaussian elimination method, it is somewhat more stable than that method and indicates precisely where the loss of precision occurs. The inversion of a unitary matrix, of course, involves no loss of precision. The place at which the precision is lost is precisely in the inverting

of the elements of the diagonal matrix D. Furthermore, the loss of precision is encountered in a quite explicit fashion in that it arises from the shifting which must be performed to keep all elements properly scaled. Thus one obtains the inverse matrix and an exact determination of its accuracy.

Let W be the unitary matrix associated with C; i.e., let

$$W^*CW = \Delta$$

where Δ is a diagonal matrix, and let

$$Y = VW$$

where V is defined above. Then if our results are absolutely accurate, we will have

$$AY - Y\Delta = 0.$$

Accordingly, we can measure the error in our calculations by evaluating the size of $AY - Y\Delta$ relative to the size of Y.

PART III - METEOROLOGY



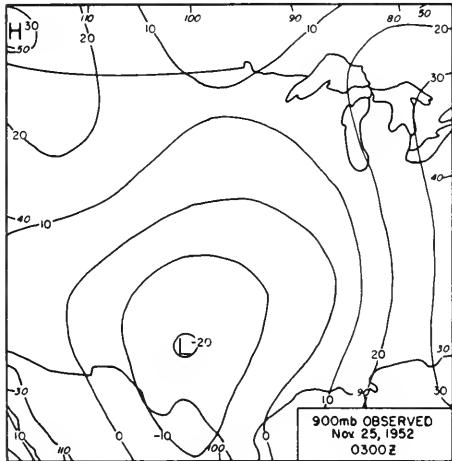
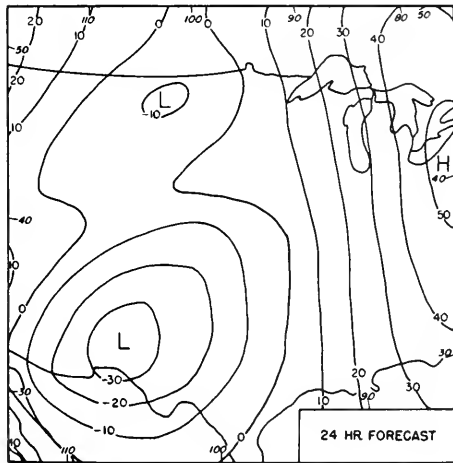
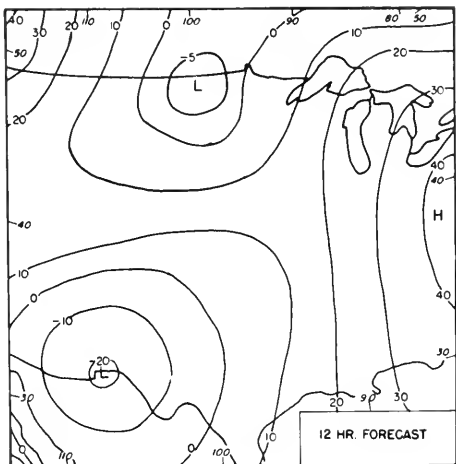
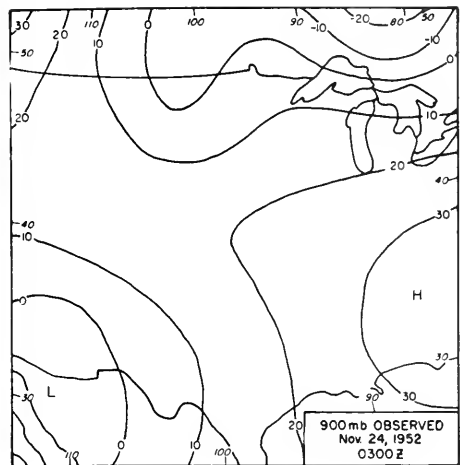
A. Computations with a three-level model.

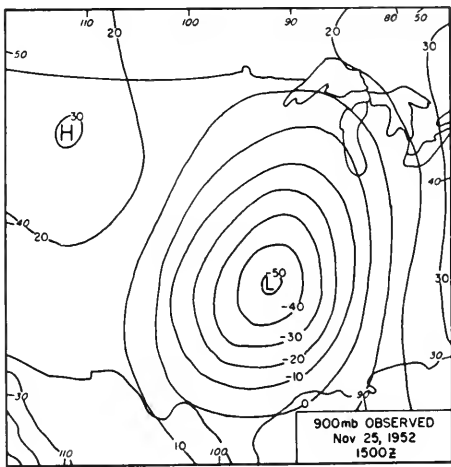
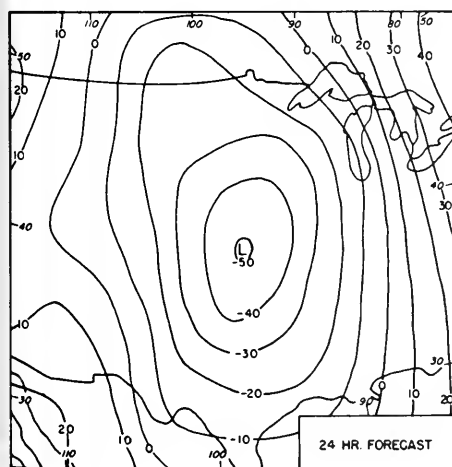
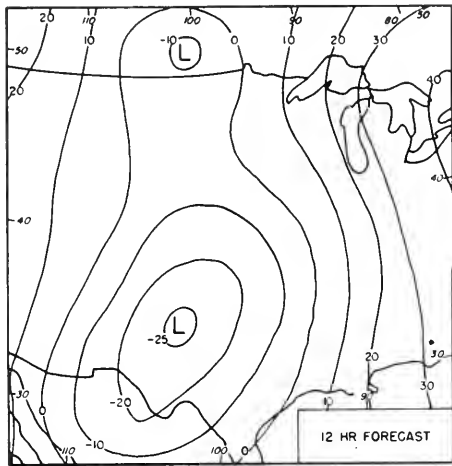
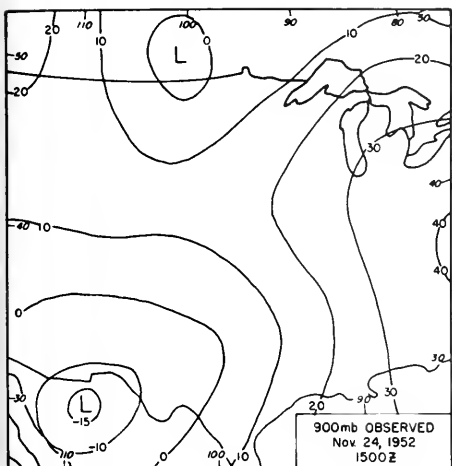
During the year several further tests were made of the three-level model* using both the ρ - and σ -coordinate systems. These 12 and 24 hour forecasts were for cyclonic developments which occurred in November 1952 (two cases), February 1953, and November 1953. A further case of cyclone filling during March 1954 is presently under consideration.

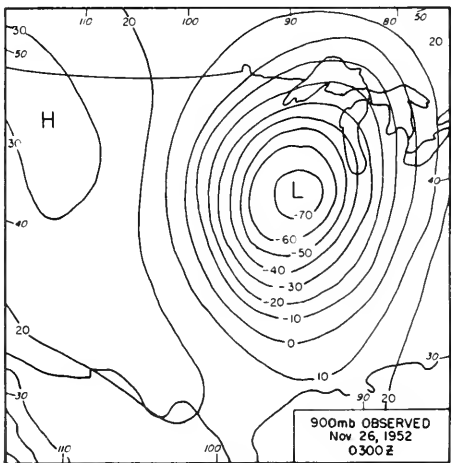
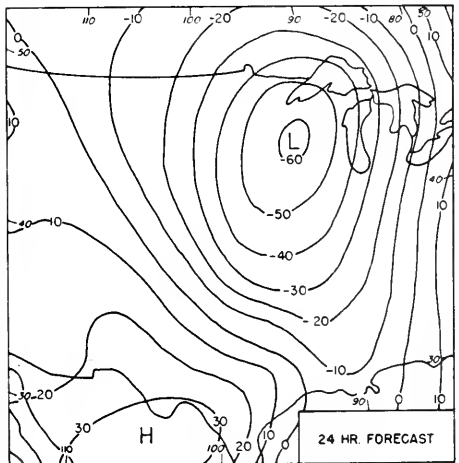
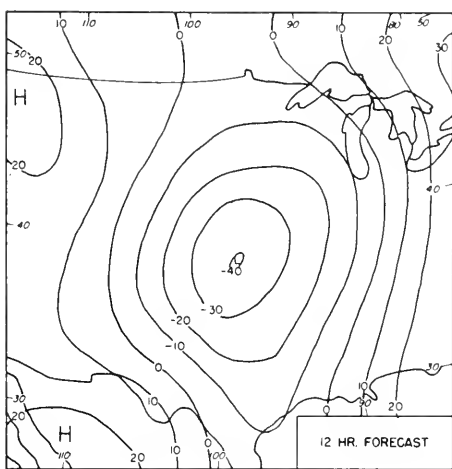
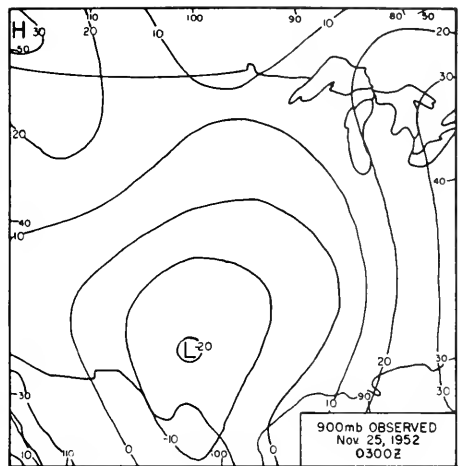
The results of these tests were considered very satisfactory. Figures 1, 2, and 3 show the 900 mb results for the forecasts of November 24/25, 1952. The forecasts were made using the σ -coordinate system with initial data at 400, 700 and 900 mb**. From these figures it will be seen that while by no means perfect the forecasts are as good, if not better, than those which could be obtained by the more conventional methods of forecasting.

* For a description of this model see Report on Contract No. N-7-ONR-388, T. O. I and Final Report on Contract No. DA-36-034-ORD-1023.

** The initial data for this case were supplied by Dr. Sverre Petterssen of the University of Chicago who requested the forecasts for use in a study of cyclogenesis currently being undertaken at Chicago.







B. Experiments with a two-level forecasting model.

During the year 1952-53 some forecasts were made with a two-level model using data at the 300 and 700 mb surfaces.* These forecasts, while improving on the barotropic, or one-level, forecasts, were not unduly successful and the model was soon superseded by a three-level model. Subsequently suggestions were made by other investigators that if data had been used at other levels, viz. the 500 and 1000 mb surfaces, much more accurate forecasts would have been obtained. As a result of these suggestions a model using ρ^2 (or σ^2 in the notation used in the description of the three-level model*) as vertical coordinate was coded for the machine. The levels at which the forecasts were made were 500 and 866 mb but the initial 866 mb data were obtained by linear interpolation with respect to pressure between 500 and 1000 mb and a corresponding 1000 mb forecast obtained by similar extrapolation from the forecast 500 and 866 mb heights.

The equations used were exactly analogous to those used in the corresponding three-level σ -system forecasts. They involved a time extrapolation with the resulting need to compute a Jacobian and the solution of a pair of simultaneous linear differential equations of the form

$$\begin{cases} \nabla^2 \phi_1 + \alpha_1 \phi_1 + \alpha_2 \phi_2 + g_1 = 0 \\ \nabla^2 \phi_2 + \beta_1 \phi_1 + \beta_2 \phi_2 + g_2 = 0 \end{cases}$$

where g_1 , g_2 are functions of the horizontal position coordinates (x , y) and ϕ_1 and ϕ_2 are the unknowns. Solutions were obtained for a 19 x 19 grid using $\phi = \text{constant}$ as the boundary condition. The solutions

* See report on Contract No. N-7-onr-388, T. O. 1, and Final Report on Contract No. DA-36-034-ORD-1023.

were obtained by the same iterative procedure used for the three-level model. Approximately 15% "over-relaxation" was used.

The results of the forecasts made with data from November 1950 and November 1953 showed no significant improvement over the previous two-level forecasts and the model was therefore not used for further forecasts.

C. Experiments with multi-layer non-linear forecasting models.

Several non-linear models were experimented with during the year. The accuracy of the forecasts was unfortunately affected by an inconsistency in the physical assumptions made. This inconsistency, resulting from the introduction of the geostrophic assumption, is apparently very difficult to remove if we wish to retain the non-linearity. Despite this difficulty the computations were valuable firstly because they brought to light this physical inconsistency and secondly because they demonstrated the feasibility of solving certain non-linear partial differential equations. In order to demonstrate the method of solving the non-linear equations a brief mathematical description of the non-linear version of the three-level model is given below.

In the report for last year* it was shown how the equations for an n-layer model could be derived. These equations are

$$(1) \quad \left\{ \begin{array}{l} \left(\frac{D}{Dt} \right)_k \left\{ \beta_k \cdot \frac{(\phi_{k-1} - \phi_k)^{\kappa_{k-1}}}{(\phi_k - \phi_{k+1})^{\kappa_{k+1}}} \right\} = 0 \quad , \quad k \neq 1, n \\ \left(\frac{D}{Dt} \right)_1 \left\{ \beta_1 \cdot \frac{1}{(\phi_1 - \phi_2)^{\kappa_{1,2}}} \right\} = 0 \quad , \quad k = 1 \\ \left(\frac{D}{Dt} \right)_n \left\{ \beta_n (\phi_{n-1} - \phi_n)^{\kappa_{n-1}} \right\} = 0 \quad , \quad k = n \end{array} \right.$$

where $\kappa_{k+1/2} = \bar{\Theta}_{k+1/2} / (\bar{\Theta}_k - \bar{\Theta}_{k+1})$ and the general notation is as in the above mentioned report, namely; ϕ is the geopotential, β is the individual derivative in an isobaric surface, $\beta = f + \frac{1}{f} \nabla^2 \phi$

* Ibid.

the vertical component of absolute vorticity, $\bar{\theta}_k$ the U. S. Standard Atmosphere potential temperature at the level k . The pressure interval $p = 0$ to $p = p_0$ is assumed divided into n equal subintervals, δp , and quantities at the mid points of each interval are denoted by the subscript k ($k = 1, 2, \dots, n$) and points at the upper and lower end-points of each interval by $k - 1/2$ and $k + 1/2$, respectively.

We now define a q_k by

$$q_k = \beta_k \frac{(\phi_{k-1} - \phi_k)^{k_{k+1}}}{(\phi_k - \phi_{k+1})^{k_{k-1}}}, \quad k \neq 1, n$$

and therefore the n -layer model equations (1) become

$$\left(\frac{D}{Dt} \right)_k q_k = 0, \quad k \neq 1, n$$

with corresponding equations for the other two levels, $k = 1$ and n .

The forecasting system then is very similar to that described for the linear version, the only difference being in the definition of q_k and thus in the method of finding the ϕ_k corresponding to a given field of q_k . The computations were performed for the case $k = 3$ using the σ -coordinate system. In this case the three equations to be solved become

$$\begin{cases} q_1 = \beta_1 \cdot \frac{1}{(\phi_1 - \phi_2)^{13}} \\ q_2 = \beta_2 \cdot (\phi_1 - \phi_2)^{23} / (\phi_2 - \phi_3)^{34} \\ q_3 = \beta_3 \cdot (\phi_2 - \phi_3)^{44} \end{cases}$$

These are clearly a very non-linear set of equations for the ϕ 's.

Having indicated the actual equations solved it is convenient for descriptive purposes to now return to the general form

$$\vartheta_k = \beta_k (\phi_{k-1} - \phi_k)^{\alpha_k} / (\phi_k - \phi_{k+1})^{\beta_k}$$

Define

$$R_k = \beta_k \cdot \frac{(\phi_{k-1} - \phi_k)^{\alpha_k}}{(\phi_k - \phi_{k+1})^{\beta_k}} - \vartheta_k$$

Now assume that a small change ϵ_k in ϕ_k causes a change δR_k in R_k

$$\therefore R_k + \delta R_k = \left(\beta_k - \frac{4}{f} \epsilon_k \right) \frac{[(\phi_{k-1} - \phi_k) - \epsilon_k]^{\alpha_k}}{[(\phi_k - \phi_{k+1}) + \epsilon_k]^{\beta_k}} - \vartheta_k$$

We now neglect second and higher powers of ϵ_k

$$\therefore R_k + \delta R_k = \frac{(\phi_{k-1} - \phi_k)^{\alpha_k}}{(\phi_k - \phi_{k+1})^{\beta_k}} \left\{ \beta_k + \beta_k \epsilon_k \left[\frac{\beta_k}{\phi_k - \phi_{k+1}} - \frac{\alpha_k}{\phi_{k-1} - \phi_k} \right] - \frac{4}{f} \epsilon_k \right\}$$

$$\therefore \delta R_k = \frac{(\phi_{k-1} - \phi_k)^{\alpha_k}}{(\phi_k - \phi_{k+1})^{\beta_k}} \left\{ \beta_k \left[\frac{\beta_k}{\phi_k - \phi_{k+1}} - \frac{\alpha_k}{\phi_{k-1} - \phi_k} \right] - \frac{4}{f} \right\} \epsilon_k$$

Now if we wish to reduce a "residual", R_k , to zero by only altering ϕ_k we must choose ϵ_k such that $\delta R_k = -R_k$, i.e. we must choose ϵ_k to be

$$- R_k / \frac{(\phi_{k-1} - \phi_k)^{\alpha_k}}{(\phi_k - \phi_{k+1})^{\beta_k}} \left\{ \beta_k \left[\frac{\beta_k}{\phi_k - \phi_{k+1}} - \frac{\alpha_k}{\phi_{k-1} - \phi_k} \right] - \frac{4}{f} \right\}$$

Thus if ϕ_k^{u+1} and ϕ_k^u are successive values of ϕ_k during the iterative process

$$\phi_k^{u+1} = \phi_k^u - \frac{1}{\chi_k} \cdot R_k$$

where

$$\chi_k = \frac{(\phi_{k-1} - \phi_k)^{\alpha_k}}{(\phi_k - \phi_{k+1})^{\beta_k}} \left\{ \beta_k \left[\frac{\beta_k}{\phi_k - \phi_{k+1}} - \frac{\alpha_k}{\phi_{k-1} - \phi_k} \right] - \frac{4}{f} \right\}$$

Similar equations clearly hold for $k = 1, n$. In the case considered in the computations the three equations were solved by the simultaneous application of procedure (4) for all three values of k at a given point (i, j) the points being scanned in the (i, j) -plane. It was found that it was not sufficient to give, as in the linear case, the criterion

$$|\phi_k^{(t+1)} - \phi_k^{(t)}| < \delta$$

as that for convergence. Rather it was found necessary to stipulate a certain minimum number of iterations (six in the cases tested) and then to require the usual criterion. No attempt was made to use "over-relaxation".

The applicability of this method clearly depends on the obtaining of a good first guess, ϕ_k^0 , in the iterative sequence. It is apparently sufficiently good in the meteorological case to take as a first guess the value of ϕ obtained by linear extrapolation from the corresponding values half hour and one hour previously. It was further found that it was necessary to restrict β_k to positive values. If any negative ones appeared in the course of the timewise application of equation (1), these values were replaced by zeros. From the meteorological view point this assumption was acceptable as the validity of the geostrophic assumption is in grave doubt for negatives β 's.

D. Barotropic forecasts for low latitudes.

In conjunction with Professor Riehl of the University of Chicago a series of twenty barotropic forecasts were made for areas extending to within 10° latitude of the equator. Separate 200 and 500 mb forecasts were made for two summer series and 500 mb forecasts for a spring series.

The only code differences between these forecasts and the barotropic forecasts previously made arose from the revised formulae necessary for the computation of the sine of the latitude and the mapping factor for regions of low latitude. The geostrophic assumption was, however, still made even for low latitudes.

The forecasts at the 500-mb level consistently brought out the major circulation features and in many cases smaller-scale features were also accurately predicted. Forecasts at the 200-mb level were much poorer and showed systematic errors which resulted in some very marked failures.

It is expected that these predictions will be of considerable assistance in the formulation of more accurate models for numerical prediction in low latitudes.

E. Computation of vertical velocities.

In the formulation of the three-level model we have at one stage equations involving w , the individual derivative of ρ , at two levels. In the normal forecasting system it is convenient to eliminate these two variables and this is in fact done. Since, however, w is proportional to the vertical velocity and is therefore highly correlated with rainfall amounts it is interesting to know its distribution at various stages in the forecast.

If the levels for which forecasts are made are numbered 1, 2, and 3, w can be evaluated at levels 1 1/2 and 2 1/2 by use of the relations

$$\left\{ \begin{array}{l} \omega_{1\frac{1}{2}} = \alpha_{1\frac{1}{2}} \left(\frac{\partial}{\partial t} \right)_2 (\phi_1 - \phi_2) \\ \omega_{2\frac{1}{2}} = \alpha_{2\frac{1}{2}} \left(\frac{\partial}{\partial t} \right)_2 (\phi_2 - \phi_3) \end{array} \right.$$

where $\alpha_{1\frac{1}{2}}$ and $\alpha_{2\frac{1}{2}}$ are constants, the operator $\frac{\partial}{\partial t} \equiv \frac{\partial}{\partial t} + V \cdot \nabla$ and the ϕ 's are the geopotentials at the various pressure surfaces indicated by the subscripts.

In order to obtain the time derivatives involved it was necessary to know the ϕ values at more than one time. In practice it was found that smooth fields of w were obtained if the time derivatives were replaced by three hour centered finite differences. Shorter time intervals resulted in too much round-off error and therefore ragged fields of w .

Used in conjunction with a three-layer model for the 400, 700 and 900 mb surfaces this code gave vertical velocities at 560 and 805 mb. Exact verifications against observation is impossible because of our inability to measure vertical velocity directly by observational



means. In the cases considered, however, the results agreed with those expected from other considerations and also agreed fairly well with observed rainfall areas.



F. Time series code.

At the request of Dr. Hans Panofsky of Pennsylvania State College a code was written to obtain certain auto-correlations and cross-correlations for given sets of observations. The observations used were obtained in the course of an investigation of small scale turbulence in the atmosphere. The code is, however, very general and can be used to treat many other types of time-series.

The input to the code consists of two sets of initial data, μ_i and ν_i , $i = 1, 2, \dots, N$. This data are first "pre-whitened" yielding sets of data X_i , Y_i defined in the following manner:

$$\left\{ \begin{array}{l} X_i = U_i + \theta_1 U_{i-1} + \theta_2 U_{i-2} + \dots + \theta_{n^*-1} U_{i-(n^*-1)} \\ Y_i = V_i + \theta_1 V_{i-1} + \theta_2 V_{i-2} + \dots + \theta_{n^*-1} V_{i-(n^*-1)} \end{array} \right.$$

where

$$U_i = \mu_i - \frac{1}{N} \sum \mu_i \quad , \quad V_i = \nu_i - \frac{1}{N} \sum \nu_i$$

for $i = n^*, n^* + 1, \dots$ where $n^* < 7$.

The auto-correlation and cross-correlation terms are then computed for $\ell = 0, 1, \dots, m$, $0 < m \leq 128$. These terms are defined in the following way:

$$A(\ell) = \frac{1}{N-\ell-n^*+1} \sum_{i=n^*}^{N-\ell} X_i X_{i+\ell} - \frac{1}{(N-\ell-n^*+1)^2} \sum_{i=n^*}^{N-\ell} X_i \sum_{i=n^*+1}^N X_i$$

$$B(\ell) = \frac{1}{N-\ell-n^*+1} \sum_{i=n^*}^{N-\ell} Y_i Y_{i+\ell} - \frac{1}{(N-\ell-n^*+1)^2} \sum_{i=n^*}^{N-\ell} Y_i \sum_{i=n^*+1}^N Y_i$$

$$C(\ell) = \frac{1}{N-\ell-n^*+1} \sum_{i=n^*}^{N-\ell} X_i Y_{i+\ell} - \frac{1}{(N-\ell-n^*+1)^2} \sum_{i=n^*}^{N-\ell} X_i \sum_{i=n^*+1}^N Y_i$$

$$D(\ell) = \frac{1}{(N-\ell-n^*)} \sum_{i=n^*}^{N-\ell} Y_i X_{i+\ell} - \frac{1}{(N-\ell-n^*)^2} \sum_{i=n^*}^{N-\ell} Y_i \sum_{\ell=n^*+1}^N X_\ell$$

The code then goes on to compute, for $k = 1, 2, \dots, m-1$, the following quantities:

$$X_k = \frac{1}{mg(k)} \left\{ \sum_{\ell=1}^{m-1} 2\epsilon(\ell) \cos \frac{k\ell\pi}{m} \cdot A(\ell) + A(0) \right\}$$

$$Y_k = \frac{1}{mg(k)} \left\{ \sum_{\ell=1}^{m-1} 2\epsilon(\ell) \cos \frac{k\ell\pi}{m} \cdot B(\ell) + B(0) \right\}$$

$$Z_k = \frac{1}{mg(k)} \left\{ \sum_{\ell=1}^{m-1} 2\epsilon(\ell) \cos \frac{k\ell\pi}{m} \cdot E(\ell) + E(0) \right\}$$

$$W_k = \frac{1}{mg(k)} \left\{ \sum_{\ell=1}^{m-1} 2\epsilon(\ell) \sin \frac{k\ell\pi}{m} \cdot F(\ell) \right\}$$

where

$$\begin{cases} E(\ell) = \frac{1}{2} \{ C(\ell) + D(\ell) \} \\ F(\ell) = \frac{1}{2} \{ D(\ell) - C(\ell) \} \\ C(\ell) = \frac{1}{2} \left\{ 1 + \cos \frac{\pi\ell}{m} \right\} \end{cases}$$

and, if only one "pre-whitening" parameter, θ , is used,

$$g(k) = 1 + \theta^2 + 2\theta \cos \frac{k\pi}{m}$$

For $k = 0$ and $k = m$, X, Y, Z, W are given by similar expressions with the additional factor $1/2$ included.

Several sets of data were treated in the way outlined above. These sets had various values of N and m but in all cases to date θ , has been taken as ~ 0.75 .

G. Objective analysis.

All methods developed to date for numerical weather prediction require input data at a regularly spaced set of grid points. Meteorological observations, however, are made at an almost random set of observing stations. We thus have the problem of obtaining from this set of observations the most probable values at the grid points as required by the forecasting code.

The usual method of solving this problem is to plot the actual observations on a map, draw a series of isopleths of the quantity concerned at suitable intervals, and then using judicious interpolation to read off the values at the grid points. The isopleths are drawn using continuity in time as well as in the three space coordinates. This method apparently depends considerably on the skill of the analyst who draws the isopleths and is therefore referred to as "subjective" analysis. The main drawback to this method is not its subjective nature so much as the fact that it is very time consuming.

In the past the numerical forecasting models have been tested only on very carefully analyzed data the preparation of which took a time incompatible with any routine forecasting system. Two questions thus arise; Is so much care necessary? Does the subjective analyst do anything that a computing machine could not also do in a considerably less time? The only way to find answers to these questions is to propose alternatives to the methods used by the subjective analyst and then to test these alternatives by using them in the preparation of forecasts. In this section one such alternative is described and results given to show its effects, firstly, on the type of analysis produced, and secondly, on numerical forecasts from data so prepared.

The method is purely two-dimensional and is based on the fitting of a second order polynomial to the observations in the area immediately surrounding the grid point at which the value of the pressure or height is required. In this description we will be concerned with the height of given pressure surfaces expressed in terms of height deviation, D , from standard atmosphere. The polynomial can be written

$$D = a_{00} + a_{10}x + a_{01}y + a_{11}xy + a_{20}x^2 + a_{02}y^2$$

Thus, if the origin of the coordinate system is taken to be the grid point under consideration, the "D" value we seek will be a_{00} . In order to determine the six coefficients a_{ij} we clearly require six independent observations of D at known positions (x, y) .

The observations give us wind values as well as D values. These wind values are incorporated in the scheme by using the geostrophic assumption. Thus, one wind observation gives us values of $\partial D / \partial x$ and $\partial D / \partial y$ at a point. Provided that there is at least one "D" value within the region being considered each wind observation is equivalent to two "D" values or pieces of information. The errors introduced by the geostrophic assumption are not random. However, due to our lack of knowledge of the geostrophic deviations we have to assume that the errors from this source are random.

Since, in general, the observations from nearby stations are not in exact agreement we usually require more than the minimum number of pieces of information and then fit the second order polynomial to these observations by the method of Least Squares. Thus we choose the a_{ij} such that we minimize

$$S = \frac{1}{\sigma_D} \sum_{n=1}^r (D_n - D'_n)^2 + \frac{1}{\sigma_W} \sum_{n=1}^3 \left\{ \left(\frac{\partial D_n}{\partial x} - \frac{\partial D'_n}{\partial x} \right)^2 + \left(\frac{\partial D_n}{\partial y} - \frac{\partial D'_n}{\partial y} \right)^2 \right\}$$

where D_n , $\partial D_n / \partial x$, $\partial D_n / \partial y$ are from the observations and the corresponding primed quantities are those computed from the polynomial (1). σ_D is the standard deviation for the errors in the \wedge observations of D and σ_W is the standard deviation of the S wind observations in the area over which the polynomial is being fitted. The ratio σ_D / σ_W is called the weighting factor. It can be shown that, if the errors have a Gaussian distribution, by choosing the a_{ij} in this way we get the most probable value of the required D . We thus have to solve the set of six linear algebraic equations:

$$\frac{\partial S}{\partial a_{ij}} = 0, \quad 0 \leq i+j \leq 2$$

for the coefficients a_{ij} and in particular the coefficient a_{00} .

These equations can be written in the form

$$\underline{y} \cdot \underline{a} = \underline{z}$$

where \underline{y} is a 6×6 matrix and \underline{a} and \underline{z} are six component vectors, the \underline{a} consisting of the six unknowns a_{ij} and \underline{y} and \underline{z} being determined by the observations.

By triangularizing the matrix \underline{y} we can reduce the equations to the form

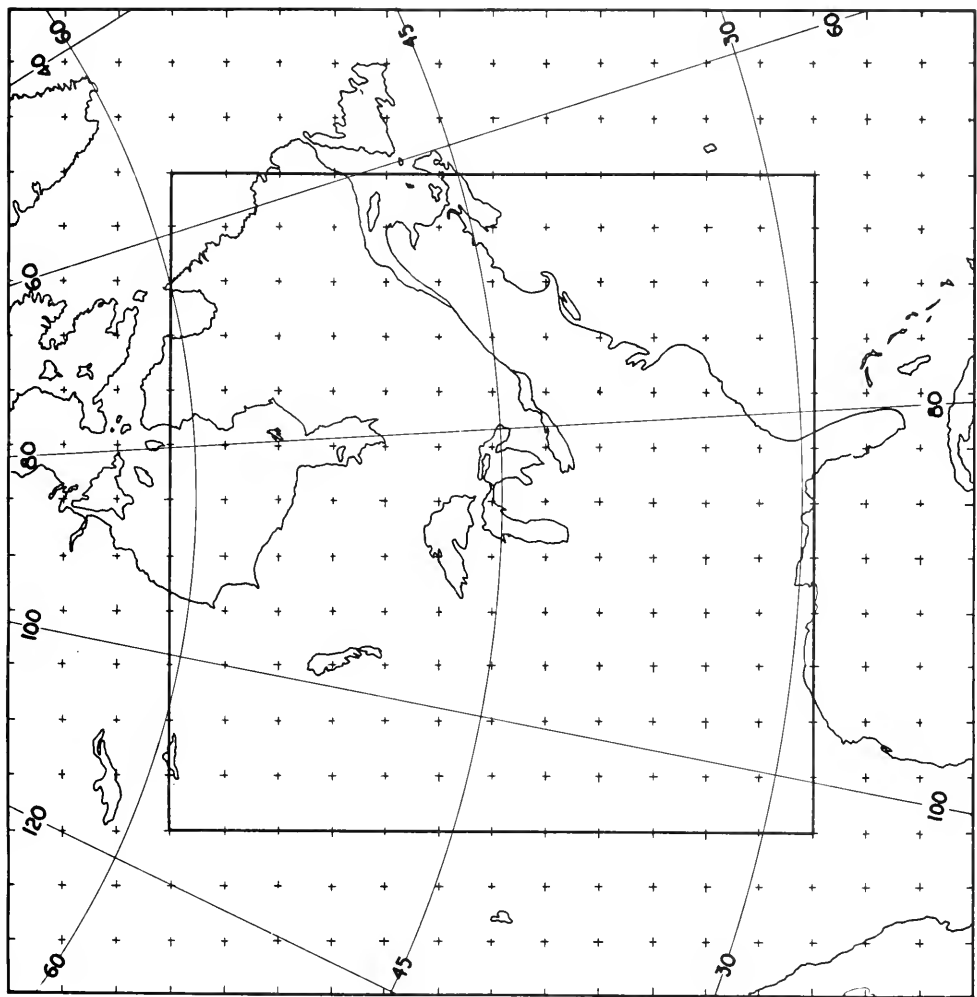
$$\underline{y}^* \cdot \underline{a} = \underline{z}^*$$

where \underline{y}^* is a lower triangular matrix. If, now y_{00}^{**} , a_{00} and z_{00}^{**} are the leading elements of the three matrices \underline{y}^* , \underline{a} and \underline{z}^* , respectively, we have directly that

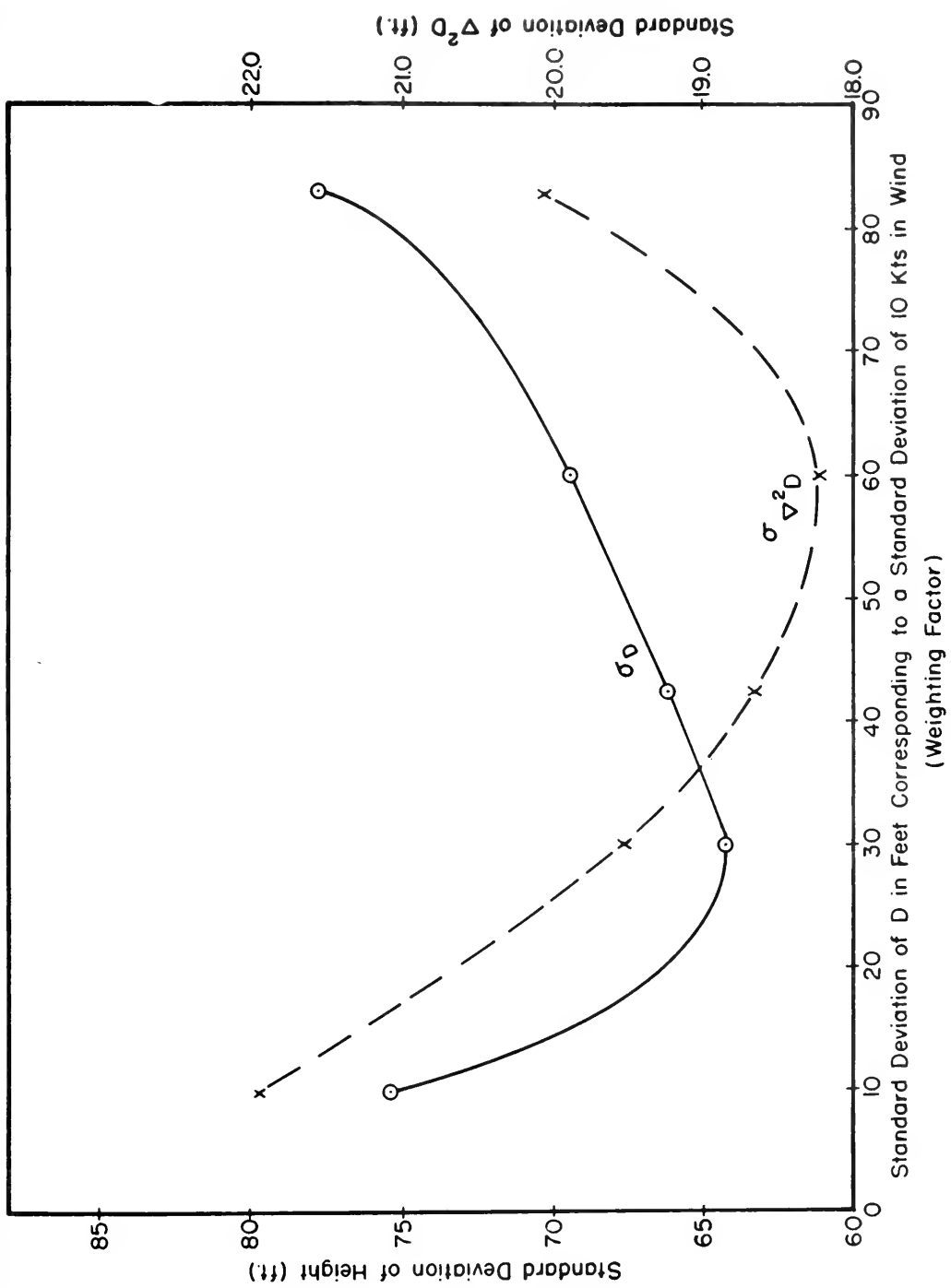
$$D = a_{00} = z_{00}^{**} / y_{00}^{**}$$

To determine the weighting factor σ_D/σ_W it is necessary to know the values of the two standard deviations. Owing to the numerous ways errors can enter into the observations and also because of the use of the geostrophic assumption it was considered best to obtain its value by the experiment described below.

A series of objective analyses was computed for the 500 mb surface for November 25, 1950, at 0300 GCT. The grid used is shown in Figure 1. Each analysis was made with a different weighting factor. The results of each analysis were then compared with the mean of three subjective analyses for the same map, prepared by three different analysts. The results are in the form of D values for 222 points and $\nabla^2 D$, the finite difference Laplacian of these D values, for 152 points. The points used were selected prior to the experiment as being those where sufficient data were available to permit a fair comparison. The means of the standard deviations of D and $\nabla^2 D$ of the objective analyses vs. the subjective analyses are shown on page III-22. It is evident from that figure that the objective analysis has the best agreement with the subjective analyses, so far as height is concerned, when wind receives a relatively small weight. However, a heavier weighting on wind produces a better agreement when $\nabla^2 D$ is considered. It was believed best to use a weighting factor giving good results for vorticity calculations, in view of the fact that the objective analyses are principally for use in numerical prediction. It may be noted that in numerical prediction one is usually more interested in expressions such as $\nabla^2 D$ and other



III-21. Location of 19 x 19 grid of points used in computation.



III-22. Standard deviations between objective and subjective analyses for various weighting factors.

derivatives of D rather than the absolute value of D. Consequently, a weighting factor corresponding to a ratio of 50 ft. height error to ten knots wind error was selected for routine use in upper air analyses.

The above type of test was not performed for other levels but a smaller weighting factor, corresponding to 30 ft. height error for a ten knot wind error, was selected for use in 1000 mb analysis. This decision was made because of the existence of greater errors in the geostrophic assumption near the ground. At high levels wind observations are more accurate with regard to direction than to speed. This would suggest that in future analysis schemes we should use separate weighting factors for the two parts of a wind observation.

An analyst, when drawing an isobar, looks at all the wind and pressure data in an area surrounding the small region in question. In a similar manner, the objective analysis program fits the quadratic surface as closely as possible to all wind and pressure data reported within a prescribed area surrounding the grid point. The limits of the area are defined by the relation

$$|x| + |y| = |a| ,$$

where x and y are the coordinates of each piece of data with respect to the grid point at which D is to be computed. This defines a square (standing on one corner) with the grid at the center. The search then consists of locating and assembling in the memory of the computer all the data reported within this area. These data are then used in the fitting of the quadratic surface and the computation of the D value at the grid point. The search is made for each grid point using a given sized area. When sufficient data are assembled for the computation, the D value is computed. If the data are inadequate in quantity, the

point is passed and a search is made around the next point. In this way the computation proceeds until all points in the grid have been considered. This leaves some points computed and some not computed.

The next step is to go back to the points which were skipped over because of lack of data, and to try to assemble more data for the computation. This is done by assembling all reported data plus all previously computed data which lie in the search area. The search area may be enlarged also. Thus, some of the points which were skipped the first time the grid was scanned can now be computed. (Points previously computed are now skipped over and left unchanged.) Some uncomputed points are still left uncomputed, due to lack of data. After the machine has proceeded through the grid a second time, the search area is enlarged again and the above process is repeated. The search routine which is currently in use has evolved through many trials and is summarized in Table I.

Passage through Grid	Size of Search area (Length of side of of square, = $a\sqrt{2}$)	Data included in search
1st	1000 km	Reported data only
2nd	1000 km	
3rd	1200 km	
4th	1400 km	
5th	1800 km	
6th	1800 km	
7th	1800 km	

Table I

The sudden increase in the size of the search area from the 4th to the 5th search is due to the fact that by the end of the 4th search the only areas remaining unanalyzed are those with practically no data at all. Searches 5 through 7 are designed to fill in these areas with values which

are not unreasonable.

Strictly speaking, one needs six pieces of meteorological information (each wind gives two pieces of information and each height value gives one) to fit a quadratic surface in the manner described above. However, in view of the fact that the data contain errors, a surplus of data is highly desirable in order that some smoothing can be done. Another reason for requiring surplus information is that, with some combinations of data, a nearly singular matrix \underline{y} is encountered in the computation of the D value. A truly singular matrix has not yet been encountered in any of the analysis runs, but nearly-singular matrices have been seen. These give solutions for D which are computed in the non-significant digits of the data and are therefore meaningless. These can never be entirely avoided, but the probability of their occurrence can be reduced to a negligible figure by requiring enough data. Experience to date has indicated that this desired result can be obtained if a minimum of ten pieces of information is required as a prerequisite to the computation of the D value.

The machine program can be outlined in the following manner:

1. Part A code is read into the computer at the start of the analysis.
2. Part A reads in data cards, one by one, converts the data from decimal to binary, and stores it. The data cards contain the index number of the station (latitude and longitude for ships), the wind direction, and speed, and the height of the pressure surface to be analyzed for each reporting station. Part A then reads in part B code.
3. Part B code reads in the station locator cards, which have the latitude and longitude for the corresponding index number of each station which can possibly report. It matches this information with the data already in the memory and converts the index numbers of the data to

latitude and longitude. All data are next converted to the coordinate system of the grid. Part B code then reads the code for parts C, D, and E into the machine.

4. Part C code is the search routine. Whenever enough data are found to enable the computation of a point, part C code transfers the control to part D.
5. Part D is the matrix code, i.e. the section which triangularizes the matrix \underline{y} , etc. It computes the D value at the grid point, using the data obtained in the search. It then transfers the control back to the search code.
6. Part E is the code which converts the results of the analysis from binary to decimal and punches the results on cards, which can then be tabulated.

It can be seen that the program is entirely automatic. The process of making the objective analysis thus proceeds in the following way:

- 1) The reported meteorological data are punched on cards.
- 2) The cards are run through a printer to produce a listing of the data. This listing is then inspected by an analyst with the aid of a plotted map of the data for the detection of any serious errors in the data. This step is unfortunately necessary because of communication errors. However, it need not delay the procedure unduly, since the maps can be plotted at the same time as the cards are being punched. It is not difficult to postulate an addition to the machine program which would check the data and reject those containing serious errors.
- 3) After any serious errors detected in the data are corrected, the data cards are added to the code cards, the resulting deck is placed in the computer, and the computation is started.

4) The machine computation then proceeds entirely automatically.

At the present, slightly under 1 1/2 hours are required for the computation of the "D" values on one pressure surface for a 19 x 19 grid of points. It is known how to rewrite the code with one slight internal change which would reduce the above computation time to under one hour. Eventual reduction to a time of less than 35 minutes is visualized for the IAS computer.

5) The output cards from part E are usually printed to enable an inspection of the analysis. These cards are also used directly as input information for the forecast problem. The printed results at each grid point consist of:

- a) the D value obtained from the analysis, in tens of feet,
- b) a two digit number which tells the number of pieces of meteorological information used in the computation of the D value, and
- c) a digit indicating at which passage through the grid the computation was made.

The subjective analyses available for comparison with the objective analysis of 500 mb, 25 November 1950, 0300 GCT, were prepared by three different individuals, and will be referred to as A, B, and C. Analyses A and B were prepared very carefully by experienced analysts, who took all the time they needed for their completion. Analysis C was made hurriedly under operational conditions. These analyses were then compared with an objective analysis (0) for the same map, using the weighting factor corresponding to fifty feet height error and ten knots wind error. The standard deviations of D and $\nabla^2 D$ in feet (for the same points referred to in the description of the determination of the weighting factor) of the difference between the various analyses are shown in

Table II.

Analysis pairs	A-B	A-C	B-C	O-A	O-B	O-C
Std. Dev. D.	50	67	60	69	72	68
Std. Dev. ∇^2	13	17	16	18	20	18

Table II

It can be seen from this table that the objective analysis did not agree with the subjective analyses quite as well as the subjective analyses agreed with each other. However, the relatively close agreement between A and B is something which cannot ordinarily be expected between subjective analyses. It should not be supposed from these results that the objective analysis was inferior to the subjective analyses, since in this case the forecast is the ultimate test of the worth of the analysis.

Previously a 24-hour numerical forecast had been made on the IAS computer for the intense cyclogenesis of November 24-25, 1950 starting from 1500 Z, November 24. The input data consisted of the 1000 and 500 mb charts prepared by analyst B (above). The same forecast was then made from objective analyses. The two resulting forecasts, expressed in the form of 24-hour forecast changes of height of the 1000 mb surface, were then correlated with each other yielding a correlation coefficient of 0.96. Both forecasts computed the cyclogenesis which developed with fair accuracy, neither forecast being observably superior to the other. From this experiment it was concluded that where a good data coverage is found, e.g. over North America, two-dimensional objective analyses, prepared for two different levels, are satisfactory for use in numerical prediction.

When three pressure surfaces in the vertical are to be analysed for use in a forecast, a new problem is encountered. This is the problem

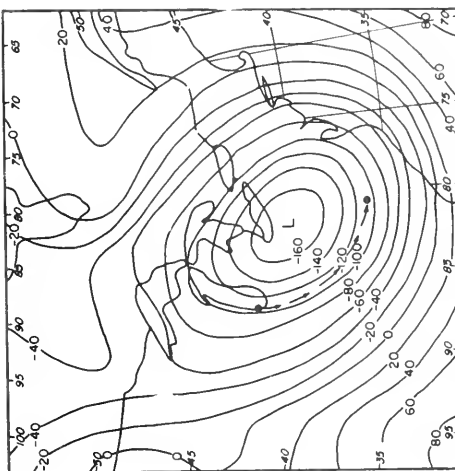
of representing accurately the horizontal variation of vertical stability. This variation is the additional feature treated in the three-parameter model, as compared with the two-parameter model. In a test of the representation of stability by the above-described objective analysis scheme, maps were prepared for 1500 Z, November 24, 1950, of a quantity directly related to vertical stability, i.e.

$$\Delta^2 D = D_{400} - 2D_{700} + D_{1000}$$

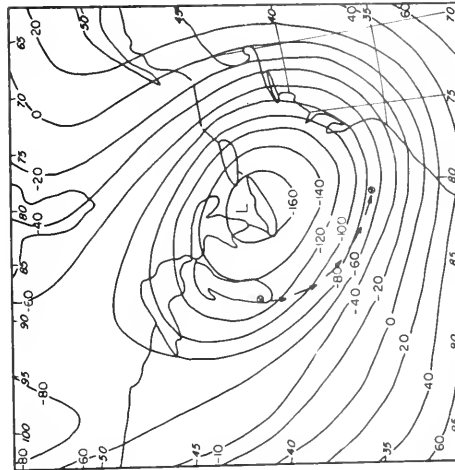
where the subscripts indicate the pressure surface at which the D value was read from the maps. This quantity was computed from data at the three pressure surfaces at each grid point from the objective and also from the subjective analyses. From the grid point values, values of $\Delta^2 D$ were interpolated at the locations of all reporting radiosonde stations.

Values of $\Delta^2 D$ were also calculated from the actual radiosonde reports. These were used as verification of the values obtained from the objective and from the subjective analyses. The values of $\Delta^2 D$ obtained by objective analysis when correlated with the values from the actual observations yielded a correlation coefficient of 0.90. The correlation coefficient between the values obtained from subjective analysis and the reports was 0.94. From this it was concluded that the two-dimensional scheme of objective analysis gives an adequate representation of the horizontal variation of vertical stability where the data coverage is good and when the pressure surfaces analyzed are at least 300 mb apart.

The next experiment consisted of using the maps prepared for 1500 Z, 24 November 1950, in two forecasts with a three-parameter model -- one to be made from the subjective analyses and the other from



OBSERVED 400 mb Nov 25, 1950 1500 Z

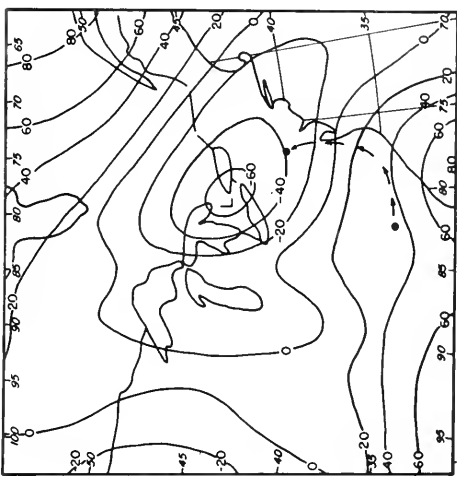
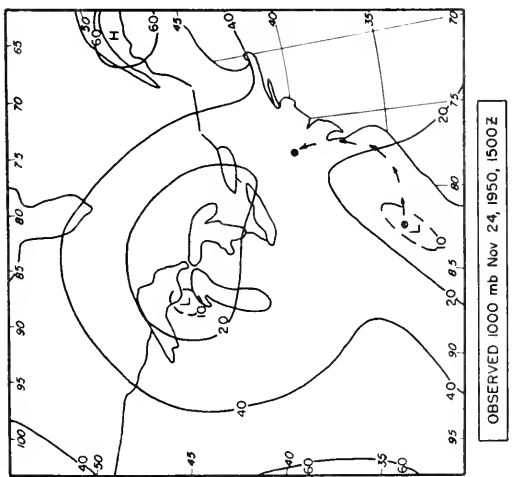
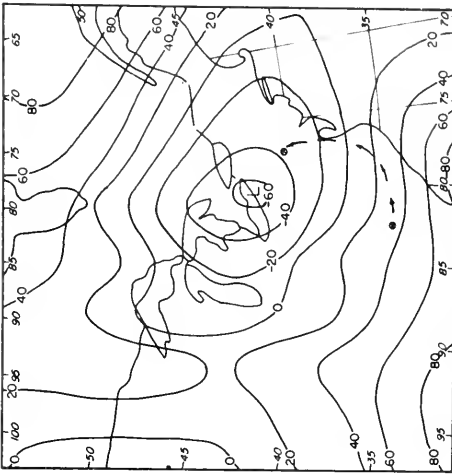
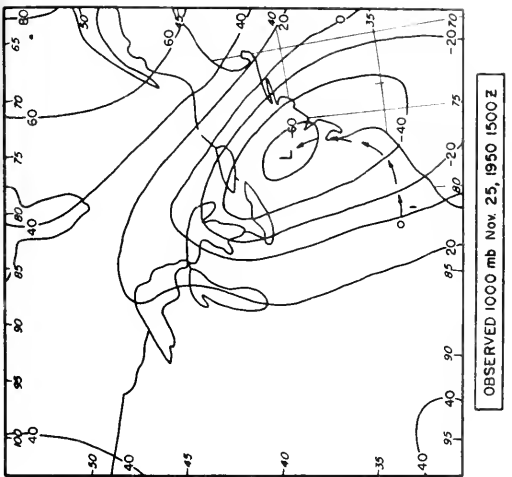


OBSERVED 400 mb Nov 24, 1950 1500 Z

24 HR FORECAST FROM OBJECTIVE ANALYSIS

24 HR FORECAST FROM SUBJECTIVE ANALYSIS

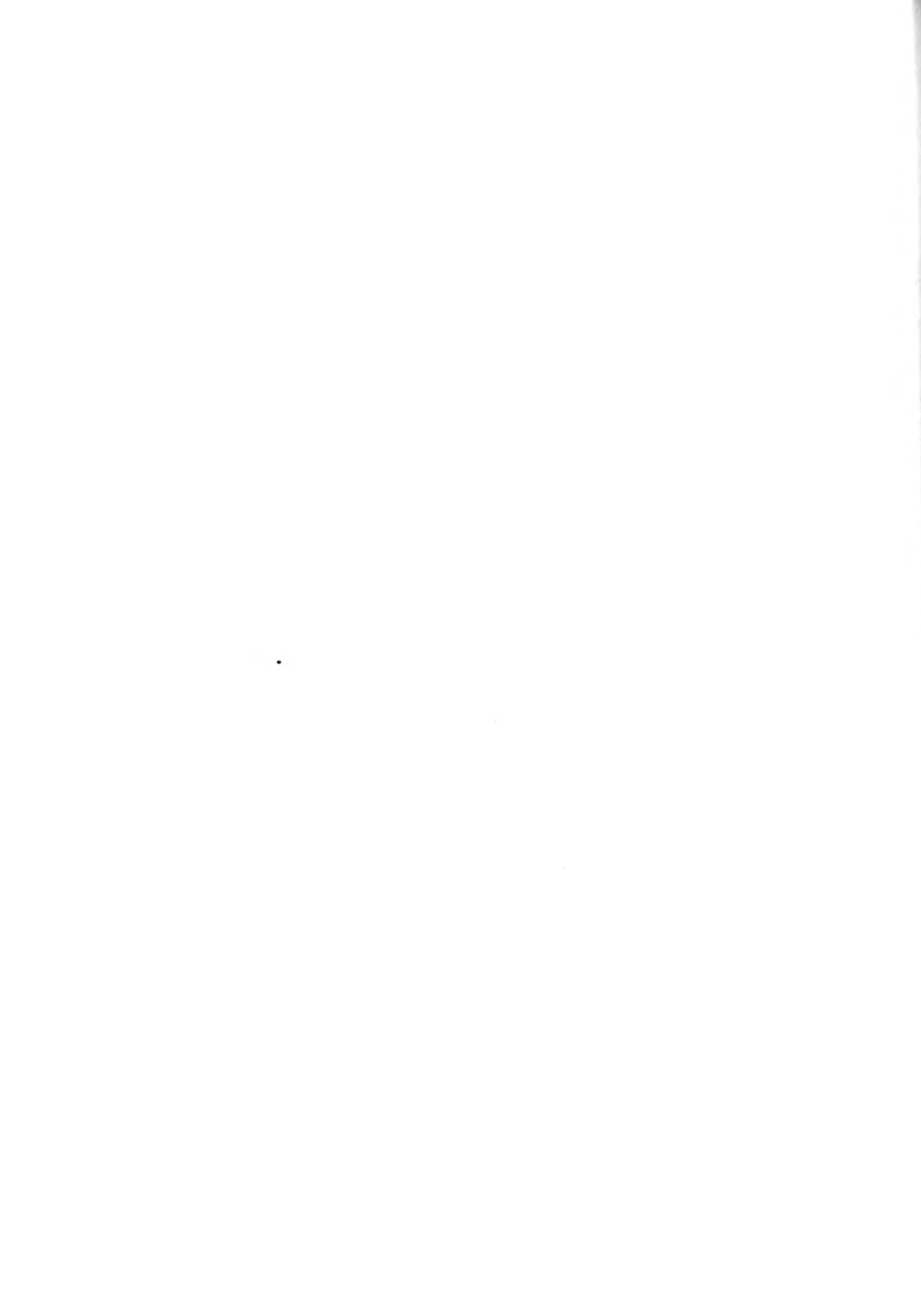
III-30. 400 mb initial, forecast and verification maps. The dashed line indicates the observed 24-hour movement of the low center.



24 HR FORECAST FROM OBJECTIVE ANALYSIS

24 HR FORECAST FROM SUBJECTIVE ANALYSIS

III-31. 1000 mb initial, forecast and verification maps. The dashed line indicates the observed 24-hour movement of the low center.



the objective analyses. The results, at 400 and 1000 mb, of these forecasts are presented in the figures on pages III-30 and III-31. The 700 mb results are very similar. These figures show the surprising result that the forecast made from the objective analyses verified better than the forecast made from the subjective analyses. Further confirmation of this is given by the correlation coefficients of forecast change vs. observed change at 400 mb, where the difference between the two forecasts was greatest. These are given in Table III.

	Correlation Coefficient
Forecast change vs. observed change--subjective analysis	0.63
Forecast change vs. observed change--objective analysis	0.79
Forecast change--objective analysis vs. forecast change --subjective analysis	0.82

Table III

The results described above can be attributed to the fact that when the objective analyses are made, the geostrophic approximation is forced on the analyses, thus giving better results when a quasi-geostrophic model is used to make the forecast. This forcing is most marked in the vicinity of pronounced troughs or lows at middle and high levels in the troposphere, where the speed and curvature of the flow are strong. It takes the form of diminishing the analyzed geostrophic wind from the actual geostrophic wind in the areas where the observed winds are markedly sub-geostrophic. This is due to the fact that observed winds as well as all the heights of the pressure surface are used in the objective analysis. The smoothing process incorporated into the objective analysis also



contributes to the same effect, particularly when the half-wave length of the wind pattern is not much larger than the dimension of the search area. The quasi-geostrophic prediction model, using the geostrophic approximation for measurement and advection of vorticity, then has a more useful representation of these quantities than it otherwise would.

The results obtained above lead to the conclusion that a simple two-dimensional scheme of objective analysis is feasible and satisfactory for the purpose of transforming raw data into input data for a two- or three-parameter numerical prediction model. In fact, such a scheme appears to be better suited for use in a quasi-geostrophic prediction model than information obtained from subjective analysis. The principal difficulty encountered so far is introduced by incomplete and erroneous meteorological observations. The detection and correction of the errors at present must be done subjectively, i.e., a skilled analyst must inspect the data very carefully for omissions and errors. One could argue that this process practically amounts to a subjective analysis. It should be pointed out that in the preparation of input data for a forecast from a subjective analysis, the analysis itself is only the beginning of the process. The reading, recording, and checking of interpolated information at the grid points is the most tedious and lengthy part of the process. All this is unnecessary when an objective analysis method is used. It is clear, however, that the reduction and eventual elimination of errors of computation and transmission of meteorological data is a subject which must receive high priority in future research and development before a truly objective analysis is possible.



H. Wind driven water waves.

Several investigations have been undertaken in the past to determine the character of the inertial oscillations initiated by an unbalanced current in the oceans. These investigations have been restricted to either the final equilibrium state or to a system in which the momentum causing the unbalanced current has been added impulsively. The present investigation is concerned with the effect on the resultant motion of the length of time during which the momentum is added.

A simple model is constructed as follows: A rotating basin of homogeneous fluid of infinite horizontal extent and of finite depth is initially at rest relative to the rotating coordinate system. At time $t' = 0$, a wind-stress is applied to an infinite strip of the surface and continues to act until time $t' = t_0'$. What are the velocity, mass, and energy distributions at time t ?

If the x' and y' axes are directed along the horizontal and the z' axis is taken positive upward, the above problem reduces to the following system of equations:

$$\left\{ \begin{array}{l} \frac{\partial v}{\partial t'} - fv = \tau_x \\ \frac{\partial u}{\partial t'} + fu = -gD \frac{\partial n}{\partial y'} \\ \frac{\partial n}{\partial t'} + \frac{\partial v}{\partial y'} = 0 \end{array} \right.$$

where u and v are the (vertically) integrated mass transports in the x' and y' directions, respectively,

n is the height of the water above the equilibrium surface,

D is the initial depth,

f denotes the (constant) Coriolis parameter,



τ_x is the wind-stress applied at the surface,

g is the gravitation acceleration, and

t' is the time.

The above set of equations can be solved analytically when the wind-stress, τ_x , is a sufficiently simple function. However, the task of computing the results by hand is formidable and the electronic computer was used. The computational problem is considerably simplified by integrating the original three differential equations directly. In order to perform the above integration the equations were first made non-dimensional.

The wind-stress, τ_x , is of the form

$$\tau_x = W \quad t' < t_0', \quad y < a,$$

$$\tau_x = 0 \quad t' > t_0', \quad \text{all } y,$$

$$\tau_x = 0 \quad t' < t_0', \quad y > a.$$

The non-dimensional equations are then given by defining

$$\lambda^2 = \frac{a^2 f^2}{gD}, \quad t = f t', \quad y = y/a, \quad \tau = \tau_x / W t_0, \quad U = u f / W t_0 \\ V = v f / W t_0, \quad H = g D / a W t_0$$

Then

$$\left\{ \begin{array}{l} \frac{\partial U}{\partial t} - V = \tau \\ \frac{\partial V}{\partial t} + U = - \frac{\partial H}{\partial y} \\ \frac{\partial H}{\partial t} + \frac{1}{\lambda^2} \frac{\partial V}{\partial y} = 0 \end{array} \right.$$

$$\left\{ \begin{array}{l} \tau = \frac{1}{t_0}, \quad |y| < 1, \quad 0 < t < t_0 \\ \tau = 0, \quad |y| > 1, \quad 0 < t < t_0 \\ \tau = 0, \quad t > t_0 \end{array} \right.$$

In centered finite difference form the equations are

$$\left\{ \begin{array}{l} \Delta_t U_i = 2\Delta T [V_i^{\gamma} + \tau_i^{\gamma}] \\ \Delta_t V_i = -2\Delta T [U_i^{\gamma} + \frac{1}{2\Delta S} \Delta_y H^{\gamma}] \\ \Delta_t H_i = -\frac{\Delta T}{\lambda^2 \Delta S} \Delta_y V^{\gamma} \end{array} \right.$$

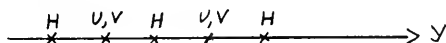
where the superscript, γ , refers to the time index and the subscript, i , refers to the space point. Thus

$$\left\{ \begin{array}{l} \frac{\partial \alpha}{\partial t} = \frac{\Delta_t \alpha_i}{2\Delta t} = \frac{\alpha_i^{\gamma+1} - \alpha_i^{\gamma-1}}{2\Delta T} \\ \frac{\partial \alpha}{\partial y} = \frac{\Delta_y \alpha^{\gamma}}{2\Delta S} = \frac{\alpha_{i+1}^{\gamma} - \alpha_{i-1}^{\gamma}}{2\Delta S} \end{array} \right.$$

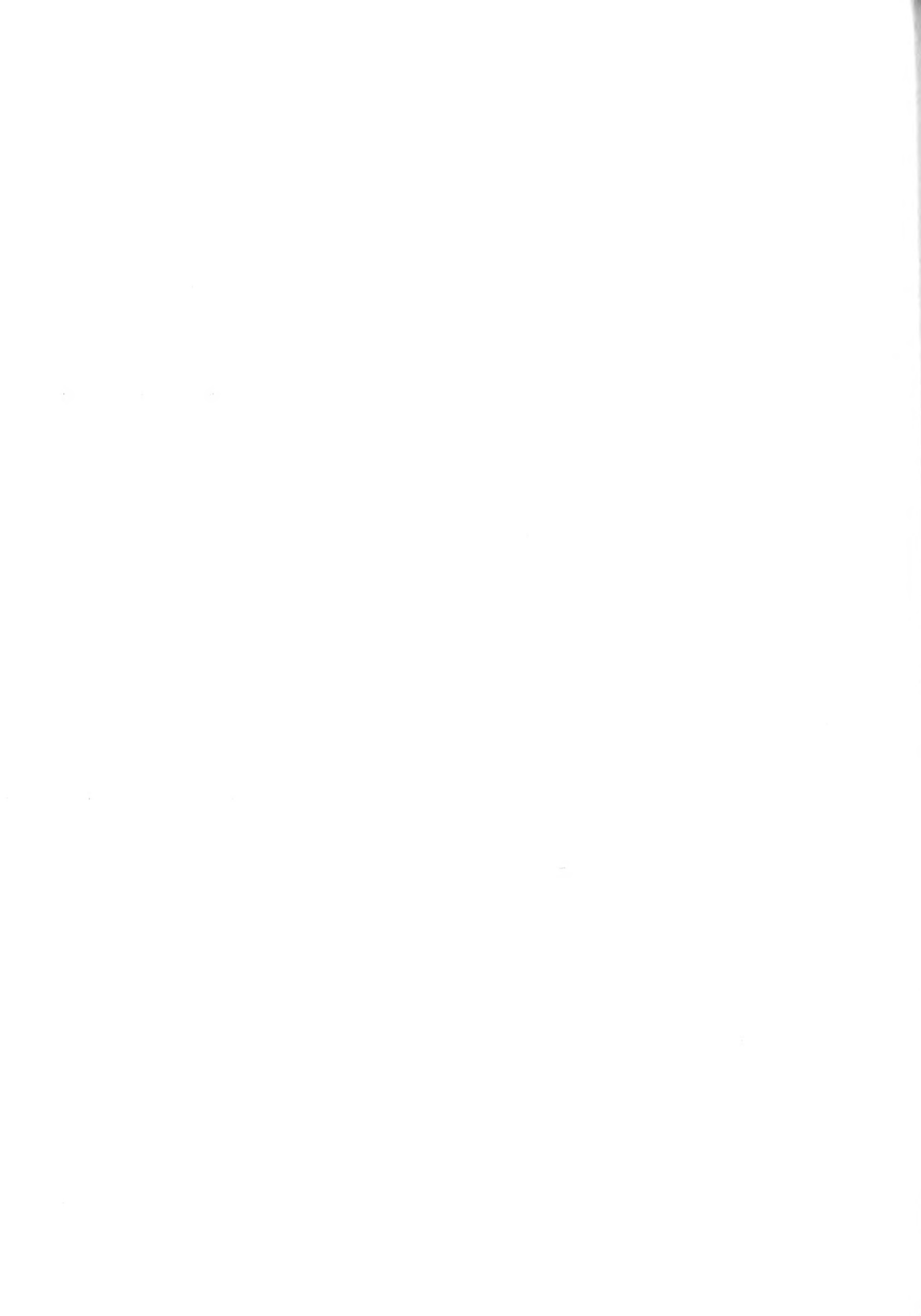
The equations can now be written

$$\left\{ \begin{array}{l} U_i^{\gamma+1} = U_i^{\gamma-1} + 2\Delta T [V_i^{\gamma} + \tau_i^{\gamma}] \\ V_i^{\gamma+1} = V_i^{\gamma-1} - 2\Delta T U_i^{\gamma} - \frac{\Delta T}{\Delta S} \Delta_y H^{\gamma} \\ H_i^{\gamma+1} = H_i^{\gamma-1} - \frac{\Delta T}{\lambda^2 \Delta S} \Delta_y V^{\gamma} \end{array} \right.$$

An inspection of the equations reveals the fact that $\Delta_t \alpha$ does not appear in the equation for $\Delta_t \alpha$. Thus, the space points can be staggered as shown below



In this case, if the U and V values are stored together with the following H value, the computation time can be reduced by a factor of 2. The equations then are changed by the definition



$$\left\{ \begin{array}{l} \Delta_y H^\delta = H_i^\delta - H_{i-1}^\delta \\ \Delta_y V^\delta = V_{i+1}^\delta - V_i^\delta \end{array} \right.$$

The numerical values of the parameters are

$$a = 100 \text{ km}, g = 10 \text{ m/sec}^2, D = 4000 \text{ m}, f = 10^{-4} \text{ sec}^{-1}$$

$$\Delta s = .5 \text{ (= 50 km in dimensional form)}, \lambda^2 = 1/400,$$

$$\Delta T = .0238 \text{ (= 1/22 pendulum days in dimensional form).}$$

These values are chosen so as to satisfy computational stability criteria. Because of the wide range of values of the variables, the equations were scaled by defining $V = 2^{-5} \bar{V}$ for all i , and $U = 2^{-5} \bar{U}$ for $i > 0$ (only one point $i = 0$ is taken in the region within which the wind-stress is acting). The two sets of equations in scaled form are thus

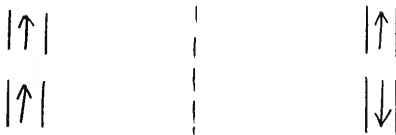
$$\left\{ \begin{array}{l} U_i^{\delta+1} = U_i^{\delta-1} + 2\Delta T \left\{ 2^{-5} \bar{V}_i^\delta + \tau_i^\delta \right\} \\ V_i^{\delta+1} = V_i^{\delta-1} - 2^{-5} \left\{ 2\Delta T U_i^\delta + \frac{\Delta T}{\Delta s} \Delta_y H^\delta \right\} \\ H_i^{\delta+1} = H_i^{\delta-1} - \frac{2^{-5} \Delta T}{\lambda^2 \Delta s} \Delta_y \bar{V}^\delta \end{array} \right. \quad i = 0$$

$$\left\{ \begin{array}{l} \bar{U}_i^{\delta+1} = \bar{U}_i^{\delta-1} + 2\Delta T \bar{V}_i^\delta \\ \bar{V}_i^{\delta+1} = \bar{V}_i^{\delta-1} - 2\Delta T \bar{U}_i^\delta - 2^{-5} \frac{\Delta T}{\Delta s} \Delta_y H^\delta \\ H_i^{\delta+1} = H_i^{\delta-1} - \frac{2^{-5} \Delta T}{\lambda^2 \Delta s} \Delta_y \bar{V}^\delta \end{array} \right. \quad i > 0$$



Because of the rapidity with which the waves move to the outlying regions, some means of confirming the computation to the region of interest ($0 \leq i \leq 100$) is necessary. This was accomplished by considering two systems of the above type with opposite boundary conditions at the extremity. The symmetry of the system of interest about the y axis enables one to specify boundary conditions which cancel when added. Because of the linear character of the equations the solutions could be superposed.

The two problems treated are shown schematically below (looking down on the surface of the ocean)



When these two problems are added (note that the system on the right in each case can be accounted for by the specification of a boundary condition along the dotted line half-way between the two systems) the effect of the right half cancels out and one is left with twice the values of the left-hand system.

Computations for 24 pendulum hours were carried through for three cases. The cases are distinguished by letting t_0 take on different values.

Case I $t_0 = 0$ corresponding to 0 pendulum hours

Case II $t_0 = 6$ corresponding to 6 pendulum hours

Case III $t_0 = 12$ corresponding to 12 pendulum hours.

The results indicate a pronounced dependence of the amplitude and energy of the oscillations on the time of duration of the wind-stress. It is shown that if the wind acts for 12 hours, the oscillations are considerably smaller in amplitude than those in which the wind is added impulsively.

The above problem was also considered for an ocean consisting of two homogeneous layers of different density with the lower layer continually adjusting in such a way as to offset any pressure gradient imposed by the surface of the ocean (such an assumption is justified when the lower layer is much deeper than the upper). The results in this case show that the amount of energy absorbed by the oscillations is very much dependent on the length of time of wind-stress duration. In fact, a wind acting for a period of 12 hours sets up oscillations which have an energy which is about 3% of that absorbed by oscillations caused by an impulsive addition of momentum.

I. Use of the primitive equations in forecasting.

Because of the limitations imposed on the accuracy of the forecast by the use of the geostrophic approximation, several attempts have been made recently to forecast the pressure and velocity fields by means of the primitive equations. By thus allowing gravity waves to enter into the solution, one encounters severe difficulties. Specifically, the effects of the boundary conditions are felt throughout the domain within three hours. As the boundary conditions are necessarily of a fictitious nature, the large-scale meteorological flow is obscured and the forecasts are practically worthless.

It has been suggested that a simple model be prescribed so that stability of boundary conditions may be easily studied. The following is a report of one such attempt.

The domain is defined by a rotating cylinder extending from $y = 0$ to $y = Y$ along the generator and from $x = 0$ to $x = X$ circumferentially. The points $x = 0$ and $x = X$ coincide, i.e., the domain is finite and the motions are periodic circumferentially. The boundaries at $y = 0$ and $y = Y$ are solid boundaries.

The primitive equations for the barotropic model are:

$$(1) \quad \frac{\partial u}{\partial t} = -u \frac{\partial u}{\partial x} - v \frac{\partial u}{\partial y} + fv - \frac{\partial \phi}{\partial x}$$

$$(2) \quad \frac{\partial v}{\partial t} = -u \frac{\partial v}{\partial x} - v \frac{\partial v}{\partial y} - fu - \frac{\partial \phi}{\partial y}$$

$$(3) \quad \frac{\partial \phi}{\partial t} = -u \frac{\partial \phi}{\partial x} - v \frac{\partial \phi}{\partial y} - \phi / \left(\frac{\partial u}{\partial x} + \frac{\partial v}{\partial y} \right)$$

where u and v are the velocities along the x and y directions, respectively, ϕ is the geopotential height and f , the Coriolis parameter, is constant.

In finite difference form, the scaled equations are

$$(4) \quad \hat{u}_{ij}^{\tau+1} = \hat{u}_{ij}^{\tau} - \frac{V\Delta T}{\Delta S} \left\{ \hat{u}_{ij}^{\tau} \Delta_x \hat{u}^{\tau} + \hat{v}_{ij}^{\tau} \Delta_y \hat{u}^{\tau} \right\} + f \Delta T \hat{v}_{ij}^{\tau} - \frac{B \Delta T}{\Delta S} \Delta_x \hat{\phi}^{\tau}$$

$$(5) \quad \hat{v}_{ij}^{\tau+1} = \hat{v}_{ij}^{\tau} - \frac{V\Delta T}{\Delta S} \left\{ \hat{u}_{ij}^{\tau} \Delta_x \hat{v}^{\tau} + \hat{v}_{ij}^{\tau} \Delta_y \hat{v}^{\tau} \right\} - f \Delta T \hat{u}_{ij}^{\tau} - \frac{B \Delta T}{\Delta S} \Delta_y \hat{\phi}^{\tau}$$

$$(6) \quad \hat{\phi}_{ij}^{\tau+1} = \hat{\phi}_{ij}^{\tau} - \frac{V\Delta T}{\Delta S} \left\{ \hat{u}_{ij}^{\tau} \Delta_x \hat{\phi}^{\tau} + \hat{v}_{ij}^{\tau} \Delta_y \hat{\phi}^{\tau} \right\} - \frac{2V\sqrt{B}\Delta T}{B\Delta S} \left(\frac{1}{2} + \frac{B}{2\sqrt{B}} \hat{\phi}_{ij}^{\tau} \right) \times \left\{ \Delta_x \hat{u}^{\tau} + \Delta_y \hat{v}^{\tau} \right\}$$

where the reference point has subscripts i, j ($0 \leq i \leq I, 0 \leq j \leq J$)

$$\begin{cases} \Delta_x \alpha = \alpha_{i+1,j} - \alpha_{i-1,j} \\ \Delta_y \alpha = \alpha_{i,j+1} - \alpha_{i,j-1} \end{cases}$$

V , ΔT , ΔS , B , $\hat{\phi}$, are scaling constants. Superscripts refer to time index. \hat{u}_{ij}^{τ} , \hat{v}_{ij}^{τ} , $\hat{\phi}_{ij}^{\tau}$ are scaled quantities (modulus < 1).

For interior points of the domain equations (4), (5), (6) suffice for evaluating the velocities and the pressure for future times. The same holds true for boundary points at $x = 0, X$ since these point may also be considered "interior" because of the periodicity.

At the boundaries $y = 0, Y$, the normal derivatives cannot be given by centered space differences. It can be seen from equation (4), however, that no difficulty arises in evaluating \hat{u}_{ij}^{τ} since each derivative normal to the boundary is multiplied by \hat{v}_{ij}^{τ} which vanishes at these points. The term $\hat{v}_{ij}^{\tau+1}$ is, of course, zero at all times at the solid boundaries. One is left, finally, with the problem of evaluating $\hat{\phi}_{ij}^{\tau+1}$ at $y = 0, Y$. Two methods have been considered.

Case I. Equation (5) written for $\tau + 1$ reduces to

$$(7) \quad \hat{\phi}_{ij}^{\tau+1} = \pm \left\{ - \frac{f \Delta S V}{B} \hat{u}_{ij}^{\tau+1} + \phi_{i,j \pm 1}^{\tau+1} \right\}$$

where \pm depends on $i = 1$ or 0 , respectively. Thus $\phi_{ij}^{\tau+1}$ can be evaluated easily and, in fact, this method indicates definite stability for a forecast of 24 hours.

Case II. In equation (6) the only unknown term is $\Delta_y \hat{v}^\tau$. If, however, we choose as $\Delta_y \hat{v}^\tau$, twice the one-sided derivative of \hat{v}_{ij}^τ at the boundary, then $\hat{\phi}_{ij}^{\tau+1}$ can be evaluated directly. Case II results are not as good as those of Case I.

A third possibility involves taking one-sided space and time derivatives for all quantities in equation (6). This method has not as yet been carried through.

2
D. 1970

36 - 045

need Study, Princeton, N. J.
er Project.
contract no. DA-36-034-ORD-
, Electronic Computer Project
llus. 28cm.

Calculating-machines, I. Title

Institute for Advanced Study
Math. - Nat. Sci. Library
Princeton, N. J. 08540

